

**POWER LAWS GOVERN MITOCHONDRIAL OPTIMIZATION OF INHERITABLE
CELLULAR MEMORY AND FATE DECISION**

by

Amin Cheikhi

Diplome de Licence, Universite Mohammed V-Agdal, Morocco, 2003

Submitted to the Graduate Faculty of
the Department of Environmental and Occupational Services
Graduate School of Public Health in partial fulfillment
of the requirements for the degree of
Doctor of Philosophy

University of Pittsburgh

2017

UNIVERSITY OF PITTSBURGH
GRADUATE SCHOOL OF PUBLIC HEALTH

This dissertation was presented

by

Amin Cheikhi

It was defended on

April 17, 2017

and approved by

Dissertation Chair:

Bruce R. Pitt, PhD

Professor

Department of Environmental and Occupational Health
Graduate School of Public Health
University of Pittsburgh

Dissertation Advisor:

Aaron Barchowsky, PhD

Professor

Department of Environmental and Occupational Health
Graduate School of Public Health
University of Pittsburgh

Committee Members:

Fabrisia Ambrosio, PhD

Associate Professor

Department of Physical and Rehabilitation Medicine
School of Medicine
University of Pittsburgh

Claudette St Croix, PhD

Associate Professor

Department of Cell Biology
School of Medicine
University of Pittsburgh

Adam C. Straub, PhD

Assistant Professor

Department of Pharmacology and Chemical Biology
School of Medicine
University of Pittsburgh

Copyright by Amin Cheikhi

2017

Bruce R. Pitt, PhD
Aaron Barchowsky, PhD

**POWER LAWS GOVERN MITOCHONDRIAL OPTIMIZATION OF INHERITABLE
CELLULAR MEMORY AND FATE DECISIONS**

Amin Cheikhi, PhD

University of Pittsburgh, 2017

ABSTRACT

Chronic environmental exposure to arsenic in drinking water is a major public health concern affecting the health of more than 130 million people worldwide. In addition to causing cancer and non-cancer diseases, arsenic causes muscle weakness and dysfunction. We found that arsenic targets muscle stem cell mitochondrial functionality to impair muscle maintenance and regeneration. Stem cell behavior was determined by their epigenetic memory. Although mitochondrial remodeling is inescapable for successful differentiation and pluripotency reprogramming and mitochondria-derived outputs shape cellular epigenetic landscape, their role in the regulation of cellular memory is poorly understood. Arsenic is a mitochondrial stressor and epigenetic modifier that alters stem-cell fate determination making it an excellent tool to determine the mitochondrial contribution to regulation of cellular memory and fate decisions. Using a model of myogenic differentiation, we imprinted a memory of arsenite-induced stress into myogenic reserve cells (RC) and monitored the fate of their progeny in arsenic-free medium. Phenotyping of primed RC revealed inherited aberrant mitochondrial dynamics that limited self-renewal capacity and enhanced their proliferation; trapping them in a poised state. Non-Gaussian statistics demonstrated that nuclear protein profiles and morphometrics were distributed as power-laws, indicating the presence of critical self-organization at the cell population level. Using graph theory, we modeled the mitochondria and showed an increased

connectivity of the primed RC progeny mitochondrial networks. We identified crucial interplay of H2A.Z acetylation with RNA polymerase II at bivalent chromatin domains that define chromatin state and transcriptional plasticity of the primed RC. Importantly, the intervention by mitochondria-targeted XJB-5-131 fully restored mitochondrial functionality and dynamics, RC cellular phenotypic identity, nuclear morphometrics, and epigenetic regulation that reset RC memory including histone modifications. Collectively, this work demonstrated that poising of chromatin regulation and cellular memory are fundamentally contingent on mitochondrial functionality and dynamics. Furthermore, we provided an innovative conceptual framework whereby cellular memory and cell fate are statistical properties defined at the cell population level by intricate mechanisms integrated at the mitochondrial level and governed by power laws. Significantly, the beneficial effects of XJB-5-131 suggest a window of opportunity for preventing or reverting disease resulting from stem cell dysfunction.

TABLE OF CONTENTS

PREFACE.....	IX
DEDICATION.....	X
1.0 INTRODUCTION.....	1
1.1 ARSENIC OVERVIEW.....	1
1.2 ARSENIC TOXICOKINETICS.....	2
1.3 ARSENIC AND LOSS OF MUSCLE MAINTENANCE AND REGENERATION	3
1.4 ARSENIC AND MITOCHONDRIAL FUNCTION	5
1.5 MITOCHONDRIAL LINKAGE TO CELL MEMORY.....	8
1.5.1 Mitochondrial linkage to linkage to H2A.Z regulation of cell fate and proliferation	8
1.5.2 Mitochondrial regulation of nuclear methylation.....	10
1.6 POWER LAW AND RELEVANCE TO OPTIMIZATION OF STEM CELL FATE.....	12
1.7 GLOBAL HYPOTHESIS AND RELEVANCE TO PUBLIC HEALTH	13
2.0 METHODS	15
2.1 CELL CULTURE.....	15
2.2 ISOLATION OF RESERVE CELLS (RC).....	15

2.3	FLUORESCENCE ASSAY OF REDUCED GLUTATHIONE (GSH), TOTAL PROTEIN THIOLS (TPT), AND LOW MOLECULAR WEIGHT THIOLS (LMWT)	16
2.4	MITOCHONDRIAL STAINING.....	17
2.5	FLOW CYTOMETRY WITH CELL SURFACE IMMUNOFLUORESCENCE STAINING	18
2.6	IMMUNOFLUORESCENCE STAINING FOR CONFOCAL MICROSCOPIC IMAGING.....	19
2.7	WESTERN IMMUNOBLOTTING.....	20
2.8	TRANSMISSION ELECTRON MICROSCOPY	20
2.9	TRANSMISSION ELECTRON MICROSCOPY	21
2.10	ANIMAL EXPOSURE.....	22
2.11	WHOLE MUSCLE GENE TRANSCRIPTS	22
2.12	C2C12 GENE TRANSCRIPTS AND CHIP ANALYSIS	23
2.13	CASPASE3/7 ACTIVITY.....	24
2.14	STATISTICAL ANALYSIS (GAUSSIAN).....	24
3.0	MITOCHONDRIAL OPTIMIZATION OF INHERITABLE CELL MEMORY	26
3.1	ABSTRACT.....	26
3.2	INTRODUCTION	27
3.3	RESULTS	29
3.3.1	Constructing a memory of stress response	29

3.3.2	Mitochondria sustain cellular memory for several generations and define RC identity	37
3.3.3	Cellular memory is contingent on mitochondrial regulation of RC heterogeneity.....	43
3.3.4	Mitochondrial maintenance of cellular memory adheres to a power-law	56
3.3.5	Mitochondria optimize bivalent chromatin domains	70
3.4	DISCUSSION.....	73
4.0	MITOCHONDRIAL DYNAMICS REGULATE MYOGENIC RESERVE CELL CELL-STATE TRANSITIONS.....	76
4.1	ABSTRACT.....	76
4.2	INTRODUCTION	77
4.3	RESULTS.....	78
4.3.1	Transient arsenic exposure hyperpolarizes mitochondria and causes aberrant mitochondrial dynamics	78
4.3.2	Aberrant mitochondrial fusion prevents resolution of cell Identity and fate decisions	82
4.3.3	Mitochondrial hyperfusion stimulates non–apoptotic Caspase 3/7 activation.....	86
4.4	DISCUSSION.....	89
5.0	CONCLUSIONS	90
5.1	NOVEL MECHANISMS FOR ARSENIC-INDUCED MALADAPTIVE RESPONSE.....	90

5.2	IMPACT OF STRESS MEMORY ON MUSCLE STEM CELL FATE AND LOSS OF HOMEOSTATIC INTEGRITY	91
5.3	IMPLICATIONS OF THE POWER-LAW FOR STEM CELL DECISIONS MAKING.....	92
5.4	SUMMARY AND FUTURE DIRECTIONS.....	93
	BIBLIOGRAPHY	95

LIST OF TABLES

Table 1. Statistical descriptors of nuclear area distributions	51
Table 2. Statistical descriptors of nuclear H2A.Z expression.....	51
Table 3. Statistical descriptors of nuclear EZH2 expression	51
Table 4. Computation of exceedance probabilities.....	59
Table 5. Goodness-of-fit results for the comparison of truncated power law and alternative methods.....	65

LIST OF FIGURES

Figure 1. Representative images of myogenic differentiation of C2C12 myogenic cells	30
Figure 2. Assessment of RC redox status	30
Figure 3. Phenotypic characterization of RC.....	31
Figure 4. Assessment of proliferative potential by flow cytometry with the cell cycle marker Ki67.....	32
Figure 5. Assessment of mitochondrial membrane potential by microplate assay measuring the accumulation of membrane-permeant potentiometric dye JC-1.....	33
Figure 6. Assessment of mitochondrial ROS and mass.....	33
Figure 7. Increased expression of the inner mitochondrial membrane protein cardiolipin synthase (CRLS) in pRC.....	35
Figure 8. Representative transmission electron microscopy of RC.....	35
Figure 9. Upregulation of autophagy markers, Atg12, Atg16 and Beclin-1 protein expression measured by flow cytometry	36
Figure 10. Expression of the bivalent chromatic marker and memory-conferring protein, H2A.Z	37
Figure 11. XJB-5-131 restores normal mitochondrial dynamics	39
Figure 12. XJB-5-131 restores mitochondrial dynamics to normal RC levels.....	39
Figure 13. RCs identity is contingent on mitochondrial maintenance of cellular memory	40

Figure 14. Characterization of RC population heterogeneity and normalization by XJB-5-131	42
Figure 15. Correlation of RC population heterogeneity and normalization by XJB-5-131	43
Figure 16. Non-parametric kernel density estimate (NPKDE) based on Silverman approach.....	47
Figure 17. Normal quantile-quantile-plots (QQ-plots).....	48
Figure 18. Nuclear morphometric analysis.....	49
Figure 19. Two-sided bootstrap Kolmogorov-Smirnov tests	50
Figure 20. Histograms of measured protein expression and nuclear area distributions and their corresponding histogram densities (insets).....	52
Figure 21. Inadequacy of Gaussian Statistics	54
Figure 22. Distribution fitting of probability density functions: nuclear area.....	55
Figure 23. Distribution fitting of probability density functions: nuclear H2A.Z.....	55
Figure 24. Distribution fitting of probability density functions: nuclear EZH2	56
Figure 25. Cumulative distribution functions (CDF) and their maximum likelihood power law fit: nuclear H2A.Z.....	60
Figure 26. Cumulative distribution functions (CDF) and their maximum likelihood power law fit: nuclear area	60
Figure 27. Cumulative distribution functions (CDF) and their maximum likelihood power law fit: nuclear area	61
Figure 28. Results from standard bootstrap procedure for the power law model: H2A.Z expression	62
Figure 29. Results from standard bootstrap procedure for the power law model: nuclear area ...	63

Figure 30. Results from standard bootstrap procedure for the power law model: nuclear area ...	64
Figure 31. Truncated power law fitting of XJB-5-131 reversion of nuclear area and protein expression	69
Figure 32. Regulation of memory for expression of DNA methyltransferases: DNMT3A	71
Figure 33. Regulation of memory for expression of DNA methyltransferases: Dnmt1	72
Figure 34. Arsenic decreases cardiolipin in RC mitochondria	79
Figure 35. Arsenic increases the abundance of RC mitochondrial outer membrane pro-fusion processing proteins Mfn1 and Mfn2	80
Figure 36. Arsenic-stimulation of inner mitochondrial membrane structural protein and protease processing and remodeling.	81
Figure 37. Arsenic stimulates RC proliferation	82
Figure 38. Arsenic-stimulated upregulation of Notch1 signaling and CD34 is associated with increased RC proliferation	84
Figure 39. Confirmation of arsenic-stimulated increase in NICD variants	84
Figure 40. Arsenic increased proliferation correlates with increased mitochondrial mass, membrane potential, and non-apoptotic caspase activity	85
Figure 41. Arsenic does not promote apoptosis in RC	86
Figure 42. Arsenic increases mitochondrial network connectivity and mass	87
Figure 43. Increased probability of higher connectivity in arsenic-exposed RC.....	88

PREFACE

ACKNOWLEDGEMENTS

I owe everything good in this thesis to Professor Aaron Barchowsky and Professor Fabrisia Ambrosio. I am forever indebted with sincere and profound gratitude for their scientific and intellectual leadership as well as their distinguished human values. I am also indebted with gratitude to Professor Valerian Kagan and Professor Hulya Bayir for giving me the opportunity to be part of their research and to further my higher education. I would like to thank the members of my PhD advisory committee, Professor Bruce Pitt and Professor Adam Straub for their critical discussions and remarks. I especially like to thank Professor Claudette St Croix for her support and guidance throughout our imaging studies. I would also like to thank all the co-authors for their help and suggestions. This work would not have been possible without the support of many EOH department faculty members, technicians and administrators. I am very grateful to every one of them. I would like to especially thank Mr. Adam Orbell for his excellent professional IT solutions.

DEDICATION

This work has been done in the hope that humanity may profit by even a small contribution to the progress of science and knowledge to cure diseases and sanctify human life

.

1.0 INTRODUCTION

1.1 ARSENIC OVERVIEW

Arsenic is a naturally occurring metalloid that occurs in both organic and inorganic forms. It is the twentieth most abundant element on the earth and is also mobilized into the environment by anthropogenic activity. In the natural environment arsenic, frequently exists in its inorganic form as a component of ores and is concentrated on the continental crust of earth at approximately 1.5 to 2 parts per million (Arsenic, 1977). Inorganic arsenic can exist in four valence states: -3, 0, +3 and +5 with the two most common oxidation states are arsenite (As (III)) and arsenate (As (V)) that exist in mildly reducing and oxidizing conditions respectively (Duker, 2005). Valence states may interchange in accordance with the pH and the presence of other substrates (Hughes, Beck, Chen, Lewis, & Thomas, 2011).

Inorganic arsenic often complexes with other elements yielding more than 245 mineral forms of arsenic (Arsenic, 1977). Arsanilic acid, methylarsonic acid and dimethylarsinic acid are the most common organic arsenic compounds (WHO, 2000). In addition, many animal species, including humans, metabolize inorganic arsenic to methylarsonic and dimethylarsinic acids, as well as their trivalent counterparts, as for more efficient excretion of the toxicant (Hughes et al., 2011).

Globally the primary source of human exposure to arsenic is drinking water, and the secondary is food. Epidemics of disease caused by arsenic in drinking water have occurred throughout the world, with countries, such as Bangladesh, India, Taiwan, Mexico, China, Argentina and Chile, reporting that more than 130 million of their people are exposed to arsenic at levels above the WHO suggested maximal containment level of 10 µg/L (Bailey et al., 2016; Hughes et al., 2011). In the United States, there are estimates that nearly 4% of the population, or 3.7 million individuals, drink water from private wells that exceeds governmental standards for arsenic contamination (US Geological Survey, <http://pubs.usgs.gov/of/2006/1376/>). For example, 39% of Arizona wells monitored in a 2000 survey contain greater than 10 µg/L of arsenic (Spencer, 2000), while in northern Pennsylvania, more than 8% of wells monitored in 2006 were above the safe levels with levels found to be as high as 188 µg/L (<http://pubs.usgs.gov/of/2006/1376/>). In Maine, the arsenic content in wells can range up to 3000 µg/L with approximately 50% of wells exceeding 10 µg/L in certain townships (Nielsen, Lombard, & Schalk, 2010).

1.2 ARSENIC TOXICOKINETICS

The primary route of inorganic arsenic exposure is oral and it is readily absorbed through aquaporin 7 and channels the gastrointestinal tract (Liu et al., 2002). Metabolism to methylated species occurs predominantly in the liver via the actions of arsenic (3) methyltransferase (AS3MT) in humans (Hughes et al., 2011; Rosen, 2002). Human tissues, blood, and urine contain a mixture of the inorganic arsenic its methylated metabolites that vary in acute and chronic toxicity (Council, 2014; Hughes et al., 2011) and rates and extent of methylation varies between different species as well as among humans (Hughes et al., 2011). The volume of

distribution of arsenic and metabolites approximates the volume of water as the trivalent arsenicals are highly soluble and distribute into cells through the aquaporin water / glycerol channels (Hughes et al., 2011; Liu et al., 2002; Rosen, 2002). As example of the scale of the internal dose expected from a low to moderate environmental exposures, epidemiological studies found that a human chronically exposed to 100 mg/L of arsenic in drinking water would have a blood total arsenic level of approximately 96 nM (Hall et al., 2006). Human autopsy data and mouse experiments indicate that the highest absolute amounts of arsenic are found in lungs, kidneys, and skeletal muscle (Hughes et al., 2011; Kenyon, Del Razo, & Hughes, 2005); however, high levels of excreted arsenic keratin metabolites accumulate in skin, nails and hair. In contrast to other metals, arsenic and its metabolites do not accumulate within the body proper (e.g. excluding hair, nails, and outer dermal layers of dead cells) and is eliminated with a half-life of approximately one day (Hughes et al., 2011).

1.3 ARSENIC AND LOSS OF MUSCLE MAINTENANCE AND REGENERATION

Arsenic exposures cause a number of cancers (e.g. lung, bladder, and skin) and non-cancer diseases (e.g. cardiovascular, obstructive lung disease, cognitive dysfunction, neuropathies) in more than 100 million individuals worldwide (Council, 2014; Oberoi, Barchowsky, & Wu, 2014). In addition, chronic arsenic exposure causes significant muscle weakness and dysfunction that is in part related to neuropathies. Muscle weakness and wasting are among the primary pathologic sequelae caused by arsenic with sensorimotor impairment and muscle atrophy observed in 10-14 million (7.5-10% of exposed) individuals exposed daily to arsenic in their drinking water (Chakraborti et al., 2003; Mukherjee et al., 2003). Epidemiological studies

in populations exposed to very high As(III) levels demonstrate rates of muscle morbidity in the range of 35-85% (Chakraborti et al., 2003; Guha Mazumder, 2003; Mukherjee et al., 2003). Lower level exposures in early development may have an even greater impact as motor functioning, strength and agility in 8-11 year-old children was found to be impaired when exposures averaged 43 $\mu\text{g/L}$ (Parvez et al., 2011), just slightly below the pre-2006 US drinking water limit of 50 $\mu\text{g/L}$. Thus, in a significant population, exposure to arsenic may be surreptitiously contributing to muscle dysfunction. This is important, as muscle weakness and change in muscle composition and metabolism are among the greatest factors contributing to declines in functional mobility (Doherty, 2003) and is a strong predictor of all-cause and cardiovascular mortality (Miljkovic et al., 2015; Rantanen et al., 2000). Globally this is an increasingly important as it causes very high numbers of Disability-Adjusted Life Years (DALY), a quantifiable measure of public health disease burden.

Muscle wasting and weakness resulting from sarcopenia and an impaired regenerative response lead to the dramatic declines in mobility, depriving a person of functional independence. Myosteatorsis is a specific form of muscle remodeling and weakness where ectopic fat infiltration within and around skeletal muscle is associated with metabolic disorders, poor musculoskeletal health, and increased risk of all-cause mortality (Miljkovic et al., 2015; Miljkovic & Zmuda, 2010; Rantanen et al., 2000). There is a significant gap in understanding the biological or environmental basis underlying these risks and relationships, as well as interventions effective in preventing these risks. Genetics play a clear role in myosteatorsis, and there are considerable disparities in mortality risk from myosteatorsis. For example, men of African ancestry are more at risk than those of European or Caucasian descent (Miljkovic-Gacic, Ferrell, Patrick, Kammerer, & Bunker, 2005; Miljkovic et al., 2015; Q. Zhao et al., 2016).

However, genetic contributions only account for a fraction of the risk factors, and aging, lifestyle and environmental exposures are clearly among the primary culprits.

Animal studies performed in our laboratory found that exposure to environmentally and human-relevant, low to moderate (10-100 $\mu\text{g/L}$) levels of arsenic in drinking water promotes ectopic fat deposition in skeletal muscle (Garciafigueroa, Klei, Ambrosio, & Barchowsky, 2013), impair muscle mitochondrial function, impairs muscle physiology, and imparts a dysfunctional memory of stress in muscle stem cells (satellite cells, MuSC) (Ambrosio et al., 2014; C. Zhang et al., 2016). In addition, these effects of disrupting mitochondrial morphology and function impair muscle regeneration after an injury, as well as remodel the muscle extracellular matrix to favor fibrogenic, and possibly adipogenic, expansion over myogenic renewal of the injured muscle (C. Zhang et al., 2016). An increased pathogenic signaling through NF- κ B-driven gene induction appears to be an underlying mechanism for arsenic effects on extracellular matrix remodeling and impaired tissue and functional regeneration of injured muscle (C. Zhang et al., 2016), and it is likely that the sustained maladaptive oxidative stress response in the muscle and MuSC mitochondria is the underlying driver of the pathogenic signaling.

1.4 ARSENIC AND MITOCHONDRIAL FUNCTION

Inorganic arsenic in drinking water is one of the most toxic environmental exposures known to target human mitochondria in several tissue and is traditionally assumed to depolarize mitochondria (Eyvani et al., 2016) , reduce ATP content, induce the generation of reactive oxygen species (ROS) and lipid peroxidation (Pace et al., 2016). Thus arsenic has been causally linked to apoptosis and necrosis via the promotion of mitochondrial permeability transition

(MMP), release of cytochrome c, activation of caspases activities and triggering of the endoplasmic reticulum (ER) stress pathway in many cell types and tissues including myoblasts (Safiedeen et al., 2017). Subcellular differential centrifugation demonstrated that the arsenic-compromised mitochondria predominantly accumulate the trivalent arsenicals such as monomethylarsonous acid MMA (III). Mitochondrial aquaglyceroporins may facilitate arsenite access to vital enzymes including oxidative phosphorylation complexes II, III and IV (Naranmandura et al., 2011) as well as pyruvate, succinate, isocitrate, and α -ketoglutarate dehydrogenases (Bergquist, Fischer, Sugden, & Martin, 2009; Hosseini, Shaki, Ghazi-Khansari, & Pourahmad, 2013), leading to the inhibition of their activity and aberrant bioenergetics. It is therefore hypothesized that arsenic-induced mitochondrial dysfunction may constitute the pathophysiological basis of arsenic adverse effects on human health. In line with this, a shift to aerobic glycolysis has been shown in several cell lines and organisms exposed to arsenic, a phenomenon known as the Warburg effect (H. Chen, Lee, Li, Tsao, & Chiu, 2016; Chowdhury, Chatterjee, Giri, Mandal, & Chaudhuri, 2010; Lee et al., 2011; Li et al., 2016; Luz et al., 2016; Sun, Board, & Blackburn, 2011; F. Zhao, Severson, Pacheco, Futscher, & Klimecki, 2013). This metabolic reprogramming is likely to reflect a maladaptation to the unexpected biosynthetic requirements (incorporation of nutrients such as nucleotides, amino acids, and lipids needed to produce daughter cells) imposed by the arsenic-induced uncontrolled proliferation (Chowdhury et al., 2010; Lee et al., 2011). One possible cause is that a high cytosolic ATP/ADP ratio can allosterically inhibit some glycolytic enzymes and shut down the glycolysis. Thus, while under aerobic respiration, the majority of ATP is of mitochondrial origin, during aerobic glycolysis, mitochondria consume glycolytic ATP rather than actually produce ATP in order to maintain a cytoplasmic ATP/ADP ratio level that is permissible of continuous glycolysis at a high rate, a

vital need for rapidly proliferating cells. This further supports the notion that disruption of mitochondrial functionality is an important mechanism that mediates adverse arsenical effects (KLINGENBERG, 1977). Overall, one common denominator of these observations is that they originate from experiments that used high doses of arsenic within the experimental paradigm of apoptosis. However, recent reports showed that arsenic stimulates mitochondrial function (Chavan et al., 2017) (Chen, Lee, Li, Tsao, & Chiu, 2016) (Samikkannu et al., 2003) emphasizing the non-linear nature of arsenic dose-response.

It is, thus, presumable that arsenic at low doses does not directly interact with mitochondria, but rather acts as an impediment to redox state of the cell. A stimulation of glycolysis will be followed by enhanced pentose phosphate pathway, producing more NADPH from NADP⁺, which is necessary for the reduction of glutathione (GSH) and enabling the GSH-dependent antioxidant defense, including glutathione peroxidase (GP), which converts hydrogen peroxide into water which potentiate the upstream ability of superoxide dismutase to convert superoxide to hydrogen peroxide. Indeed it has been shown that arsenic induces a strong antioxidant response including an elevation in GSH levels (Barchowsky, Dudek, Treadwell, & Wetterhahn, 1996) supporting an alternative explanation for the arsenical effect on mitochondria. Further supporting this view, we recently reported that muscle progenitor cells from a mouse model of subchronic exposure to the low-dose arsenic exhibited persistently increased levels of mitochondrial activity and autophagy, long after their isolation from hind limb muscles and expansion in culture, in total absence of arsenic (Ambrosio et al., 2014). Similar overactive mitochondria have been directly linked to the stemness of hematopoietic stem cells, corroborating a potential role of mitochondria in mediating arsenic effects on stem cells.

1.5 MITOCHONDRIAL LINKAGE TO CELL MEMORY

1.5.1 Mitochondrial linkage to linkage to H2A.Z regulation of cell fate and proliferation

Cellular identity is determined by a dynamic constellation of mechanisms which the interplay define the cell fate decisions that occur during a regenerative event or the adaptation to the fluctuations of environmental cues. Epigenetic regulatory mechanisms are of utmost importance in these processes as cell fate decisions are translated into chromatin states that determine a wide array of transcriptional outcomes. Stem cells are typified by an epigenetic plasticity that permits cell-state transitions which the ultimate goal is to balance the stem cells capacity of self-renewal and their differentiation potential. Thus, during a regenerative event, the chromatin dynamically transition from a permissive to a restrictive configuration as the cells gradually commit to differentiation.

The maintenance of a tissue homeostasis and its regenerative potential depend on the integrity of the stem cell pool. During a regenerative event, the stem cells exit their quiescent state that is characterized by repressed pro-differentiation programs, become activated, proliferate and commit to a terminally differentiated state as the repressive mechanisms are relieved. This intricate balance of quiescence and readiness to promptly respond to instructive regenerative or environmental cues is ensured by the stem cells cellular memory. The latter, involve poising of genes that are epigenetically repressed yet transcriptionally competent to swiftly adjust to the crucial spatio-temporal requirements of stem cell-state transitions.

The nuclear genomic DNA is packaged into chromatin, which is composed of basic repeat units, called nucleosomes, which have approximately 146 bp of DNA wrapped around an octamer of core histones (two molecules of each histone H2A, H2B, H3 and H4). Chromatin

compaction is a highly fine-tuned and dynamic process that restricts the access of cellular machinery to DNA (Cutter & Hayes, 2015; C. Jiang & Pugh, 2009; Christopher M Weber & Steven Henikoff, 2014). N-terminal tails of histones extend from the nucleosome and have no specific structure, and thus are readily accessible to enzyme-catalyzed modifications. Histone post-translational modifications (PTM) combinations form a “histone code” and constitute a fundamental epigenetic mechanism to regulate genes expression (T. Chen & Dent, 2014; Turner, 2002). They facilitate the recruitment of specific factors and their interactions with existing sites, or conversely, to alter existing sites so as to obliterate such interactions. The capacity of these histone modifications to configure of DNA–protein interactions, allows a dynamic control of gene expression in function of the maintained or disrupted interactions and thereby define cell-fate decisions (Aguilar et al., 2016; Rohlf et al., 2012; Watanabe et al., 2012).

H2A.Z is an evolutionary conserved histone variant of the canonical H2A family, with has approximately 60% amino-acid sequence similarity. H2A.Z deletion is lethal in many organisms, including mammals, suggesting a vital function (L. Jiang et al., 2007; Zlatanova & Thakar, 2008). Indeed, H2A.Z has been implicated in critical cellular processes, such as cell cycle progression, genes transcription, nucleosome turnover, antagonism of DNA methylation and stem cell differentiation (Zlatanova & Thakar, 2008). H2A.Z is a multifunctional protein in the sense that it can have repressive, poisoning or activating roles (M. Ku et al., 2012; Sura et al., 2017; C. M. Weber & S. Henikoff, 2014). One mechanism that dictate H2A.Z function is the acetylation of its lysines K4, K7 and K11 (Doyen et al., 2006; Ishibashi et al., 2009; Millar, Xu, Zhang, & Grunstein, 2006; Morales & Richard-Foy, 2000) which has been correlated with promoting transcriptional activity notably during differentiation (M. Ku et al., 2012) (Law & Cheung, 2015) .

H2A.Z genome-wide mapping in mammalian ES cells and neural progenitors revealed H2A.Z presence at poised promoters with bivalent chromatin domains and at active promoters with H3K4 methylation. In Contrast, H2A.Z was absent from stably repressed promoters that are specifically enriched for H3K27 trimethylation. Taken together, these published data support an important role H2A.Z in stem cell-fate decision making. Arsenic is an endocrine disruptor and its effects on estrogen receptor-mediated gene expression in vivo and in cell culture are known (Davey, Bodwell, Gosse, & Hamilton, 2007). Moreover, Arsenic is also a regulator of Cyclin D1 (Beezhold, Klei, & Barchowsky, 2017; Sharma, Sharma, Arora, & Kaul, 2013). Intriguingly, the removal of non-acetylated H2A.Z and acetylation of the remaining H2A.Z-containing nucleosomes at the promoter and enhancer in estrogen receptor (ER) positive MCF-7 is indispensable for the expression of the oncogene cyclin D1 (M Dalvai et al., 2013; Dalvai, Fleury, Bellucci, Kocanova, & Bystricky, 2013). It is not known whether mitochondria regulate H2A.Z activities, however, it is reasonable to consider H2A.Z expression and acetylation as potential mechanism that mediate arsenic sustained impairment of skeletal muscle and muscle progenitor (Ambrosio et al., 2014) and thus to consider a possible mitochondria and H2A.Z link.

1.5.2 Mitochondrial regulation of nuclear methylation

The notion of a “mitocheckpoint” (Chandra & Singh, 2011; Kulawiec, Ayyasamy, & Singh, 2009; Minocherhomji, Tollefsbol, & Singh, 2012; Singh, 2004, 2006) emerged from realization that the pathology of many mitochondrial diseases is intimately associated with significant alterations of the epigenetic landscape. This observation provided a plausible explanation to the mitopathology complexity (Minocherhomji et al., 2012; D. J. Smiraglia, Kulawiec, Bistulfi, Gupta, & Singh, 2008). Notably, an important role for mitochondria in the regulation of DNA

methylation, which occur via the modulation of S-adenosylmethionine availability or the control of ATP synthase by modulating ATP synthase gene methylation status, has been demonstrated (Minocherhomji et al., 2012; Xie et al., 2007; Yang et al., 2016). In line with these reports, another study suggested that global DNA methylation levels are modulated by specific mitonuclear interactions that affect the efficiency of the oxidative phosphorylation (Bellizzi, D'Aquila, Giordano, Montesanto, & Passarino, 2012).

It's increasingly recognized that mitochondrial metabolism is consequential for epigenetic modifications. This implies that the availability of mitochondrial metabolites may be a rate-limiting factor that determine the frequency of putative sites for epigenetic modification (e.g. Methylation) of nuclear genome (Guantes et al., 2015; Martinez-Pastor, Cosentino, & Mostoslavsky, 2013; Shaughnessy et al., 2014). In line with this, it has been recently demonstrated that the pro-activation histone modifications H4K16, H3K4me3, and H3K36me2 are modulated by the mitochondrial content (Canals-Hamann et al., 2013; Guantes et al., 2015; Henikoff & Shilatifard, 2011). Taken together, these reports strongly support the notion of an permissive mitochondrial influence on the epigenome and genes expression (Iain G Johnston et al., 2012; Muir, Diot, & Poulton, 2016).

Changes in mitochondrial functionality can induce significant compartmentalization in the nuclear genome into transcriptionally repressed or active regions by affecting directly or indirectly many epigenetic mechanisms. Despite the fact that cellular memory is physically stored in local chromatin states that are associated with DNA methylation patterns and/or histone modifications. A role of mitochondria in cellular memory has not been reported. Modulation of DNA methylation constitutes for the cell a means of producing heritable changes that can prime genes for transcription-activation events that may not necessarily be initiated immediately and

that may be reversed if the need arises. An additional characteristic of DNA methylation is that its alteration at multiple CpG sites is usually necessary for change in expression to occur, thus providing cells with a means of modulating their levels of readiness for adapting gene expression. The mitonuclear communications are of obvious importance in the cell fate decisions. Mitochondria is the central environmental sensor of the cell and the mitochondrial dynamics are pivotal regulators of myriad of cellular activities. These attributes poise mitochondria to play a fundamental role in coordinating cell-autonomous and non- autonomous processes that the outcome defines the cell fate. Arsenic is a well-established mitochondria poison and epigenetic modifier, making arsenic an excellent tool to investigate the mitonuclear communications contribution to cellular memory.

1.6 POWER LAW AND RELEVANCE TO OPTIMIZATION OF STEM CELL FATE

Many empirical metrics cluster around a typical value e.g. the temperature in Pittsburgh in mid-august, driving speed back and forth from work every day, etc. This means that the entropy of these quantities and measurements is reduced, and thus, probabilities of occurrences far from their typical value are quasi- negligible. This makes such a typical value a reliable representative of most occurrences related to that quantity. For instance, a typical 5 feet 7 inches height is representative of 300,000,000 Americans because deviations very far from that height are probabilistically extremely rare if not inexistent. Even when a large deviation happens it will be still within a reasonable limit that can be accounted for by a normal distribution's mean and standard deviation as described by the central. Under power law distributions, extreme events

become much more probable. Example of such events are earthquakes, stock markets meltdowns or the rise of companies like Google and Facebook, etc.

One concept that is intimately linked to the generation of power law distributions is self-organized criticality. This concept tries to explain power-law scaling observed in real-life phenomena by emphasizing that complex dynamical systems, including biological systems, that consist of many interacting components will spontaneously organize, under certain conditions, into a state with specific properties akin to a phase transition. Because this unpredictable complex behavior emerges spontaneously without external cues, this phenomena is called self-organized criticality. Systems that exhibit self-criticality are also typified by a permanent flux of matter and energy from and to the environment and thus are intrinsically far from the equilibrium. A corollary to this concept is its hypothetical universality, that is the collective behavior of a given system and its components become independent of the system microscopic details. (Clauset, Shalizi, & Newman, 2009).

1.7 GLOBAL HYPOTHESIS AND RELEVANCE TO PUBLIC HEALTH

Owing to the scaling and fractal properties of the mitochondrial network, mitochondria are poised to integrate cell-autonomous and non-autonomous processes to dynamically direct stem cell state transitions. We further hypothesize that is achieved by mitochondrial optimization of cellular memory and that epigenetically imprinted memory within a heterogeneous cell population results in the population dynamically organizing into behavior that is best described as a power law. The consequence is that normal cell homeostatic integrity is lost and pathogenic behavior is acquired within the population that ultimately, in the case of muscle stem cell state

transitions, results in compromised muscle maintenance and regeneration. Globally, chronic exposure to arsenic drives this muscle stem cell power law behavior to cause debilitating muscle morbidity. The findings of this thesis suggest that mitochondrial reversion of memory towards normal central tendencies restores normal stem cell fate decisions. If proven to be effective in vivo, this strategy would have immense public health impact in preventing or treating arsenic promoted muscle and muscle-derived metabolic disease in millions of exposed individuals worldwide.

2.0 METHODS

2.1 CELL CULTURE

Mouse C2C12 myoblasts were cultured in coating-free 75 cm² tissue culture flasks in Dulbecco's modified Eagle's medium (low pyruvate, cat #: 12430-054, ThermoFisher) growth medium supplemented with 10% fetal bovine serum, 1mM L-glutamine, and 0.2% antibiotics (penicillin/ streptomycin, Invitrogen) under an atmosphere of 5% CO₂ and at 37°C and in a humidified chamber. Myogenic differentiation was induced in confluent cultures by changing the growth medium to Dulbecco's modified Eagle's differentiation medium supplemented with only 2% horse serum and antibiotics (penicillin/streptomycin, Invitrogen). Differentiation was allowed over 4 days.

2.2 ISOLATION OF RESERVE CELLS (RC)

Near confluent proliferating myoblasts were incubated in differentiation medium in absence or presence of one single dose of 20 nM arsenite. Differentiation medium was not changed throughout the 4 days of differentiation process. At the 4th day of differentiation, C2C12 cultures were isolated into undifferentiated reserve cells from myotubes by mild trypsinization (cat #: 12430-054, ThermoFisher). Briefly, myotubes were specifically detached by mild trypsinization

(Cat#: ICN1689149, MP Biomedicals), 3 min, in Dulbecco's modified Eagle's medium, whereas undifferentiated reserve cells remained adherent to the dish. These cells were then all detached by trypsinization, passed through a 40 μm cell strainer (Corning, Inc. 352340, ThermoFisher) to obtain a uniform single-cell suspension, and re-seeded (10000 cells/ cm^2) onto a new dish in growth medium. After at least 30 min, the growth media including cellular debris including fragments of resting floating myotubes were removed and replaced with a fresh growth media with or without the mitochondrially targeted drug XJB-5-131. The reserve cells were left to proliferate for 3-4 days then harvested for different analyses.

2.3 FLUORESCENCE ASSAY OF REDUCED GLUTATHIONE (GSH), TOTAL PROTEIN THIOLS (TPT), AND LOW MOLECULAR WEIGHT THIOLS (LMWT)

Protein concentration of the cell samples was determined using working reagent (Bio-Rad) with a Bovine Serum Albumin (BSA) standard (0.1mg/ml). A standard curve was established by addition of GSH (0.04-4mM) to 50 mM Na, Na-phosphate buffer, and pH 7.4 containing 10 mM ThioGloTM-1 (Calbiochem), a maleimid reagent that produces a highly fluorescent product upon its reaction with thiol groups. GSH concentrations were determined by addition of GSH peroxidase and cumene hydro peroxide to the brain homogenates with ThioGloTM-1 working solution, and the resultant fluorescence response was subtracted from the LMWT measured by the fluorescence response of the same specimens with only the addition of ThioGloTM-1 (Calbiochem). Levels of total protein sulfhydryls were determined as fluorescence response after adding 4 mM SDS to each LMWT sample. A Fusion alpha plate reader (PerkinElmer) was used to detect fluorescence at excitation and emission wavelengths of 388 and 500 nm, respectively.

2.4 MITOCHONDRIAL STAINING

For assessment of mitochondrial mass cells were stained with 100 nM MitoTracker Deep Red FM (Ex: 644 nm / Em: 665 nm, cat #: M22426, ThermoFisher) for 20 minutes at 37°C in the dark. Cells were then collected by trypsinization, washed with Ca²⁺ and Mg²⁺ free Hank's Balanced Salt Solution (HBSS) (Cat #: 14170112, ThermoFisher), re-suspended in 0.5ml of PBS and analyzed immediately using a Canto flow cytometer to quantify relative fluorescence intensity as measurement of mitochondrial mass.

For measurement of mitochondrial ROS, cells were stained with 250 nM of MitoSOX red (Ex: 488 nm / Em: 575 nm, cat #: M36008, ThermoFisher) for 15 minutes at 37°C in the dark. The cells were then collected by trypsinization and washed with HBSS, fixed in 1.5% paraformaldehyde for 10 min, washed to remove any residual paraformaldehyde, re-suspended in 0.5ml of PBS and flow cytometry was carried out to quantify relative fluorescence intensity as measurement of mitochondrial ROS.

For mitochondrial potential evaluation, cells were seeded and grown at 37 °C and 5% CO₂ in a humidified chamber in a 96 well black culture plate at 50000 cells/well for same day measurement (about 6 hours after plating) or 10000 cells/well 3 to 4 days post-plating rescue experiments with mitochondrially targeted XJB-5-131. Medium was discarded and wells were manually washed using a multichannel pipette and replaced with 200 µl per well of assay medium (140 mM NaCl, 2.5 mM KCl, 1.8 mM CaCl₂, 1 mM MgCl₂ and 20 mM HEPES, pH=7.4, mOsm=300) containing JC-1 (1 µM) and incubated at 37 °C and 5% CO₂ in a humidified chamber for at least 90 minutes. Because JC-1 is a ratiometric assay, it does not require any washout steps when used in plate-based assays. When mitochondria are polarized JC-1 forms aggregates which display strong fluorescent intensity with excitation and emission at

353 nm and 595 nm, respectively. When mitochondria are depolarized JC-1 exists as monomers which show strong fluorescence intensity with excitation and emission at 485 nm and 535 nm, respectively. The ratio of fluorescent intensity of J-aggregates to fluorescent intensity of monomers can be used as an indicator of mitochondrial membrane ($\Delta\Psi_m$) potential. Because JC-1 is ratiometric, it was left in excess in wells with cells during plate-based profiling and traces of $\Delta\Psi_m$ were collected of up to 3 hours.

2.5 FLOW CYTOMETRY WITH CELL SURFACE IMMUNOFLUORESCENCE STAINING

Cytofluorimetric analysis was performed on reserves cells and progeny using antibodies to Alexa Fluor® 647 Rat anti-Mouse CD34 at 1:100 (cat #: 560233, BD Biosciences) and Alexa Fluor® 647 Rat anti-Mouse CD133 at 1:100 (cat #: 315-2C11, Biolegend) individually. Cells were then collected by trypsinization, washed with free HBSS (Cat #: 14170112, ThermoFisher), re-suspended in 0.5ml of HBSS and incubated in the dark at room temperature for 15 min. Cells were then pelleted, washed and re-suspended in 0.5ml of HBSS, fixed in 1.5% paraformaldehyde for 10 min, washed with PBS then PBS plus 0.5% BSA (PBB) to remove any residual paraformaldehyde and re-suspended in 0.5ml of PBS. Flow cytometry analysis was carried out to quantify relative fluorescence intensity as measurement of CD34 and CD133 abundance.

2.6 IMMUNOFLUORESCENCE STAINING FOR CONFOCAL MICROSCOPIC IMAGING

Cells were grown on coverslips in 24 well-plate washed three times with HBSS, fixed with 2% paraformaldehyde for 10 minutes at room temperature, and permeabilized with 0.1% Triton X-100 made in PBS solution for 15 min. The cell monolayer was then washed with PBS. A second round of washing was done using PBS plus 0.5% BSA (PBB). Cells were then blocked with 2% BSA for 45 minutes, washed with PBB and incubated with rabbit-anti Histone H2A.Z at 1:100 (Cat #: 2718S, Cell Signaling) and rabbit-anti EZH2 at 1:100 (Cat #: AC22, Cell Signaling) overnight. The cell monolayers were washed with PBB and incubated with species specific secondary antibodies conjugated to appropriate fluorophores. Cell monolayers were washed with PBB and stained with DAPI for 30 seconds and washed again with PBS. Coverslips were adhered with gelvatol to a slide and stored at 4 C⁰ with minimal exposure to light until scoped. Same protocol was applied to conduct intracellular staining for flow cytometry in Eppendorf tubes except the cells were processed after being trypsinized, washed and suspended in PBS. The following primary antibodies were used; mouse monoclonal Atg12 (C-6) (Cat #: sc-271688, Santa Cruz) at 1:50, mouse monoclonal Atg16 (E-10) (Cat #: sc- 393274, Santa Cruz) at 1:50 and rabbit anti-Beclin1 (Atg6) (Cat #: 500-249, Novus Biologicals) for assessment of autophagy and rabbit anti-Ki67 (Cat #: ab15580, Abcam) to determine the cells proliferation capacity.

2.7 WESTERN IMMUNOBLOTTING

For immunoblot analysis, 15 μ g whole-cell extracts from undifferentiated reserve cells were loaded onto a 4-12% Bis-Tris pre-cast protein gels (ThermoFisher). After electrophoresis, proteins were electro-blotted onto a nitrocellulose membrane (Odyssey, Licor) and blocked with Blocking Buffer (PBS) (Odyssey, Licor) for 1 hour at room temperature. The membranes were then probed with antibodies against rabbit-anti Histone H2A.Z at 1:1000 (Cat #: 2718S, Cell Signaling) and goat-anti Cardiolipin Synthase at 1:1000 (SAB2501839, Sigma-Aldrich) and β -actin at 1:10000 (Cat #: A5441, Sigma-Aldrich) in blocking buffer overnight at 4°C. Fluorescently labeled secondary antibodies IRDye® 680LT Donkey anti-Rabbit IgG (H + L), 0.1 mg IRDye and 800CW Donkey anti-Goat IgG (H + L), 0.1 mg at 1:20000 respectively were incubated for 1 hours at room temperature. After Five washes with PBST for 5 minutes each, antibody binding was visualized with an Odyssey CLx imaging system (Licor). Image Studio 5.2 software was used for quantification of intensities.

2.8 TRANSMISSION ELECTRON MICROSCOPY

Cells grown on tissue culture plastic ware were fixed in 2.5% glutaraldehyde in 100 mM PBS (8 gm/l NaCl, 0.2 gm/l KCl, 1.15 gm/l Na₂HPO₄·7H₂O, 0.2 gm/l KH₂PO₄, pH 7.4) overnight at 4°C. Monolayers were then washed in PBS three times then post-fixed in aqueous 1% osmium tetroxide, 1% Fe₆CN₃ for 1 hr. Cells were washed three times in PBS then dehydrated through a 30-100% ethanol series then several changes of Polybed 812 embedding resin (Polysciences, Warrington, PA). Cultures were embedded in by inverting Polybed 812-filled BEEM capsules on

top of the cells. Blocks were cured overnight at 37°C, and then cured for two days at 65°C. Monolayers were pulled off the coverslips and re-embedded for cross section. Ultrathin cross sections (60 nm) of the cells were obtained on a Riechart Ultracut E microtome, post-stained in 4% uranyl acetate for 10 min and 1% lead citrate for 7 min. Sections were imaged using a JEM 1011 TEM (JEOL, Peabody, MA) at 80kV. Images were taken using a side-mount AMT 2k digital camera (Advanced Microscopy Techniques, Danvers, MA).

2.9 TRANSMISSION ELECTRON MICROSCOPY

Cells grown on tissue culture plastic ware were fixed in 2.5% gluteraldehyde in 100 mM PBS (8 gm/l NaCl, 0.2 gm/l KCl, 1.15 gm/l Na₂HPO₄·7H₂O, 0.2 gm/l KH₂PO₄, pH 7.4) overnight at 4°C. Monolayers were then washed in PBS three times then post-fixed in aqueous 1% osmium tetroxide, 1% Fe₆CN₃ for 1 hr. Cells were washed three times in PBS then dehydrated through a 30-100% ethanol series then several changes of Polybed 812 embedding resin (Polysciences, Warrington, PA). Cultures were embedded in by inverting Polybed 812-filled BEEM capsules on top of the cells. Blocks were cured overnight at 37°C, and then cured for two days at 65°C. Monolayers were pulled off the coverslips and re-embedded for cross section. Ultrathin cross sections (60 nm) of the cells were obtained on a Riechart Ultracut E microtome, post-stained in 4% uranyl acetate for 10 min and 1% lead citrate for 7 min. Sections were imaged using a JEM 1011 TEM (JEOL, Peabody, MA) at 80kV. Images were taken using a side-mount AMT 2k digital camera (Advanced Microscopy Techniques, Danvers, MA).

2.10 ANIMAL EXPOSURE

Five to 6 week old male wild type C57BL/6NTac (Taconic Farms, Hudson NY) mice were exposed for five weeks to drinking water containing 0 or 100 µg/L trivalent arsenite. All studies were approved by the Institutional Animal Care and Use Committee of the University of Pittsburgh. Arsenite was used in these studies as it is the most relevant toxic inorganic arsenic species. Further, these levels are within the range of exposures found in large epidemiological studies of arsenic effects on motor function demonstrating motor deficits in children. Fresh arsenite-containing water or culture media is provided every 2-3 days mice or cultured cells to insure that there is little arsenite oxidation to arsenate.

2.11 WHOLE MUSCLE GENE TRANSCRIPTS

RNA was extracted with Trizol (Invitrogen) from the tibialis anterior muscles of animals exposed to 0 or 100ppb As(III) drinking water for five weeks (n=8 each group), and analyzed for transcript levels by quantitative RT-PCR, essentially as described (26). Gene transcripts were quantified using standard curves for the respective cDNA products and changes in resulting inducible cDNA levels were normalized to changes in the housekeeping transcript Rpl41 levels to calculate the pg of normalized product per ml of reaction. Specific primer pairs include DNMT3a (Forward:5' 3': Reverse:5' 3'), and Rpl41 (Forward:5'AAGATGAGGCAGAGGTCCAA3': Reverse:5'GGTTGTAAGAAAGGCGGTCA3').

2.12 C2C12 GENE TRANSCRIPTS AND CHIP ANALYSIS

RNA isolated from C2C12 cells using the AllPrep DNA/RNA/miRNA Universal Kit (Qiagen, Germantown, MD) was treated with DNaseI and reverse transcribed using iScript™ gDNA Clear cDNA Synthesis Kit (BIO-RAD, Hercules, CA). The mRNA levels of the *Dnmt1* and *Dnmt3a* genes were quantified by SYBR Green-based real-time PCR (qPCR) using SsoAdvanced™ Universal SYBR® Green Supermix (BIO-RAD, Hercules, CA). Transcript levels of *Dnmt1* and *Dnmt3a* were normalized to the expression level of *Rpl44*, and the fold changes of *Dnmt1* or *Dnmt3a* relative to universal mouse reference RNA was calculated using $2^{-\Delta\Delta C_t}$ method. Each sample was measured in duplicates. Primers sequence: *Rpl44* (Forward: 5'-AGATGAGGCAGAGGTCCAA-3' and Reverse: 5'-GTTGTAAGAAAGGCGGTCA-3'); *Dnmt1* (Forward: 5'-GTCGGACAGTGACACCCTTT -3' and Reverse: 5'-TTTAGTGGGGCCCTTCGTG -3') and *Dnmt3a* (Forward: 5'-GGGCCACACGGCAGAG-3' and Reverse 5'-TGCCGTGGTCTTTGTAAGCA-3').

For ChIP analysis, C2C12 cells were fixed with 1% formaldehyde for 15 minutes followed by quenching with 125mM glycine solution. Crosslinked cells were pelleted and washed with PBS containing protease inhibitor cocktail. Chromatin isolation and immunoprecipitation was performed using ChIP-IT kit (Active Motif, Carlsbad, CA), following the manufacturer's instructions. One to two μ g of ChIP-validated antibodies against RNA Polymerase II (A2032, Epigentek, Farmingdale, NY), DNMT1 (A1001, Epigentek, Farmingdale, NY), DNMT3A (39206, Active Motif, Carlsbad, CA), H3K9M2 (ab1220, Abcam, Cambridge, MA), H3K27M3 (ab6002, Abcam, Cambridge, MA), H2A.Zac (ab18262, Abcam, Cambridge, MA), EZH2 (39876, Active Motif, Carlsbad, CA) or nonspecific negative control mouse IgG (Active Motif, Carlsbad, CA) were used for immunoprecipitation of each sample. Non-

immunoprecipitated chromatin was used as input. Following reverse cross-linking and elution of chromatin, DNA from each sample was purified with QIAquick PCR purification kit (Qiagen, Germantown, MD). Purified DNA sample concentrations were quantified by Qubit[®] DNA HS assay kit (Thermo Fisher Scientific, Waltham, MA). Ten ng of purified DNA was used for PCR of *Dnmt1* or *Dnmt3a* promoters. The primers were designed for *Dnmt1* and *Dnmt3a* promoter regions: *Dnmt1* (Forward: 5'- ATGGTCTTCCCCCACTCTCT -3' and Reverse: 5'- TGCAGACGACAGAACAGCTC -3') and *Dnmt3a* (Forward: 5'- ACTGAGGGAGCCAGGTCTAGT -3' and Reverse: 5'- TGTCCAAAAAGAGTTGGATGC -3'). The percent of immunoprecipitated DNA relative to the input was calculated.

2.13 CASPASE3/7 ACTIVITY

Apoptosis Wash Buffer was diluted 1:10 with diH₂O. FLICA was Reconstituted with 50 μ L DMSO then diluted 1:5 by adding 200 μ L PBS. The diluted FLICA to each sample at 1:30 (e.g., add 10 μ L to 290 μ L of cultured cells), incubated approximately 1 hour then washed and span cells three times. Analyze with a by FACS. FAM-FLICA excites at 492 nm and emits at 520 nm.

2.14 STATISTICAL ANALYSIS (GAUSSIAN)

Data in bar graphs are expressed as mean \pm SEM. Significance between groups was determined by student's t-tests or one-way ANOVA followed by Tukey's test for multiple comparisons. A

priori, differences were considered to be significantly different at $p < 0.05$. Statistical analysis was performed using Graphpad Prizm v5 software.

3.0 MITOCHONDRIAL OPTIMIZATION OF INHERITABLE CELL MEMORY

3.1 ABSTRACT

Genetically homogenous stem cell populations exhibit a remarkable phenotypic heterogeneity and divergence of cell fates even when grown in a uniform environment. One determinant of this cell-autonomous heterogeneous behavior is cellular memory. The latter is the outcome of a complex interplay of transcription factors, DNA methylation and histone modifications. Despite the contingency of all these processes on global outputs derived from mitochondria, the mitochondrial role in maintenance of cellular memory remains poorly understood. To delineate how mitochondria influence cellular memory and identity-actuating outputs, we transiently exposed myogenic progenitor cells to arsenic to induce a cellular memory of stress. Memory-bearing cells progeny resolved to a poised cellular state characterized by an increased mitochondrial membrane potential, fusion, and mass, as well as distinct distributions of epigenetic modifiers and nuclear morphometrics at the cell population level. Mechanistically, the poised cellular state was maintained by a balance of acetylated H2A.Z-rich bivalent chromatin marks and heightened RNA polymerase II transcriptional activity. Importantly, a multifaceted normalization of mitochondrial function with a mitochondrially targeted electron scavenger, XJB-5-131, led to dynamic reorganization of bivalent chromatin domains and attenuation of RNA polymerase II activity, reset the inherited cellular memory and thus reestablished the memory-bearing cell progeny identity and heterogeneity. Altogether, this work demonstrated that

mitochondria are the locus of retrievable cell-autonomous outputs that sustain cellular memory and resilience to environmental changes. Moreover, these studies revealed that cellular memory is a mitochondrially optimized statistical property that is quantized by the heterogeneity of the cell population.

3.2 INTRODUCTION

The integrity of tissue homeostasis depends on a lifelong provision of stem cells to substitute differentiated cells without exhausting the reserve pool. Such dynamics imply an intrinsic functional heterogeneity in stem cell populations that optimizes their differential response to a complex and diverse array of extrinsic factors. The integration of these cell autonomous and non-autonomous cues confer either metastable or definitive states to self-renewing cells or their differentiating progeny, respectively (Almada & Wagers, 2016; Blau, Cosgrove, & Ho, 2015; A. S. Brack & Rando, 2007; Dumont, Wang, & Rudnicki, 2015). The differentiation of proliferating myoblasts induced in culture by serum deprivation results in a heterogeneous cell population of post-mitotic multinucleated myotubes, an incipient form of muscle fibers, and mono-nucleated myoblasts that refract differentiation, i.e. myogenic reserve cells (RC) (N. Yoshida, S. Yoshida, K. Koishi, K. Masuda, & Y. Nabeshima, 1998). The latter exhibit expression patterns of cell state markers and behavioral properties reminiscent of the muscle precursor satellite cells in vivo, including the capacity to sustain quiescence, transition into an activated state, maintain a proliferative state, differentiate, and self-renew (Rapizzi, Donati, Cencetti, Nincheri, & Bruni, 2008). These collective dynamics can be iteratively recapitulated by the RC, thereby propagating the original heterogeneous cell population (N. Yoshida et al.,

1998). Cellular memory is a crucial regulatory mechanism underpinning this process (Vionnie et al., 2016). Either permitting return to the ground cell state or perpetuating an acquired state as epigenetic marking can suppress or activate specific chromatin states and select gene expression configurations (Rui et al., 2015). Significantly, mitochondrial functionality and dynamics impinge on several aspects of nuclear gene expression, and on stemness (Chandel, 2015; das Neves et al., 2010; Guantes et al., 2015; I. G. Johnston et al., 2012; A. Kasahara & Scorrano, 2014; Salminen, Kaarniranta, Hiltunen, & Kauppinen, 2014; D. Smiraglia, Kulawiec, Bistulfi, Ghoshal, & Singh, 2008), and, thus, may play a role in bolstering or resetting memory responses during cell state transitions. Delineating cause and effect in the mitonuclear communications that define cellular memory is of utmost importance in understanding cell fate decision-making and devising novel regenerative therapeutic strategies.

We previously reported that skeletal muscle progenitor cells from a mouse model of subchronic exposure to the metallotoxicant, arsenic, exhibited persistently increased levels of mitochondrial activity and autophagy long after their isolation and expansion in culture in the absence of arsenic (Ambrosio et al., 2014). Here, we report a simple culture model to construct a cellular memory in RC by exposure to arsenic. Using this model, we determined the extent of the mitochondrial contribution in imprinting the memory of stress, and demonstrated that mitochondrial functionality optimizes the expression of crucial modulators of epigenetic memory, including nuclear morphometrics. This implies mitonuclear coordination in safeguarding cellular identity. Using a mitochondrially-targeted, electron scavenger, we performed non-Gaussian statistical modeling and chromatin immunoprecipitation (ChIP) assay of modified histones and DNA, as well as histone-modifying enzymes. Our work reveals that mitochondria causally account for the epigenetic memory and underlying cell population

dynamics, and underscore the need for a more comprehensive understanding of the interplay between intrinsic and extrinsic factors that define cell plasticity and cell population heterogeneity.

3.3 RESULTS

3.3.1 Constructing a memory of stress response

We reasoned that the resilience of myogenic RC (N. Yoshida et al., 1998) vis-à-vis the instructive differentiation medium likely involves an active cellular memory (L. Wang et al., 2009). To imprint a memory of stress into RC memory, we exposed differentiating C2C12 myoblasts to the mitochondrial stressor and epigenetic modifier (Bailey & Fry, 2014; Rainbolt, Atanassova, Genreux, & Wiseman, 2013), inorganic arsenic. After 4 days of differentiation with (Control RC; cRC) or without 20 nM arsenic (As(III)-exposed RC; eRC), cultures were evaluated for myotube formation and retention of undifferentiated mononuclear RC (figure 1). For future experiments where the RC were separated from myotubes and replated in cultured in arsenic-free growth medium, the control RC progeny are referred to as naïve RC and the arsenic exposed RC progeny are referred to as primed or poised RC.

Cellular redox state, indicated by levels of low-molecular-weight thiols (LMWTs), reduced glutathione, and protein sulfhydryl groups (measured using ThioGlo®1) was measured to establish that the exposed RC retain a stress response. As we previously reported in vascular cells (Barchowsky et al., 1996), arsenic exposure elicited a significant antioxidant response that increased intracellular reduced thiol content (Fig. 2, $P \leq 0.001$).

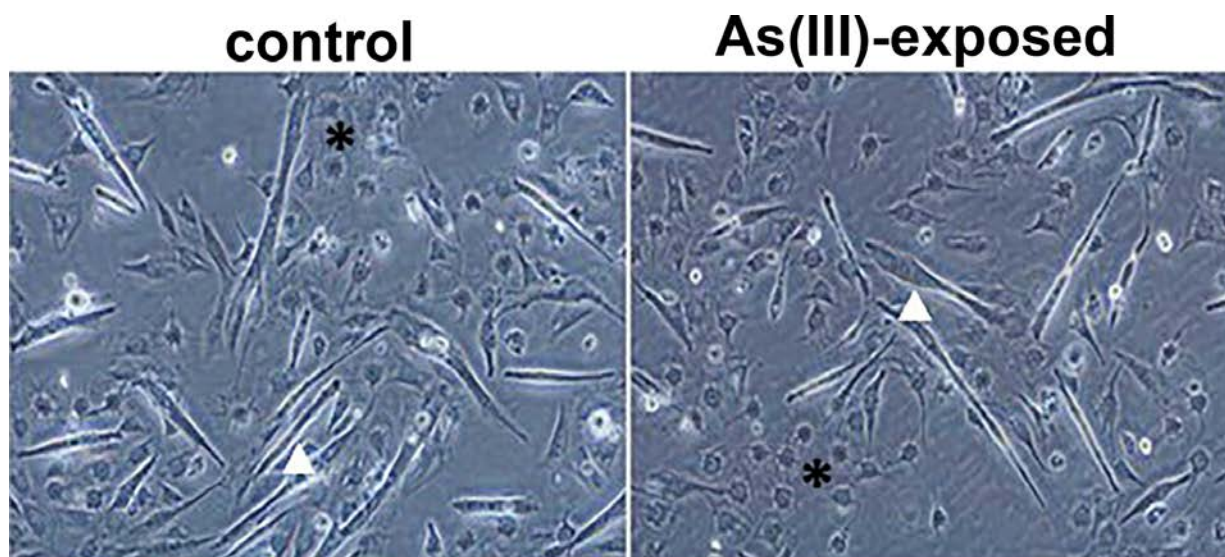


Figure 1. Representative images of myogenic differentiation of C2C12 myogenic cells
 C2C12 cells were cultured in low serum differentiation medium for four days in the absence or presence of 20 nM arsenite (As(III)). The resulting heterogeneous culture contained fused multinucleated myotubes (triangle) and mononucleated reserve cells in an undifferentiated state (stars).

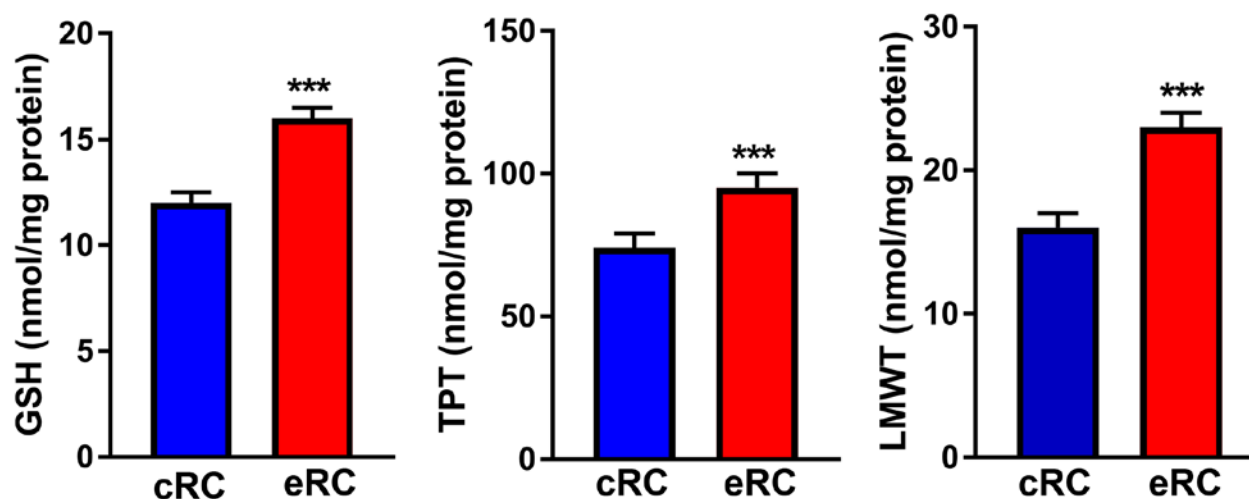


Figure 2. Assessment of RC redox status
 Levels of glutathione [GSH], total protein thiols (TPT), and low-molecular-weight thiols (LMWT), in As(III)-exposed RC (eRC), relative to control RC (cRC). Representative results of 3 separate experiments.

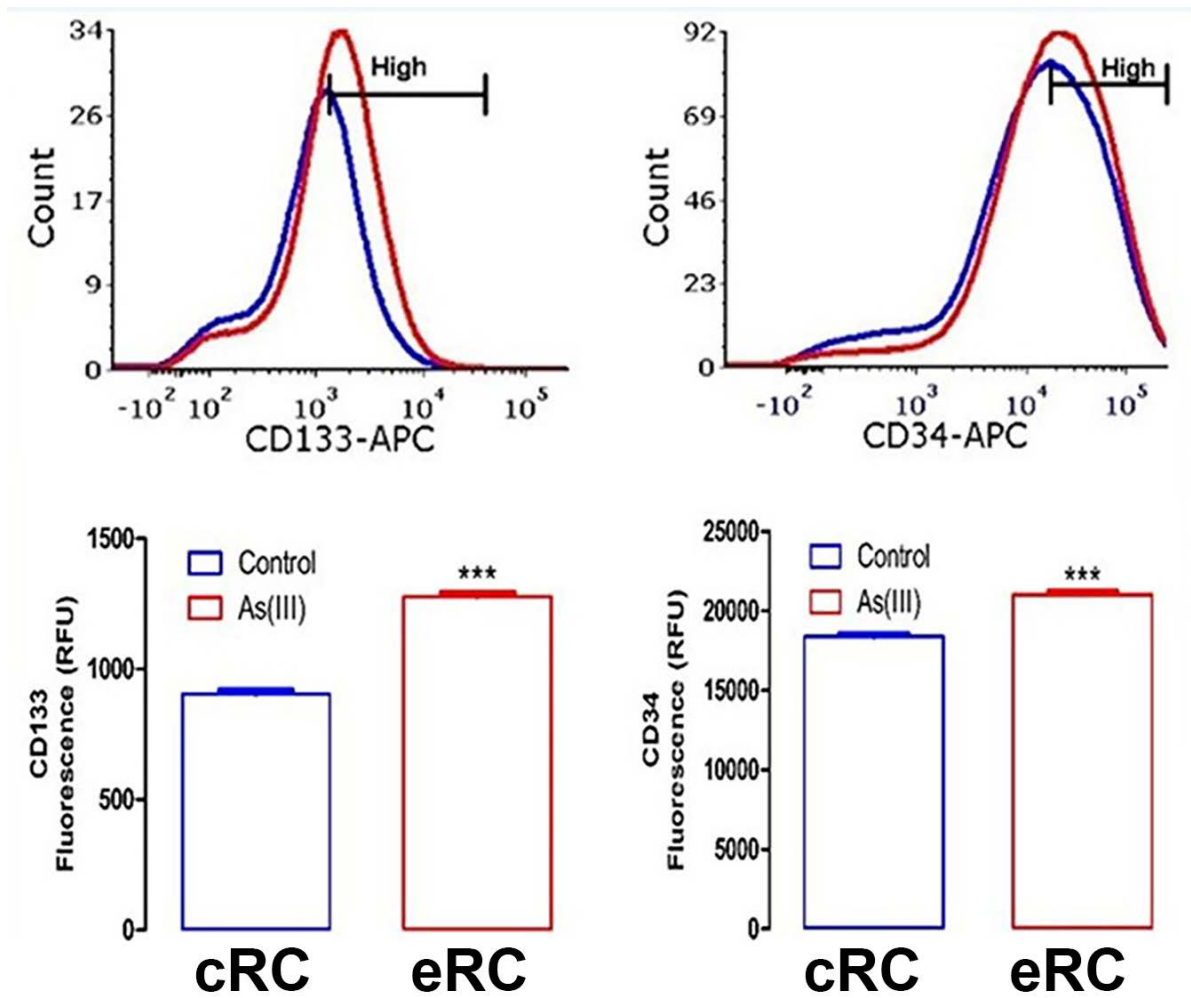


Figure 3. Phenotypic characterization of RC

Flow cytometric analysis showed an increase in the self-renewal markers CD34 and CD133. Representative results of 3 separate experiments.

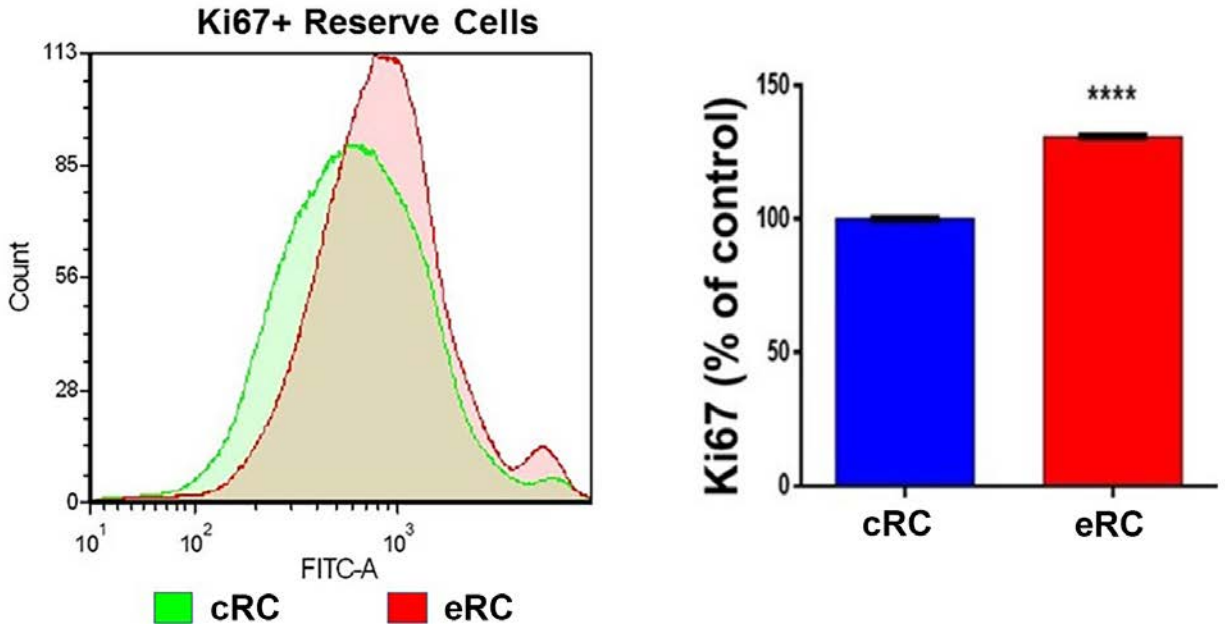


Figure 4. Assessment of proliferative potential by flow cytometry with the cell cycle marker Ki67

Representative results of 3 separate experiments.

Having confirmed the occurrence of an adaptive stress response, we next examined expression levels of the myogenic stem cell self-renewal markers, CD34 and CD133 (Kitzmann et al., 2006; Negroni et al., 2009). eRC had stem cell markers that were $13.39 \pm 0.84\%$ and $39.72 \pm 3.6\%$ higher than cRC, including an increase in the CD34^{High} and CD133^{High} subpopulations of $15.93 \pm 0.46\%$ and $81.33 \pm 7.57\%$, respectively (Figure 3, $n=3$, $P \leq 0.01$). This suggested that eRC were more prone to proliferation and less committed to differentiation (Kitzmann et al., 2006; Negroni et al., 2009). Indeed, analysis of the Ki67 antigen revealed a heightened cycling capacity in the eRC ($+79.7\%$, $n=3$, $P \leq 0.01$; Fig.4).

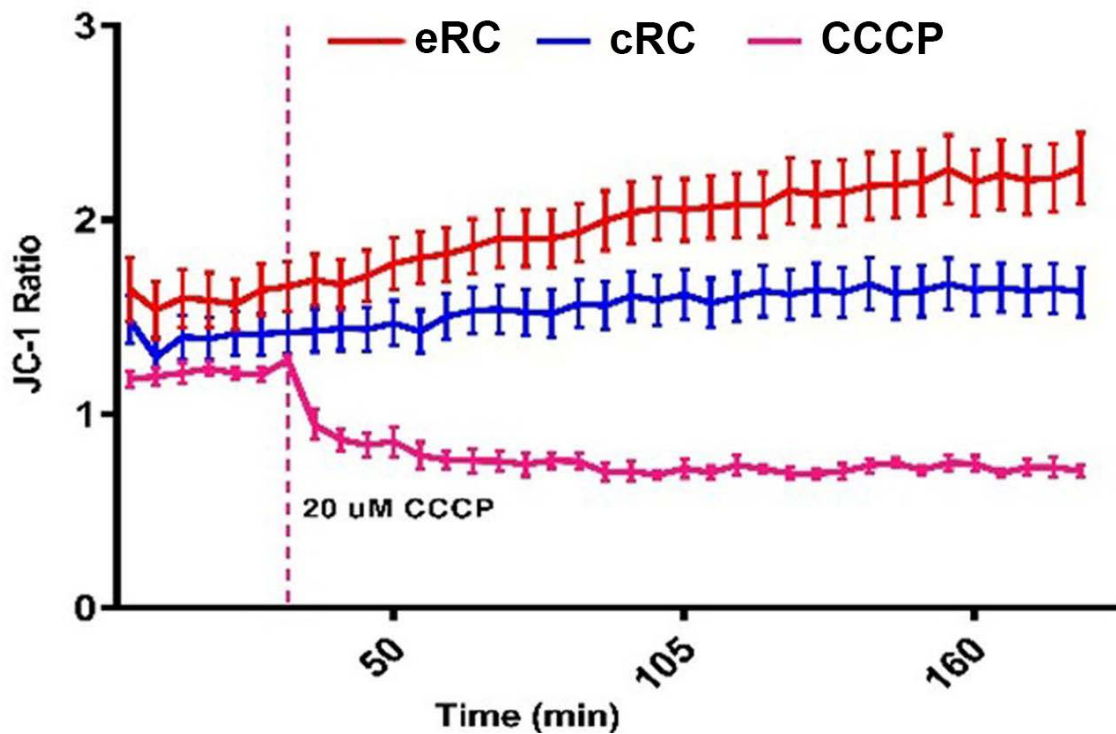


Figure 5. Assessment of mitochondrial membrane potential by microplate assay measuring the accumulation of membrane-permeant potentiometric dye JC-1
Representative results of 4 separate experiments.

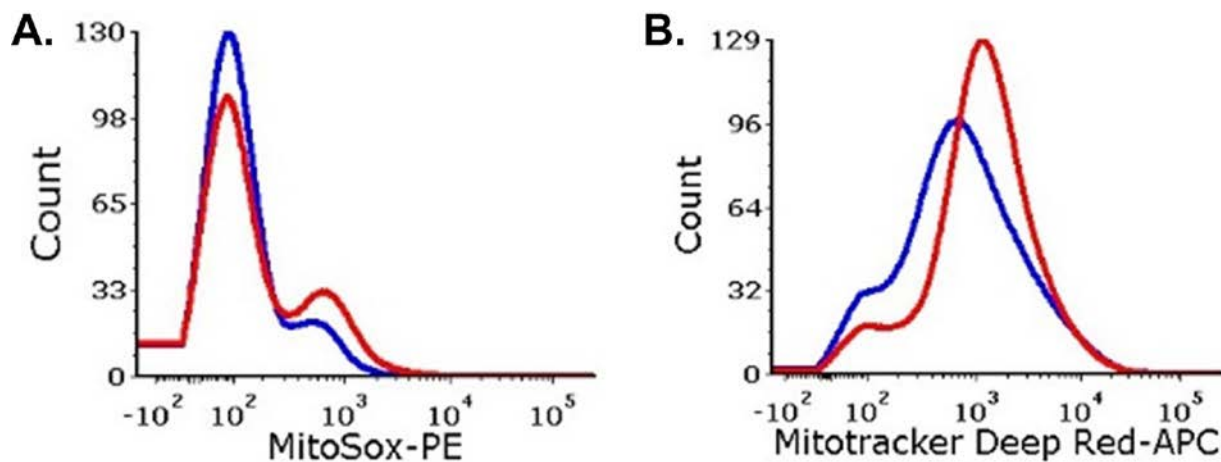


Figure 6. Assessment of mitochondrial ROS and mass

A. mitochondrial ROS generation was measured cell by flow cytometric analysis of the fluorescent intensity of the mitochondrial superoxide indicator, MitoSOX. Representative results of 2 separate experiments. B. Flow cytometric analysis of mitochondrial mass with fluorescent mitotracker deep red .cRC (blue) and eRC (red) .Representative results of 3 separate experiments.

As with previous reports (Song et al., 2015), we observed that upregulation of CD133 expression was linked to increased mitochondrial membrane potential, as measured with the ratiometric probe JC1 ($+39.28 \pm 11.19\%$, $n=4$, $P \leq 0.001$, Figure 5). Mitochondrial superoxide generation, measured by fluorescence of MitoSox Red dye, was also elevated ($+78.07 \pm 16.17\%$, $n=2$, $P \leq 0.001$, Figure 6A), consistent with the increase in membrane potential and the adaptive stress response. Mitochondrial mass, measured by flow cytometry using MitoTracker Deep Red (MTDR) dye, was increased by $23.17 \pm 8.35\%$, as well ($n=3$, $P \leq 0.001$, Figure 6B). Since MTDR can produce false positive results due to membrane potential sensitivity, western analysis of the expression level of the inner mitochondrial membrane protein, cardiolipin synthase, was used to confirm the mass increase ($+54.84\%$, $n=3$, $P \leq 0.01$; Figure 7).

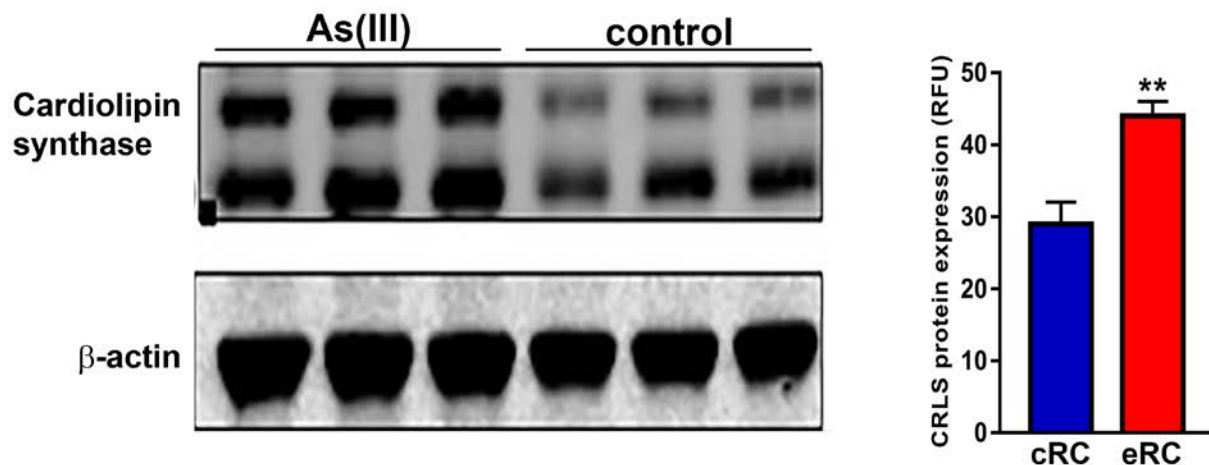


Figure 7. Increased expression of the inner mitochondrial membrane protein cardiophilin synthase (CRLS) in pRC

Data in bar graphs are mean + SEM relative fluorescent units of specific protein immunofluorescence normalized to b-actin and significance difference ($p < 0.01$, Student's t test, $n = 3$ separate experiments).

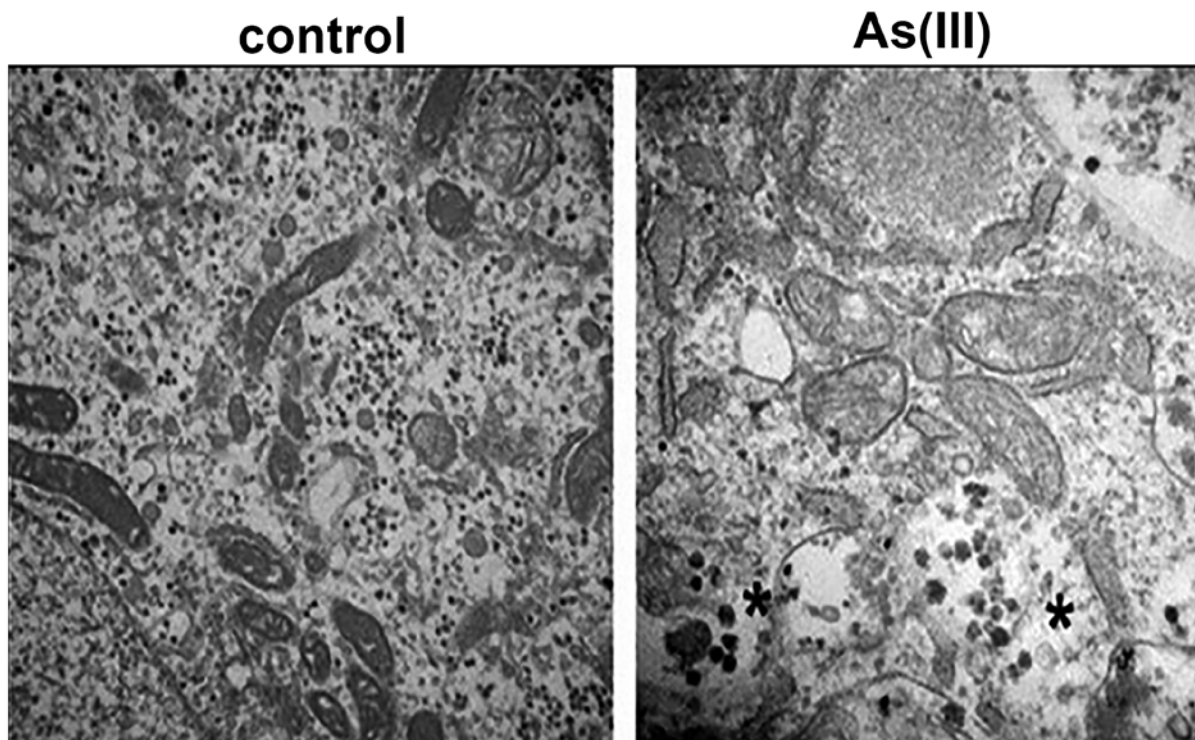


Figure 8. Representative transmission electron microscopy of RC

The image shows the remodeling mitochondrial cristae and enhanced autophagy as reflected by the abundance of autophagosomes and autolysosomes in eRC (right panel).

We further examined mitochondrial status by morphological assessment with transmission electron microscopy. Unlike the cRC, mitochondria in eRC were relatively larger with remodeled cristae (Figure 8). We also observed enlarged endoplasmic reticulum (ER), increased numbers of small vesicles and lysosomes, and increased autophagosomes (early/initial autophagic compartments) and autolysosomes (late autophagic compartments). Furthermore, flow cytometry analysis showed increased expression of macroautophagy markers Atg12, Atg16 and Beclin-1 in eRC (Figure 9).

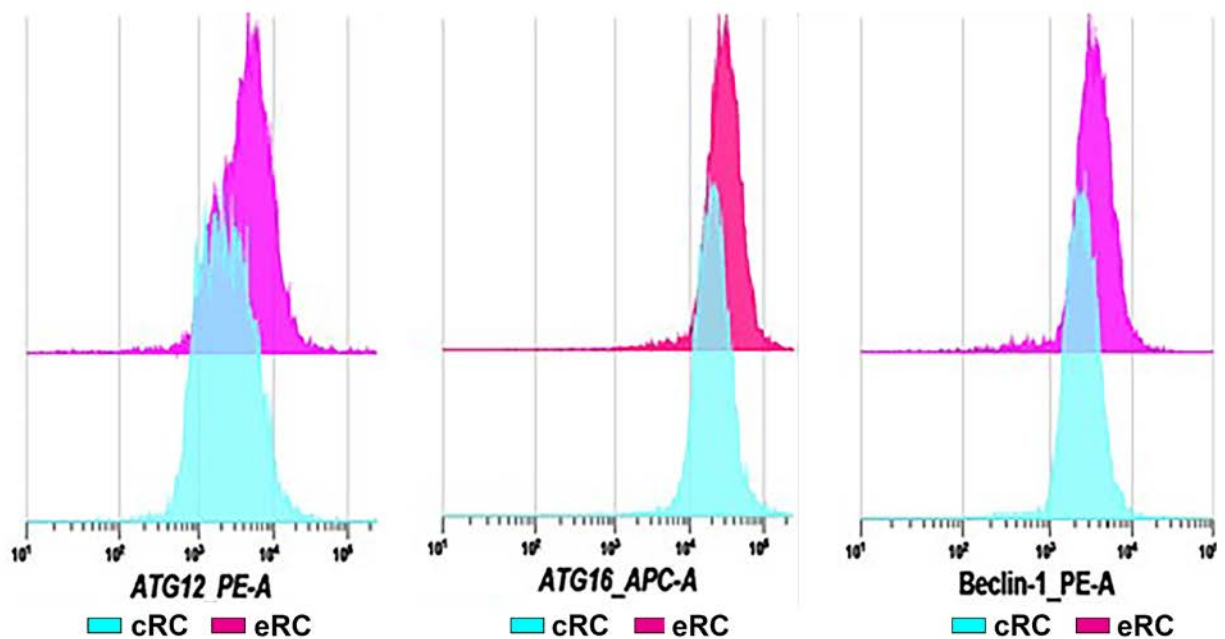


Figure 9. Upregulation of autophagy markers, Atg12, Atg16 and Beclin-1 protein expression measured by flow cytometry

The figures are representative of two separate experiments.

We found that expression of the memory-conferring histone variant, H2A.Z that promotes cell cycling and blocks myogenic differentiation (Brickner et al., 2007; Raisner et al., 2005; Sutcliffe

et al., 2009; H. Zhang, Roberts, & Cairns, 2005), was increased in eRC (+24.22%, n=3, $P \leq 0.01$; Supplementary Fig. 10). Collectively, these results substantiate successful imprinting of an adaptive stress response and memory (Kroemer, Marino, & Levine, 2010; Quiros, Mottis, & Auwerx, 2016) in primed RC.

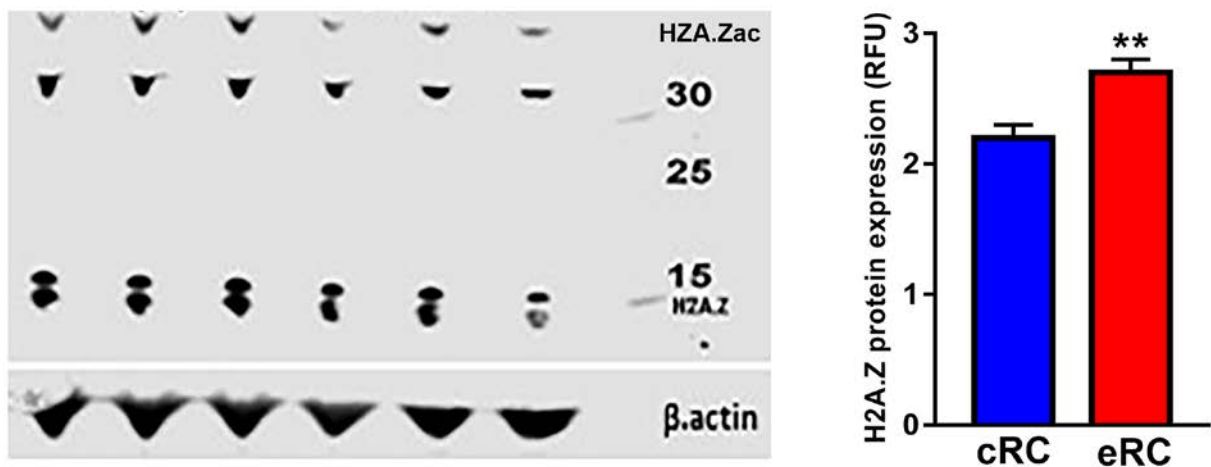


Figure 10. Expression of the bivalent chromatic marker and memory-conferring protein, H2A.Z

Western blot analysis of whole-cell protein lysates from control (cRC) and As(III)-exposed (eRC) RC revealed significant upregulation of memory-conferring histone variant H2A.Z total protein (n=3, $p < 0.01$).

3.3.2 Mitochondria sustain cellular memory for several generations and define RC identity

A correlate of cellular stress-memory is the persistence of stressor-specific alterations long after the transient exposure to the stressor. Thus, we examined whether such a protracted response was captured at the mitochondrial level in our model. We harvested the eRC and cRC after the fourth day of differentiation, thoroughly washed them with cell culture medium, and re-cultured them in arsenic-free growth medium for 3-4 days (i.e. 6-8 generations). To determine the extent of

mitochondrial influence, the isolated cRC and eRC were cultured in the presence or absence of the mitochondrially targeted electron scavenger, XJB-5-131 (Fink et al., 2007; Kagan, Chu, Tyurina, Cheikhi, & Bayir, 2014; Polyzos et al., 2016). Consistent with our previously reported in vivo effects (Ambrosio et al., 2014), as well as in vitro models of synthetic stress memory (Burrill, Inniss, Boyle, & Silver, 2012; Burrill & Silver, 2011), we found that the mitochondria of primed RC progeny (pRC) sustained a higher mitochondrial potential ($+19.51 \pm 1.97$, $n=3$, $P \leq 0.001$; Figure 11a), increased superoxide generation ($+23.55 \pm 2.39$, $n=2$, $P \leq 0.01$; Figure.11b), increased mass ($+95.29 \pm 3.524$, $n=2$, $P \leq 0.01$; Figure.11c), and enhanced oxygen consumption. These acquired attributes due to the transient exposure to arsenite by the pRC ancestors indicated an inherited memory of the original stress generations after the stressor was removed.

Changes in mitochondrial functions are inextricably coordinated to mitochondrial shape transitions. Immunofluorescence staining for the mitochondrial protein Tom20 and quantitative assessment of mitochondrial networks indicated a predominantly interconnected network in pRC (Figure 12A). Strikingly, addition of XJB-5-131 attenuated the mitochondrial overactivity and restored the mitochondrial morphology (Figure 12C) and mass (Figure 12C) compared to nRC.

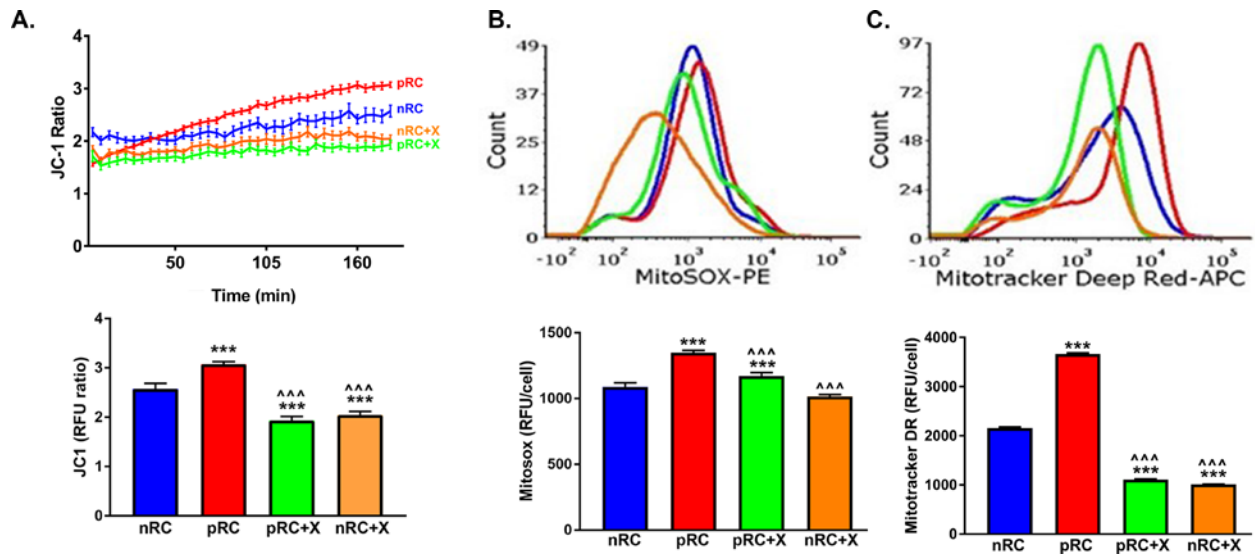


Figure 11. XJB-5-131 restores normal mitochondrial dynamics

A. Mitochondrial membrane potential assessed by the accumulation of JC-1 (n=3 separate experiments). The treatment groups were naive RC progeny (nRC, blue), As(III)-primed RC progeny (pRC, red), and the nRC or pRC cultured with 0.1 μ M XJB-5-131 (nRC+X, orange; pRC+X, green). **B.** Mitochondrial ROS quantified by MitoSOX Red (n=3 separate experiments). **C.** Mitochondrial mass measured with mitotracker deep red (n=3). Results in graphs are presented as mean \pm SEM. Differences from control progeny (nRC) are designated by ***, $p < 0.001$, while differences from arsenic-primed progeny pRC are designated by ^^^, $p < 0.001$.

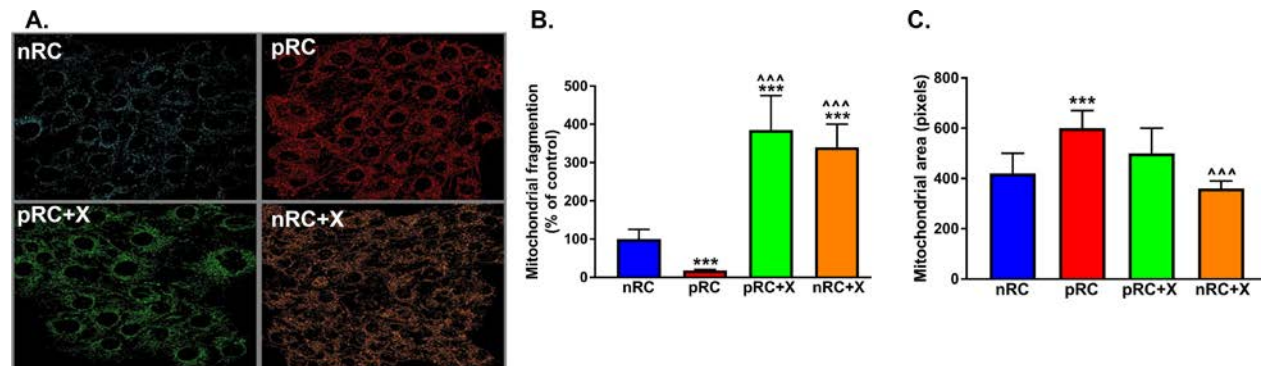


Figure 12. XJB-5-131 restores mitochondrial dynamics to normal RC levels

A. Tom20 immunofluorescence; Representative confocal images of mitochondrial morphology pseudocolored to match treatment group colors. **B.** Measure of mitochondrial networks fragmentation **C.** Measure of the area as a correlate of mitochondrial mass. Results in graphs are presented as mean \pm SEM. Differences from control progeny nRC are designated by ***, $p < 0.001$, while differences from arsenic-primed progeny pRC are designated by ^^^, $p < 0.001$.

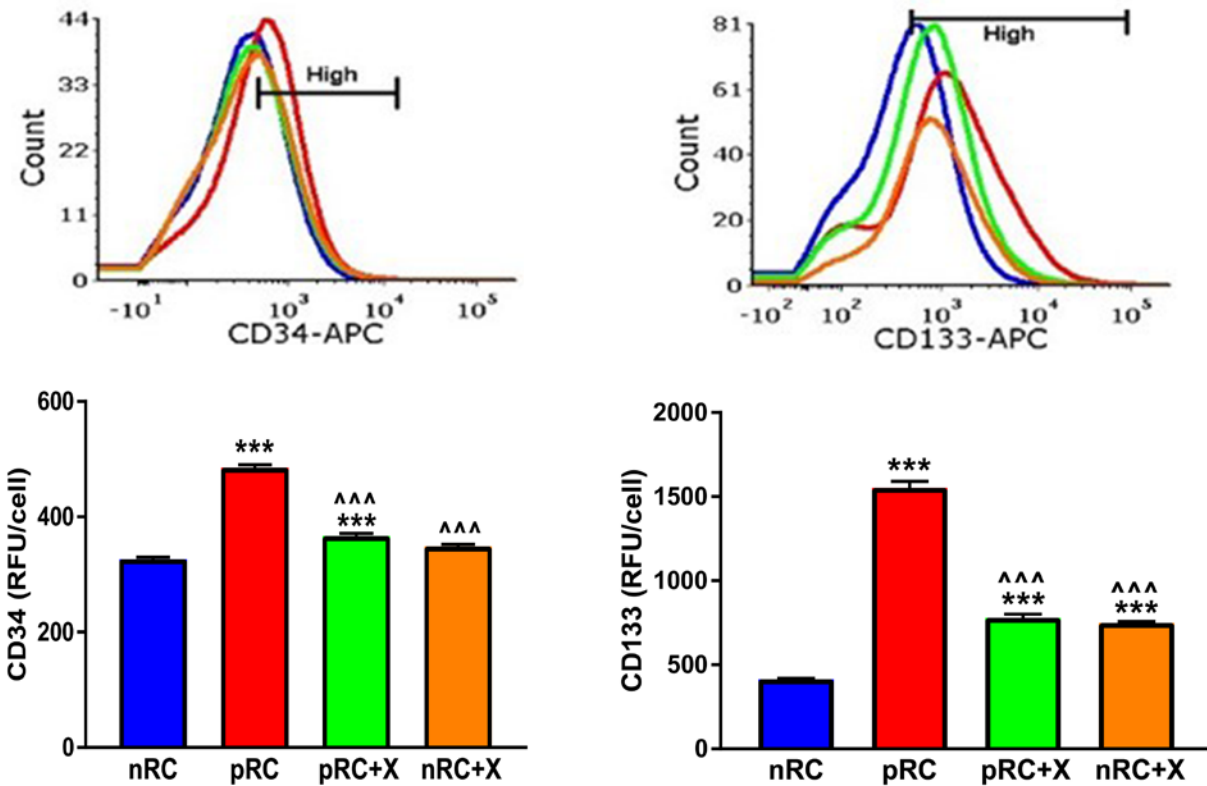


Figure 13. RCs identity is contingent on mitochondrial maintenance of cellular memory

Restoration of mitochondrial function and dynamics with XJB-5-131 significantly restored pRC identity as reflected by the return of stem cell self-renewal markers CD34 and CD133 expression levels, measured by flow cytometry, to those of nRC. Results in graphs are presented as mean \pm SEM. Differences from control nRC are designated by ***, $p < 0.001$, while differences from arsenic-primed RC are designated by ^^, $p < 0.001$, determined using one-way ANOVA with Tukey's post hoc test for multiple comparisons.

Restoring the pRC mitochondrial function and dynamics to nRC levels with XJB-5-131 significantly restored the pRC identity, as reflected by the consequent attenuation of the stem cell self-renewal markers, CD34 and CD133, in pRC to nRC expression levels ($P \leq 0.01$; Figure 13). This suggested erasure of prior exposure history. In contrast to what has been shown in stress models of cellular synthetic memory (Burrill & Silver, 2011), these data provided the first evidence that the inherited overactive mitochondrial state observed in the progeny of the

transiently pRC ancestors is not a collateral transcriptional response. Instead, it has a permissive role in maintaining the operability of static memory and in driving dynamic memory processes. Collectively, these results indicate that priming of mitochondrial function by exposure to transient mild stress results in a poised cellular state, which closely mirrors the “alert” state recently described in muscle stem cells (Rodgers et al., 2014).

Conspicuously, recent studies support the notion that mitochondrial dynamics control stem cell self-renewal (Mireille Khacho et al., 2016). Altogether, these results show that the RC phenotypic state is a manifestation of mitochondrial influence on cellular memory

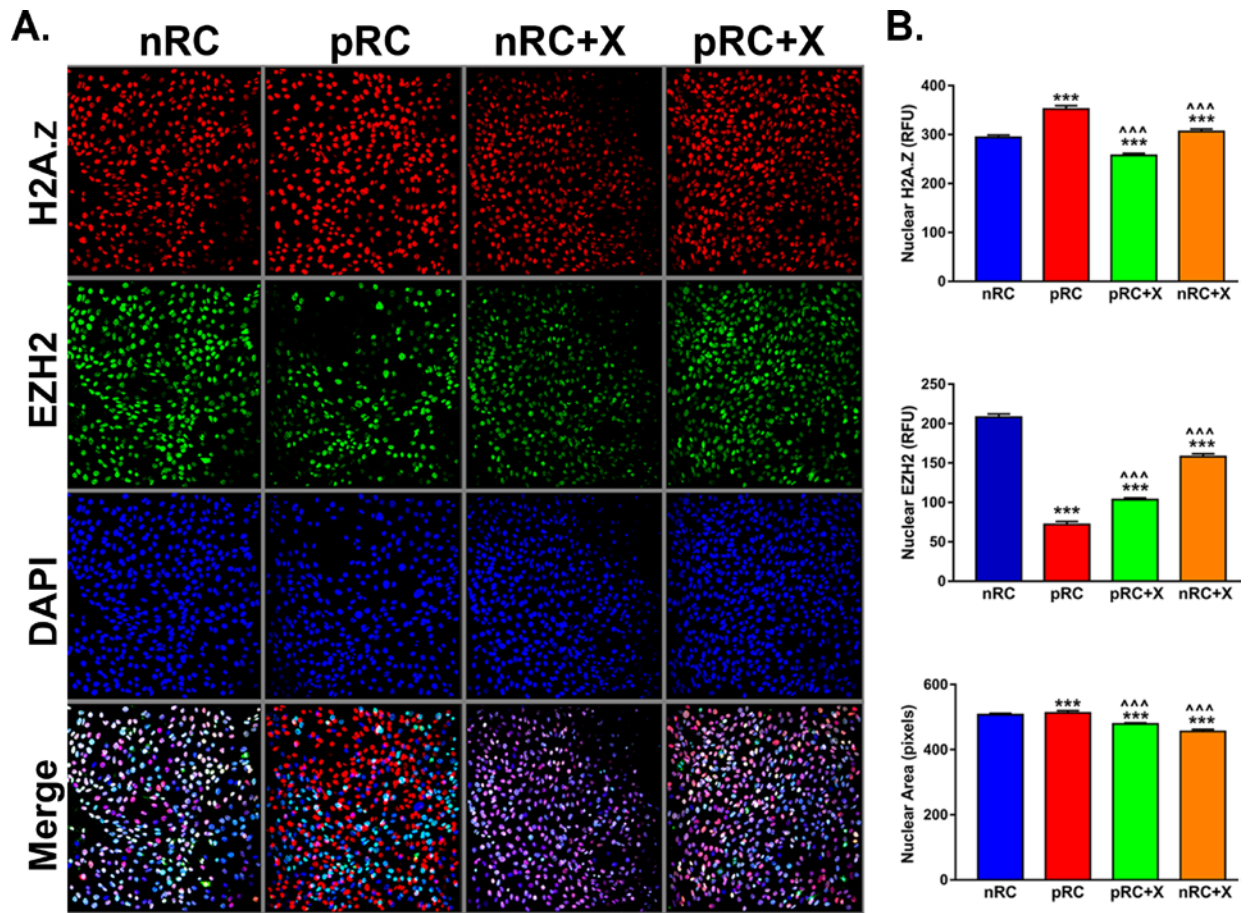


Figure 14. Characterization of RC population heterogeneity and normalization by XJB-5-131

A. Representative confocal microscopic images of naïve RC (nRC), primed RC (pRC), as well as nRC and pRC treated with 0.1 μ M XJB-5-131. Cells were immunostained for H2A.Z (red) and EZH2 (green) and then counterstained with DAPI. **B.** Quantification of H2A.Z and EZH2 immunostaining presented as mean + SEM of nuclei relative fluorescent intensity nuclei from four to five separate experiments. Significant difference from nRC is designated by ***($p < 0.001$) and significant difference from pRC is designated by ^^^($p < 0.001$).

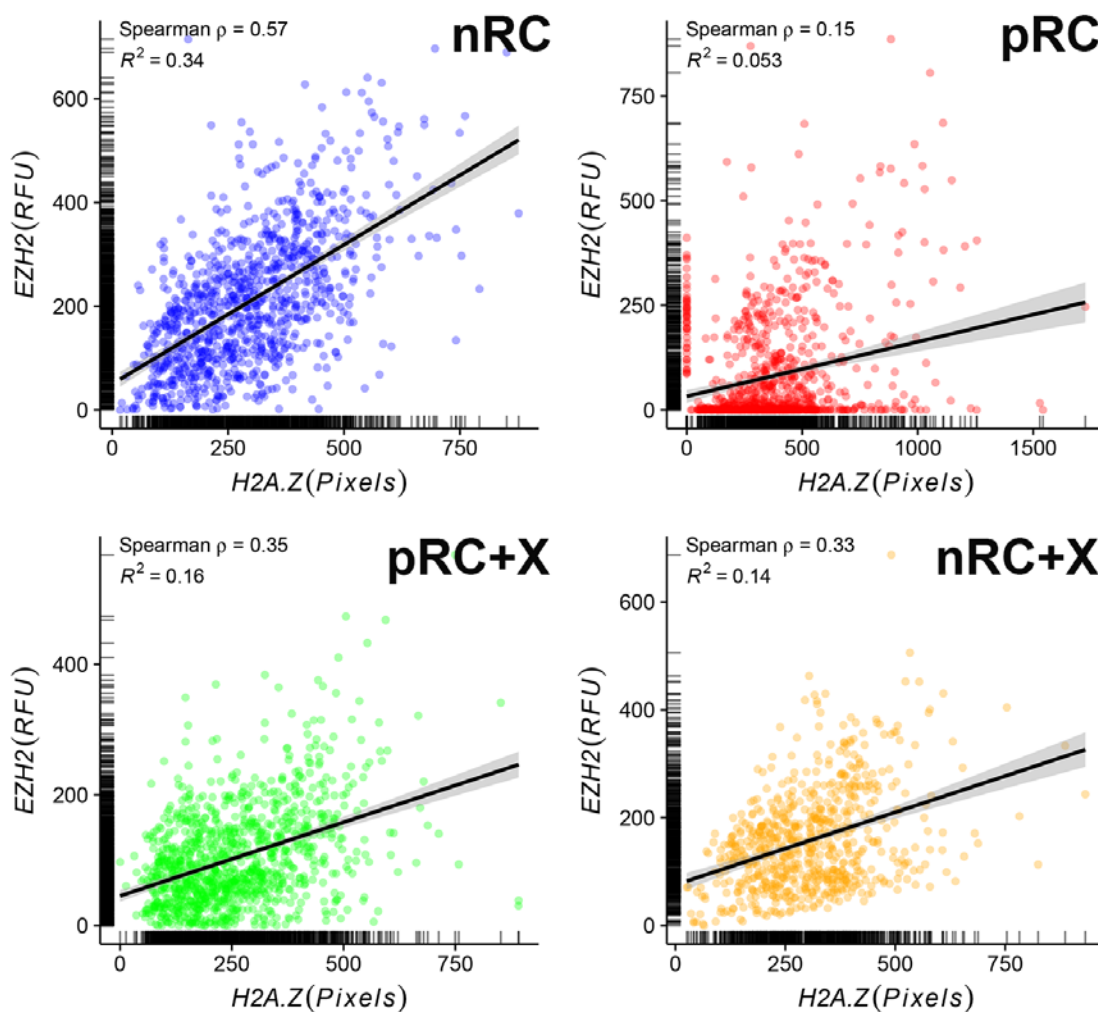


Figure 15. Correlation of RC population heterogeneity and normalization by XJB-5-131

Positive correlation of H2A.Z and EZH2 protein expression with Spearman's correlation coefficient and R^2 .

3.3.3 Cellular memory is contingent on mitochondrial regulation of RC heterogeneity

Next, we examined the mechanism that could mediate such mitochondrial capacity to alter cellular memory and the identity of RC. The highly significant upregulation of histone variant, H2A.Z, in the primed RC (Figure 10) suggested that memory was imprinted by marking active genes and poising silenced genes for reactivation (Kelly et al., 2010; C. M. Weber & S.

Henikoff, 2014). This is a phenomenon that has been functionally (Law & Cheung, 2015) and phenotypically (Abraham, Cui, Tang, & Zhao, 2013; Cui et al., 2009) linked to the blockage of myogenic differentiation and expression of both CD34 and CD133 markers. Equally significant is the expression of EZH2 which, co-localizes with H2A.Z at silenced gene loci (M. P. Creighton et al., 2008; Margueron & Reinberg, 2011), and thus contributes to the transmission of repressive memory. Assessment of nuclear H2A.Z protein expression levels using immunofluorescence microscopy revealed a significant increase in primed RC progeny, compared to naïve RC progeny, (+19.1%, $P \leq 0.001$, $n=5$; Figure 14A & B), and confirmed the persistence of total H2A.Z protein expression pattern in the progeny of stress memory-bearing RC, despite the removal of the stressor and throughout many cellular generations. In contrast, EZH2 protein nuclear expression levels were significantly decreased in pRC (-34.8%, $P \leq 0.001$; Figure 14A & B). Comparing different nuclei across all conditions demonstrated that the primed RC progeny exhibited a distinct H2A.Z / EZH2 co-expression pattern. We therefore assessed the degree of correlation between H2A.Z and EZH2, using the nonparametric rank-based Spearman's correlation coefficient (PEARSON'S, 2011) (Figure 15). This test provides a measure of the monotonic relationship between the two continuous variables and yields more robust estimate of correlation than a linear coefficient such as Pearson's, which can be strongly biased by outliers. Nuclear data were pooled from five separate experiments across the four conditions A high mean correlation coefficient ($\rho=0.57$) was observed when comparing H2A.Z and EZH2 expression levels in the progeny of naïve RC. In contrast, this correlation was considerably lower ($\rho=0.15$) in the primed RC progeny. Importantly, administration XJB-5-131 completely restored H2A.Z protein expression in primed RC to naïve RC levels, reduced the gap in EZH2 expression level between naïve, and primed RC progeny by 15%. Although this reduction was not statistically

significant compared to naïve RC progeny, it corresponded to a net increase of 42% when comparing primed RC to primed RC treated with XJB, indicating an important role for mitochondria in regulating EZH2 expression levels. In similar vein, XJB-5-131 treatment resulted in a twofold amelioration of H2A.Z and EZH2 correlation ($\rho=0.35$). However, there was also a decrease of correlation in XJB-5-131-treated control RC progeny due to a slight increase in mean H2A.Z expression level and a simultaneous decrease of mean EZH2 expression level by +4.22% and -24.09%. In aggregate, these data support the conclusion that modulation of mitochondrial activity and morphology transitions impact epigenetic modifiers of cellular memory. Strikingly, fluorescence microscopy shed light on a large quantitative and qualitative cell-to-cell variation in protein expression and nuclear area (a proxy of cell size) even though the RC progeny were grown under a uniform condition.

Given that cell phenotype is chiefly determined by its protein expression level, it is important to understand how this variability and emergence of stress-memory in the RC population relate to mitochondrial changes. Thus, we first performed a preliminary non-parametric analysis of H2A.Z and EZH2 expression using a kernel density estimator (KSE) (Figure 16). This robust method has the advantage of not assuming any particular functional form and, thus, is based upon minimal assumptions about the underlying model. The KSE plots showed broad and right-skewed distributions of H2A.Z and EZH2 expression, as well as nuclear area, regardless of the experimental condition. However, the primed RC progeny tended to exhibit a behavior akin to heavy-tailed distributions over a greater range of the upper tail.

The tendency for heavy-tailed behavior was graphically corroborated by the normal Q-Q plot (Figure 17). The number of quantiles was selected to match the size of experimental samples data. If the experimental data was normally distributed (i.e. bell-shaped), the points in the plot

should form a straight line. The Kolmogorov-Smirnov Two Sample Test of proteins expression and nuclear area distribution (with the correspondent KS statistic D and p-value) confirmed the beneficial effects of the mitochondrially targeted-drug XJB-5-131. These data suggest that the heterogeneity of RC is the outcome of a constellation of correlated mechanisms (Maheshri & O'Shea, 2007) that integrate at a cellular level of organization, and are not the result of unique molecular or cellular mechanisms. XJB-5-131 intervention had a significant impact on the primed RC progeny proteins and nuclear morphometrics distribution bodies and completely restored their upper tails to naïve-like distributions (Figure 18).

The XJB-5-131 rescue effect was confirmed by the Kolmogorov-Smirnov two-sample test. (Figure 19), the computed special moments, quantiles and extremals (Tables 1-3), and graphically by histogram density plots (Figure 20). Indeed, the beneficial impact of XJB-5-31 became obvious when considering the reduction of the gap in median EZH2 expression, compared to naïve RC, from +1998.24% to 224.251% in primed and XJB-5-131-treated primed RC progenies, respectively (Figure 18).

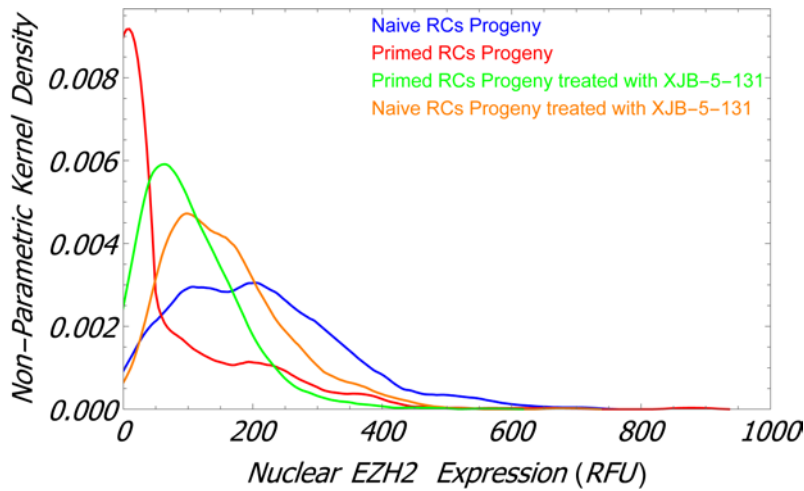
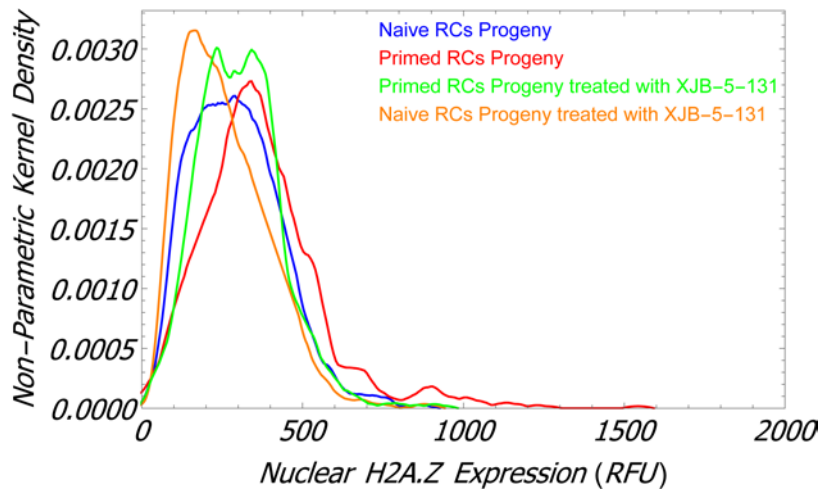
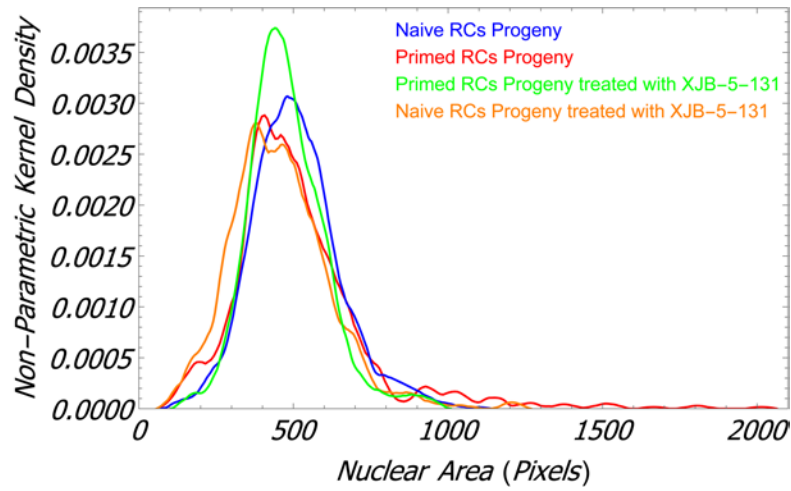


Figure 16. Non-parametric kernel density estimate (NPKDE) based on Silverman approach

Multiple bandwidths were modeled and the representative images were obtained with bandwidth $c=50$.

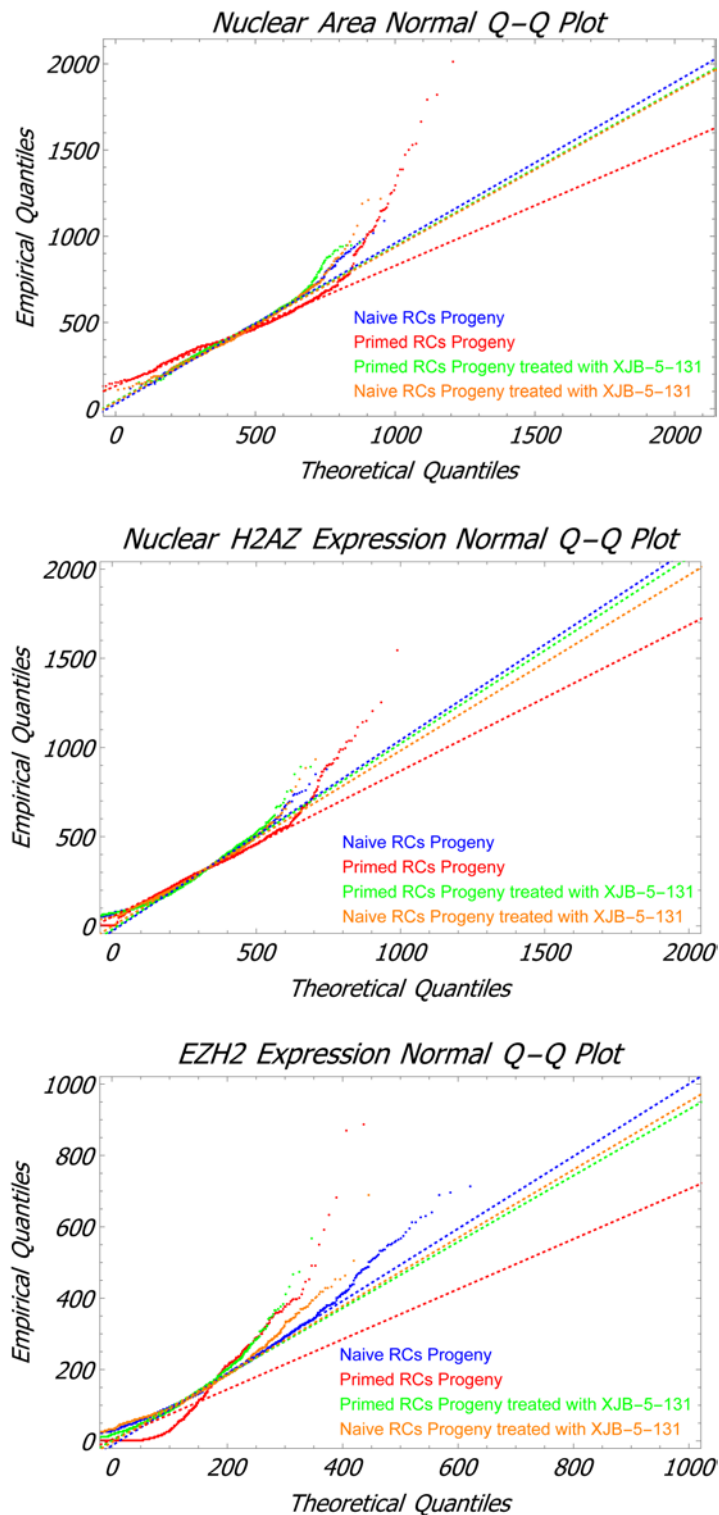


Figure 17. Normal quantile-quantile-plots (QQ-plots)

Comparing the experimental quantiles of protein expression values against the computed quantiles from a theoretical normal distribution of random protein expression values.

Area	1091.75	Area	1823.38
Length	41.8208	Length	60.526
Width	33.8346	Width	38.8961
Circularity	0.756709	Circularity	0.607051
Total{R,G,B}	{876.604, 379.145, 0.}	Total{R,G,B}	{905.831, 19.0431, 0.}
Shape	 nRC	Shape	 pRC

Area	1218.12	Area	958.875
Length	40.6014	Length	46.7094
Width	38.2744	Width	26.6129
Circularity	0.593664	Circularity	0.608194
Total{R,G,B}	{932.31, 243.616, 0.}	Total{R,G,B}	{443.137, 375.682, 0.}
Shape	 nRC+X	Shape	 pRC+X

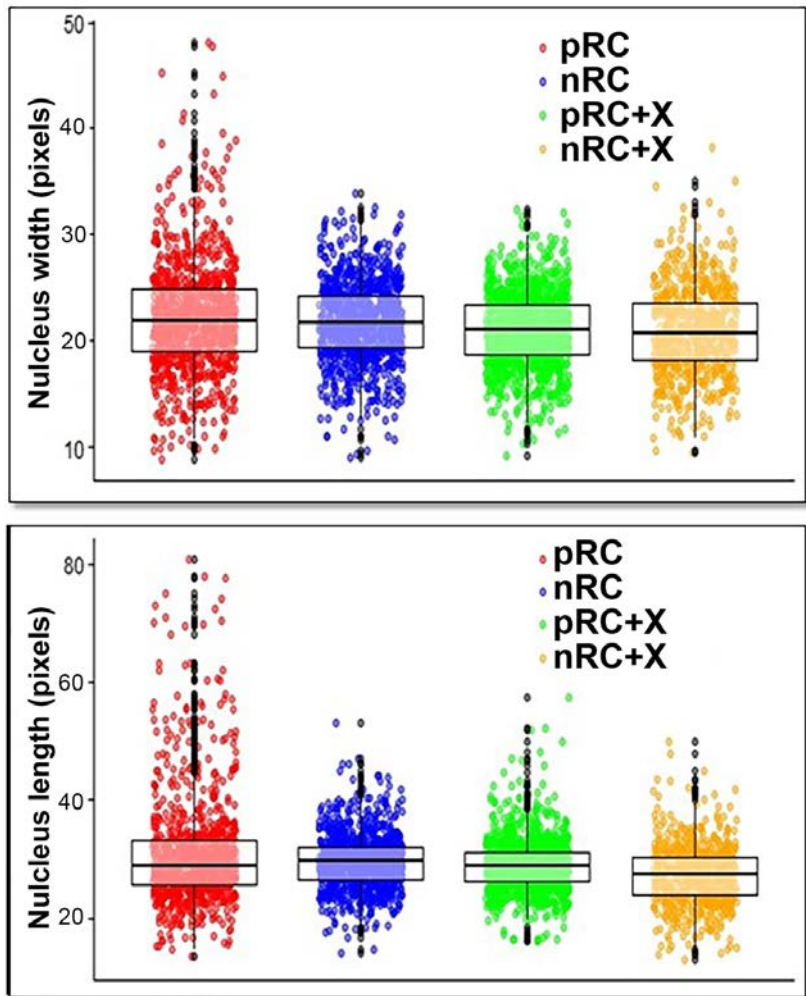


Figure 18. Nuclear morphometric analysis

Representative nuclei for each group are shown in the top panel. Box plots display the distribution of nuclear length and width.

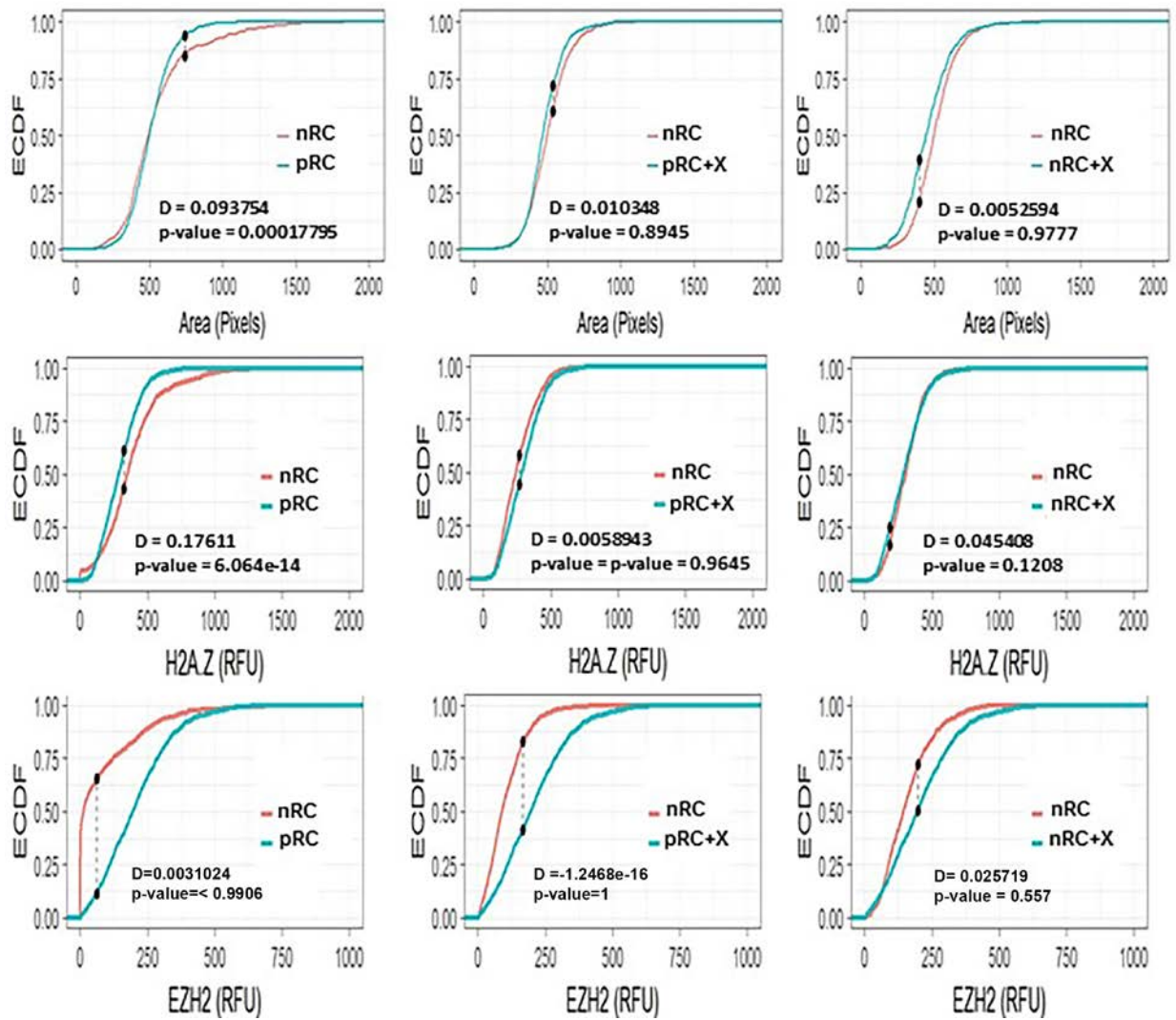


Figure 19. Two-sided bootstrap Kolmogorov-Smirnov tests

Bootstrap version of the univariate Kolmogorov-Smirnov test that provides correct coverage even when the distributions compared are not entirely continuous. Ties were allowed with this test unlike the traditional Kolmogorov-Smirnov test. The bootstraps are Monte Carlo simulations that were performed in order to determine the proper p-value from the empiric.

Table 1. Statistical descriptors of nuclear area distributions

Nuclear Area	nRCs	pRCs	pRCs+X	nRCs+X
mean	507.09 (+/- 4.48)	512.63 (+/- 7.28)	478.55 (+/- 3.72)	455.92 (+/- 6.09)
variance	20 072.3	47 394.8	15 148.4	25 553.8
skewness	0.52	2.19	0.71	0.86
kurtosis	3.83	11.64	4.46	5.08
median	498.31	475.37	465.62	442.31
first quantile	410.5	386.	399.	351.
interquantile range	178.12	206.31	149.28	193.43
third quantile	588.75	592.37	548.37	543.87
Max	1091.75	2014	958.87	1218.13
min	118.37	108.87	153.75	106.87

Table 2. Statistical descriptors of nuclear H2A.Z expression

H2A.Z Expression	nRCs	pRCs	pRCs+X	nRCs+X
mean	294.32 (+/- 4.45)	352.08 (+/- 6.68)	257.52 (+/- 4.05)	306.07 (+/- 4.93)
variance	19 729.3	40 368.6	17 897.4	16 785.4
skewness	0.62	1.1	0.88	0.7
kurtosis	3.45	6.16	4.06	4.45
median	282.58	337.5	236.7	303.77
first quantile	184.94	228.21	154.1	213.3
interquantile range	202.59	221.41	187.95	171.78
third quantile	387.48	449.95	342.22	384.76
min	17.08	0	0	25.75
Max	876.6	1542.44	891.72	932.31

Table 3. Statistical descriptors of nuclear EZH2 expression

EZH2 Expression	nRCs	pRCs	pRCs+X	nRCs+X
mean	208.05 (+/- 4.09)	72.4 (+/-3.84)	103.51 (+/- 2.27)	157.93 (+/- 3.54)
variance	16 705.8	13 245.6	5 662.15	8 657.88
skewness	0.77	2.31373	1.32	1.06
kurtosis	3.59	10.57	6.03	4.76
median	195.75	9.4	87.29	143.19
first quantile	109.29	0.015	49.67	87.01
interquantile range	176.52	108.892	94.1628	119.704
third quantile	285.95	108.98	143.97	206.73
min	0	0	0	0
Max	715.1	885.83	567.33	687.4

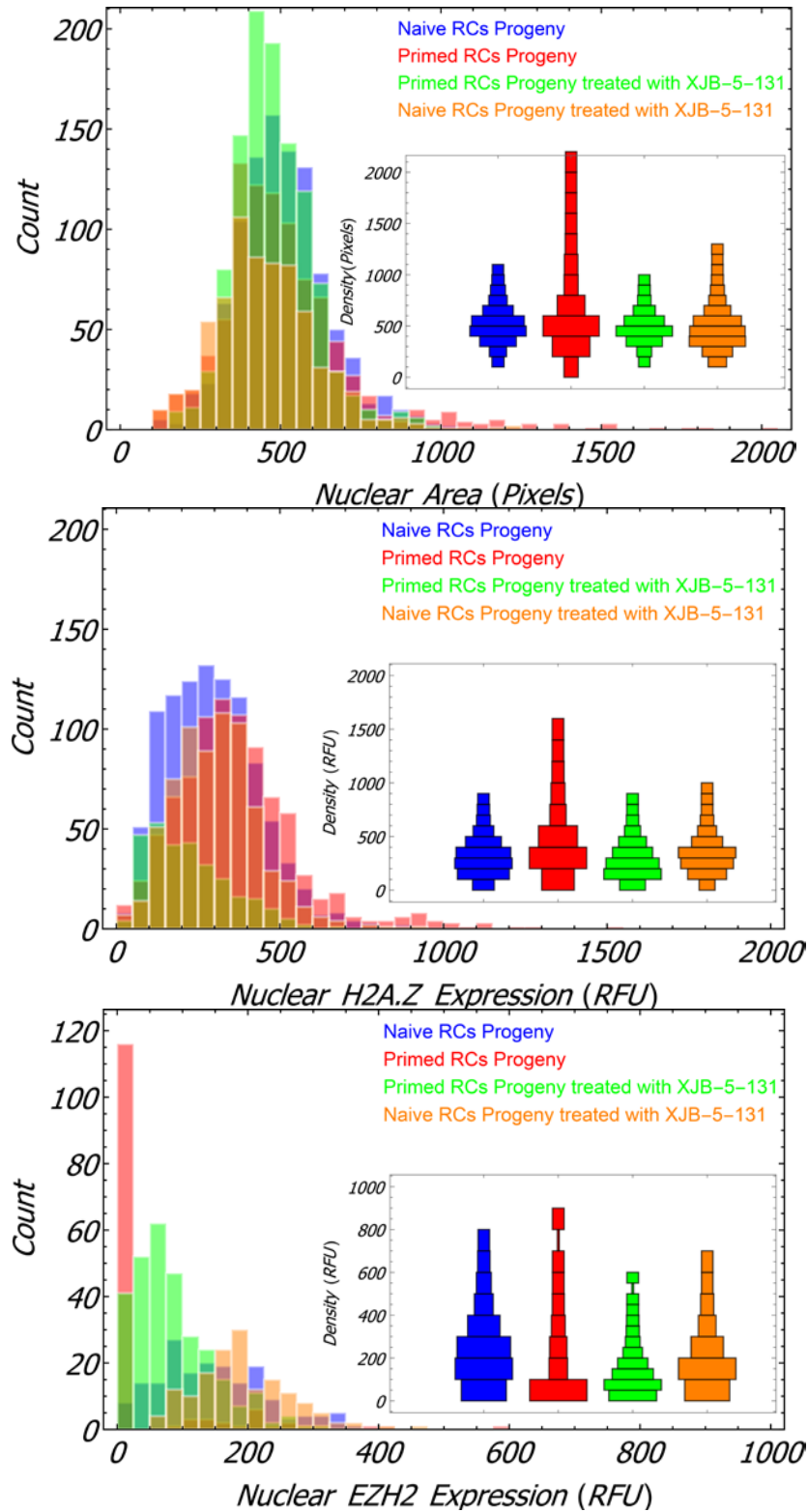


Figure 20. Histograms of measured protein expression and nuclear area distributions and their corresponding histogram densities (insets)

Collectively, these findings demonstrate that H2A.Z, nuclear area and, to a lesser extent, EZH2, are strongly coupled to mitochondrial functionality. Moreover, these findings illustrate a previously unexplored role for mitochondria in the regulation of cell population dynamics. Notably, these data demonstrate that memory of stress is encoded, at the cell population level, in RC heterogeneity by quantized distributions of epigenetic modifiers. From a statistical point of view, these results suggest that the classical Gaussian analysis (Normal) is ill suited for studying the extremal realizations aggregated in this type of distribution tail. In fact, the Central Limit Theorem (CLT) focuses on average behavior of stochastic processes around the mean. However, it does not imply that extremal events (maxima and minima) and the extremes of the limiting normal distribution obey the same laws. Thus, in an aggregation process, variable values around the average are approximable by the bell-shaped distribution. However, the tail events, which might be governed by an extreme value distribution (Fisher-Tippett theorem) (Beirlant, Teugels, & Vynckier, 1996), can be ejected towards large values of the variable and thus tend to gradually get unnoticed for the sums of random variables despite their consequential asymptotic effect. These subtle but crucial considerations refer to either rare (but probable) occurrences of events with high values, or the many occurrences of events with small values (Figure 21). A corollary is that the investigation of the memory-bearing RC can be better modelled under the Extreme Value Theory (EVT)(Reiss, Thomas, & Reiss, 2007).

Distribution fitting of nuclear proteins and area revealed the presence of power-law generative statistical models (Figures 22-24). Comparison of the protein expression and nuclear area histograms to their three best PDFs derived from the immunofluorescence data. All models were fitted to the data using the maximum likelihood estimation technique. Goodness-of-fit was measured based on Anderson-Darling (AD),Kolmogorov-Smirnov(KS) and Cramer-Von Mises

(CVM) ($\alpha=0.05$) . A cutoff α is chosen such that H_0 is rejected only if $p < \alpha$. The value of α used was controlled by the significance level option. By default, α was set to 0.05. Additionally, the Bayesian information criterion (BIC) and Akaike Information Criterion (AIC) were used to penalize each model's relative complexity and over-fitting. The insets show the comparison between the exponentially truncated power law and alternative models and further support the power laws models goodness-of-fit.

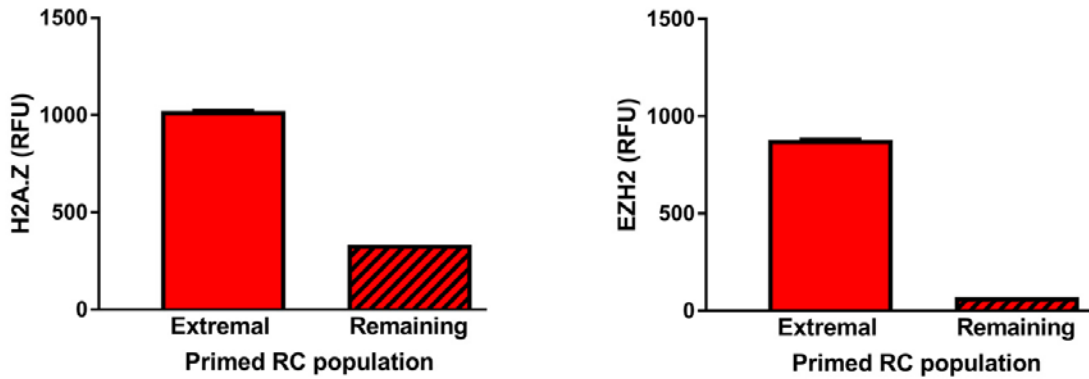


Figure 21. Inadequacy of Gaussian Statistics

Mean values are dominated by the extremals, and therefore are not faithfully describing the data. Data are mean + SEM.

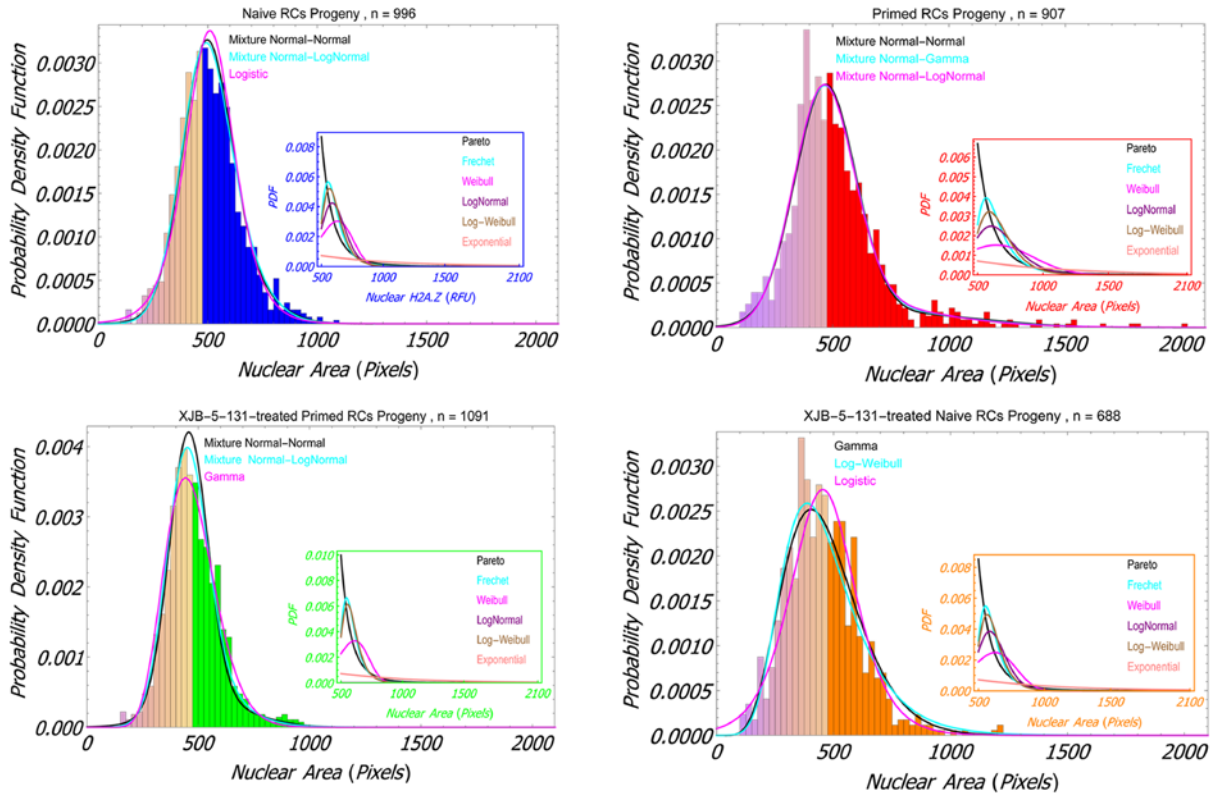


Figure 22. Distribution fitting of probability density functions: nuclear area

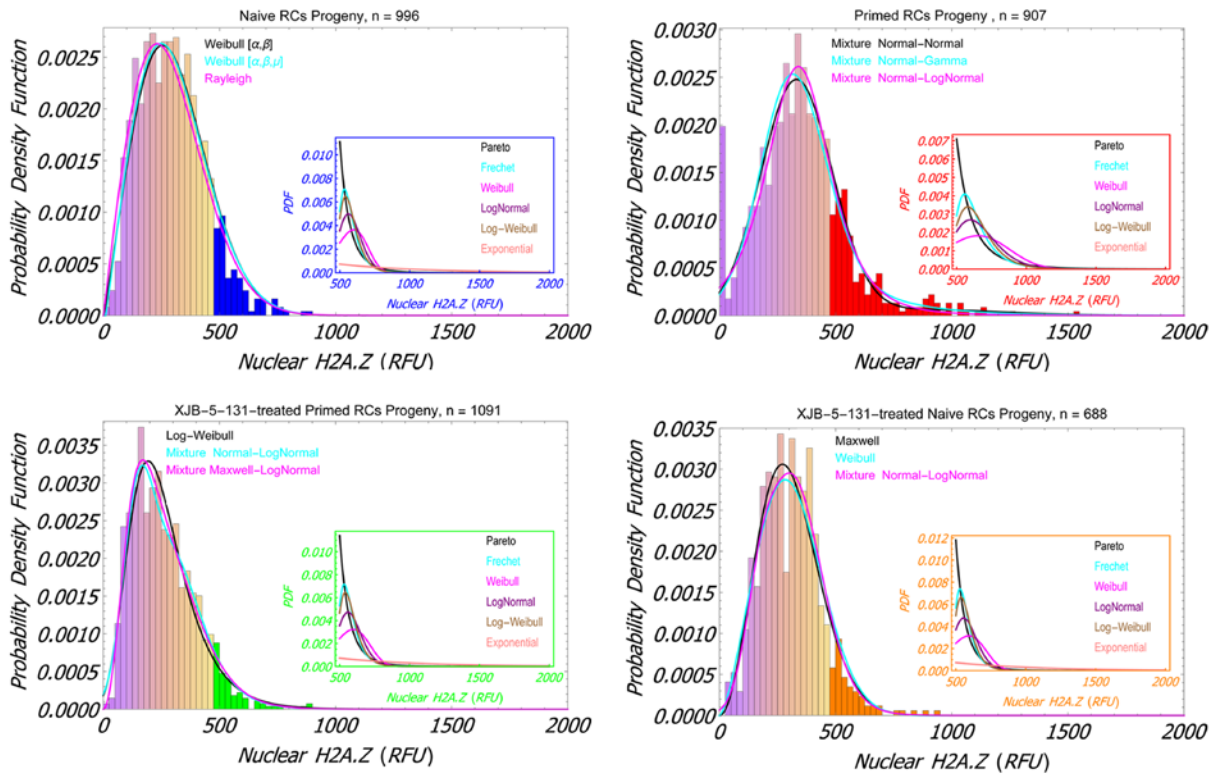


Figure 23. Distribution fitting of probability density functions: nuclear H2A.Z

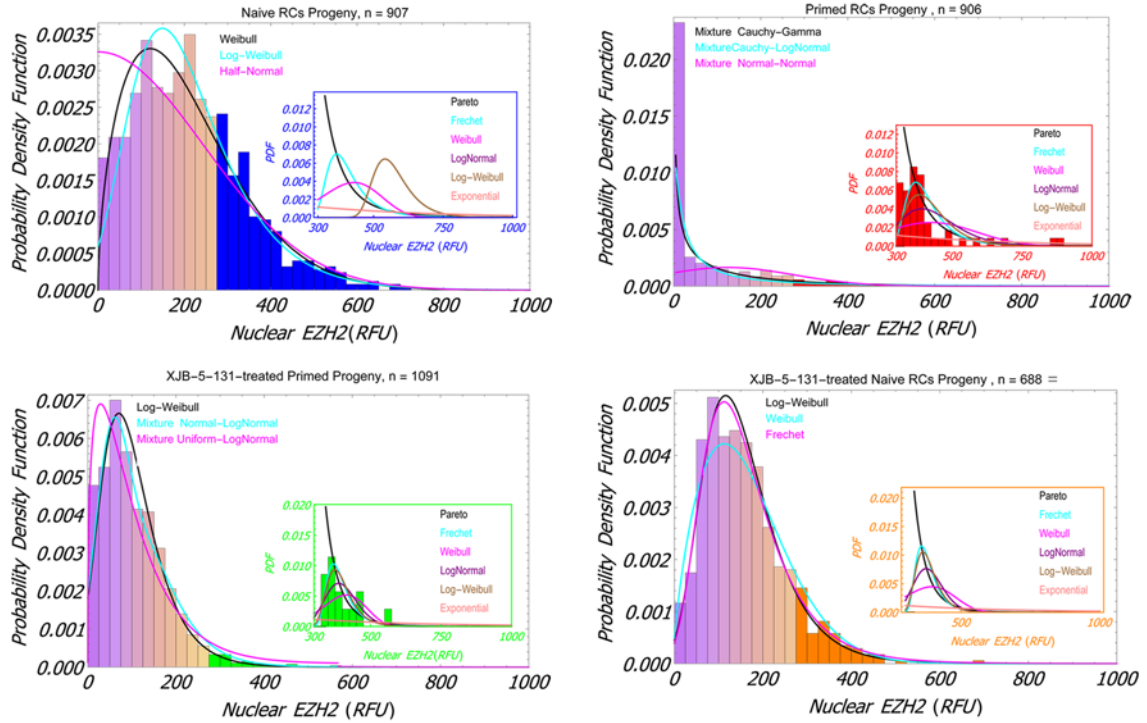


Figure 24. Distribution fitting of probability density functions: nuclear EZH2

3.3.4 Mitochondrial maintenance of cellular memory adheres to a power-law

For insight into the potential generative models of the RC progeny right-skewed distributions, we computed the probability density functions (PDFs) of H2A.Z, EZH2 and nuclear area (Figures 22-24). All models were fitted to experimental data using the maximum likelihood estimation technique that maximizes agreement with the data. To assess the goodness-of-fit, we employed Anderson-Darling (AD) and the Kolmogorov-Smirnov (KS) tests that have increased power against fatter tails and deviations in the middle curve respectively. We also employed the Cramer-von Mises (CVM) test that is in between, but relatively close to KS (Razali & Wah, 2011). To account for potential over-fitting, we considered the Bayesian information criterion

(BIC) and the Akaike information criterion (AIC) that are both likelihood criteria that measure the goodness-of-fit and penalize models complexity and other selection statistics (Dziak, Coffman, Lanza, & Li, 2012). BIC is an estimate of a function of the probability of a model being true. AIC is an estimate of a constant plus the relative distance between the unknown true likelihood function of the data and the fitted likelihood function of the model. Lower values indicate that a model is more likely to be the true model. However, BIC is a stronger penalizing criteria and favors more parsimonious models. Therefore when BIC and AIC do not agree, we favor BIC. Thus, the best-fit selection was based on the convergence of all the above mentioned tests (Table 5). Corroborating the heterogeneity revealed by fluorescence microscopy across all conditions, we found that all these three variables were best empirically fitted by unimodal generalized extreme value distributions (e.g. Weibull) or mixture of distributions. These included: linear combination of normal distributions with different standard deviations; combination of normal and heavy tail distributions (e.g. Lognormal) or exponential-related distributions (e.g. Gamma); and composite of power law distributions (e.g. Cauchy) and heavy tail or exponential-related distributions. These data support the idea of discrete RC subpopulations that likely possess distinctive characteristics. Furthermore, this type of statistical mixtures promptly raises the possibility of presence of power law tails (Farmer & Geanakoplos, 2008; Mitzenmacher, 2004; Xu, Liu, & Liang, 2009). Power laws can be generated in many heterogeneous complex systems by the superposition of normal distributions both within the context of canonical statistical mechanics equilibrium or non-equilibrium superstatistical systems (Patriarca, Heinsalu, Marzola, Chakraborti, & Kaski, 2016; Touchette & Beck, 2005). Significantly, many of the best-fit distributions we measured (e.g. Frechet, Cauchy and Student T) were de facto power laws in their own right. To investigate the possibility of power law tails,

we employed the R (R Core Team 2014) (powerLaw) statistical package that provides a principled methodology to power law and other heavy-tailed distributions fitting (Clauset, Shalizi, & Newman, 2009; Gillespie, 2014). First, we determined the point estimates for x_{min} , which define the length of the tail and the scaling exponent parameter α for the power-law model $f(x) = c x^{-\alpha}$. Then, we used the method of maximum likelihood to fit a power-law distribution to the observed tail data. Based on the x_{min} , the scaling exponent, α , was then numerically calculated. These two variables (i.e. x_{min} and α) are then utilized to create a large number of simulated datasets from a synthetic true power-law distribution using a bootstrapping procedure (for our analysis, we performed 1000 iterations). Each of these true power-laws was then compared with the empirical dataset using the Kolmogorov-Smirnov statistic that reflects the closeness between the empirical and the model distribution. This provides a goodness-of-fit test, which generates a p-value that quantifies the validity of the power-law hypothesis, with small p values indicating that the data are not consistent with being drawn from power-law distribution. (We choose $p > 0.05$ to suggest significant*, and $p > 0.1$ to suggest very significant** results, Figure 28).

Table 4. Computation of exceedance probabilities.

Area

Exceedance probability:Pr[Area (Pixels) \geq x]	Naive RCs	Primed RCs	Primed RCs treated with XJB	Naive RCs treated with XJB
x = 25 th Naive percentile	1	0.6959	0.7119	0.5848
x = 50 th Naive percentile	0.9411	0.4615	0.3579	0.3762
x = 75 th Naive percentile	0.4507	0.2515	0.1184	0.2117
x = 90 th Naive percentile	0.1913	0.1263	0.0423	0.1031
x = 95 th Naive percentile	0.0998	0.0857	0.0236	0.0574
x = 99 th Naive percentile	0.0218	0.0495	0.0049	0.0131
x = 99.9 th Naive percentile	0.0037	0.0262	0.0004	0.0019

H2A.Z

Exceedance probability:Pr[H2A.Z (RFU) \geq x]	Naive RCs	Primed RCs	Primed RCs treated with XJB	Naive RCs treated with XJB
x = 25 th Naive percentile	0.7641	0.8376	0.6591	0.8184
x = 50 th Naive percentile	0.5158	0.6431	0.3631	0.5392
x = 75 th Naive percentile	0.2722	0.3873	0.1614	0.2531
x = 90 th Naive percentile	0.1385	0.2184	0.0797	0.1098
x = 95 th Naive percentile	0.0757	0.1337	0.0462	0.0513
x = 99 th Naive percentile	0.0101	0.0461	0.0107	0.0041
x = 99.9 th Naive percentile	0.0006	0.0277	0.0022	0.0001

EZH2

Exceedance probability:Pr[EZH2 (RFU) \geq x]	Naive RCs	Primed RCs	Primed RCs treated with XJB	Naive RCs treated with XJB
x = 25 th Naive percentile	0.7319	0.2205	0.3899	0.6664
x = 50 th Naive percentile	0.4581	0.1303	0.0982	0.2792
x = 75 th Naive percentile	0.2423	0.0793	0.0199	0.0884
x = 90 th Naive percentile	0.1101	0.0489	0.0037	0.0249
x = 95 th Naive percentile	0.0526	0.03341	0.0009	0.0086
x = 99 th Naive percentile	0.0128	0.0178	0.0001	0.0014
x = 99.9 th Naive percentile	0.0024	0.0095	8.5×10^{-6}	0.0002

Computation of exceedance probabilities at different thresholds showed that naïve RCs progeny distributions tails decreased exponentially for large values of any given quantity whereas these probabilities decrease rather algebraically in primed RCs progeny. The exponential behavior remain unaltered in XJB-5-131 treated naïve RCs progeny whereas the algebraic behavior in converted to an exponential one in XJB-treated primed RCs progeny.

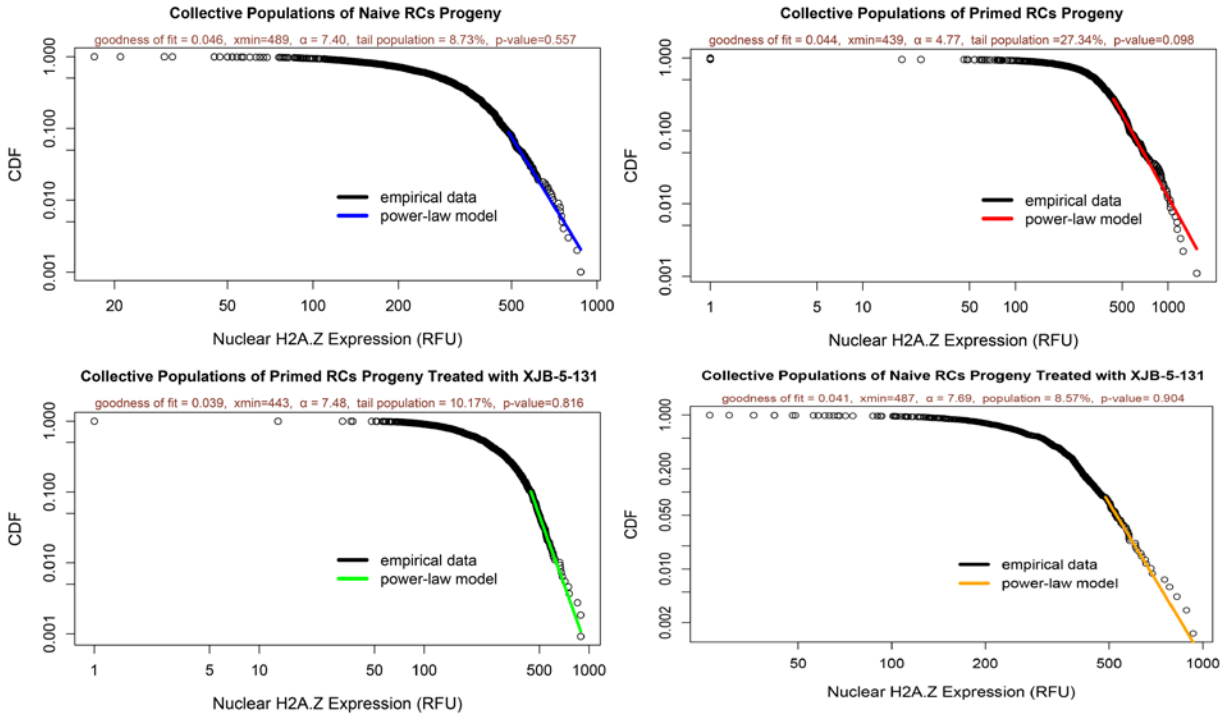


Figure 25. Cumulative distribution functions (CDF) and their maximum likelihood power law fit: nuclear H2A.Z

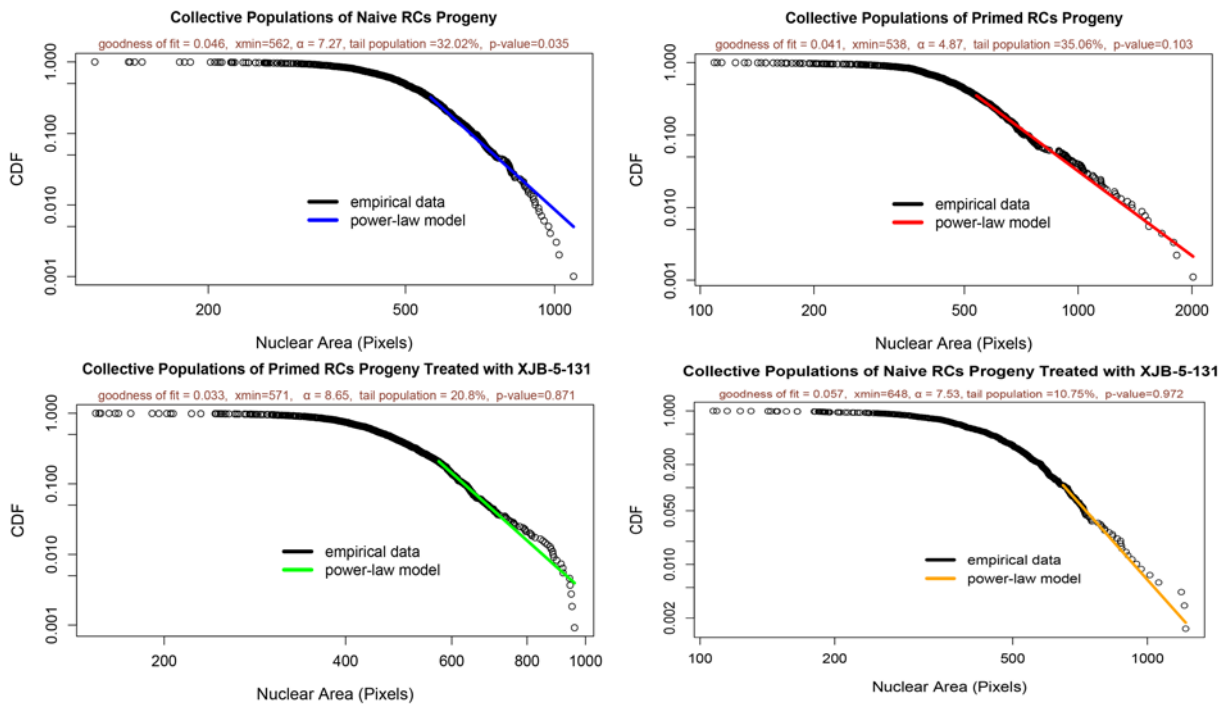


Figure 26. Cumulative distribution functions (CDF) and their maximum likelihood power law fit: nuclear area

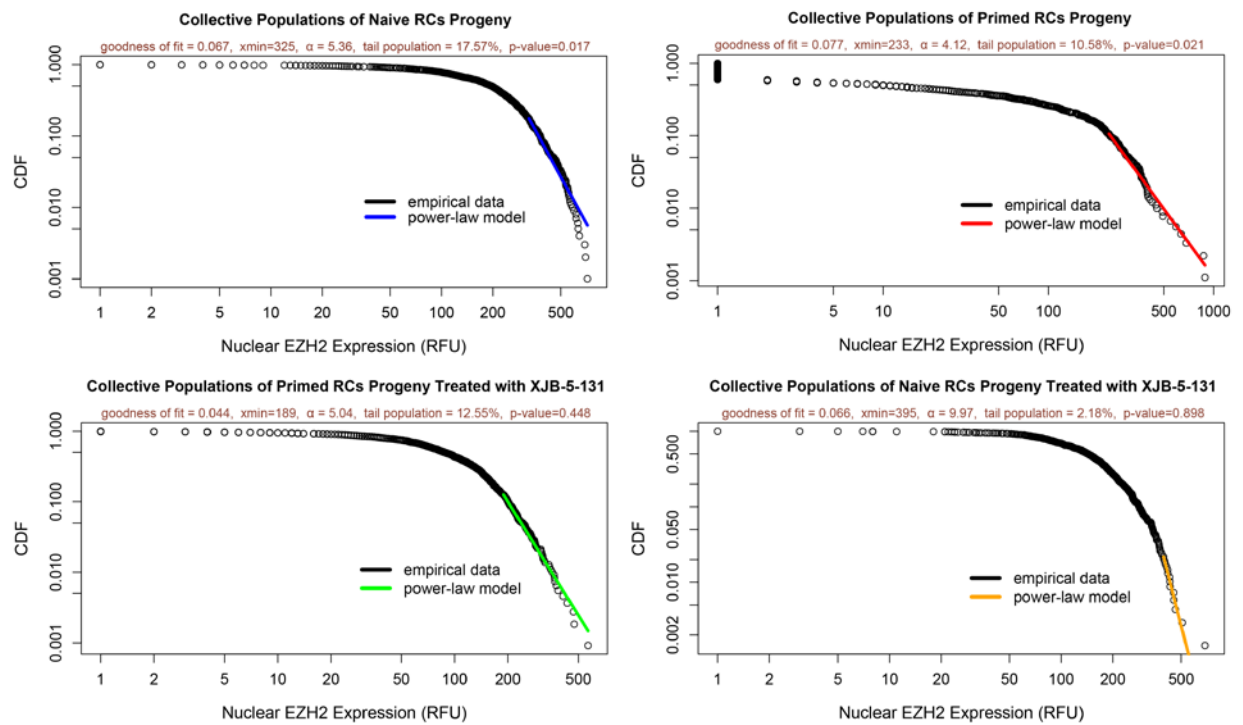


Figure 27. Cumulative distribution functions (CDF) and their maximum likelihood power law fit: nuclear area

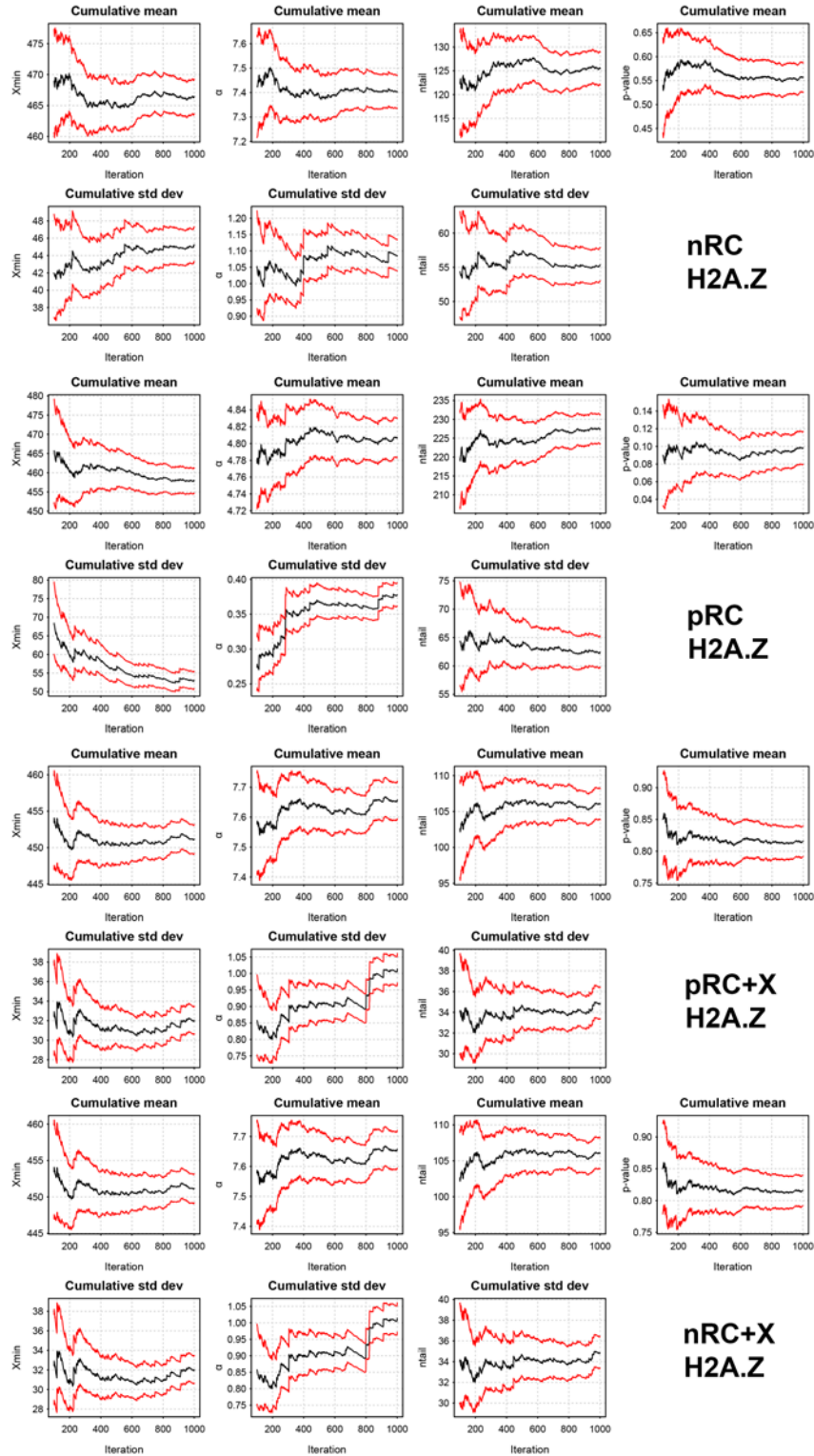


Figure 28. Results from standard bootstrap procedure for the power law model: H2A.Z expression

The black line shows the mean estimate for the model and the red line represent the 95% confidence intervals after 1000 simulations.

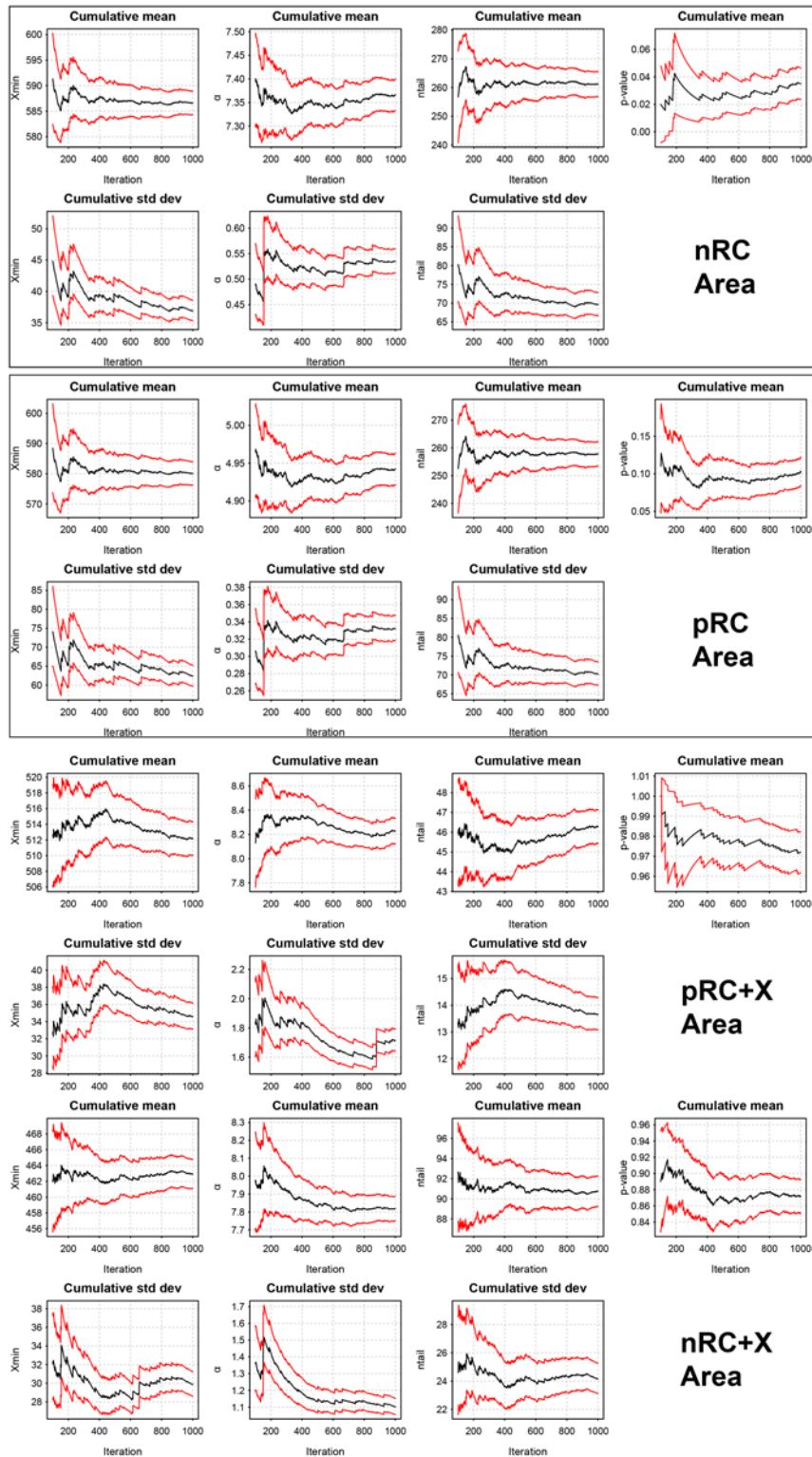


Figure 29. Results from standard bootstrap procedure for the power law model: nuclear area

The black line shows the mean estimate for the model and the red line represent the 95% confidence intervals after 1000 simulations.

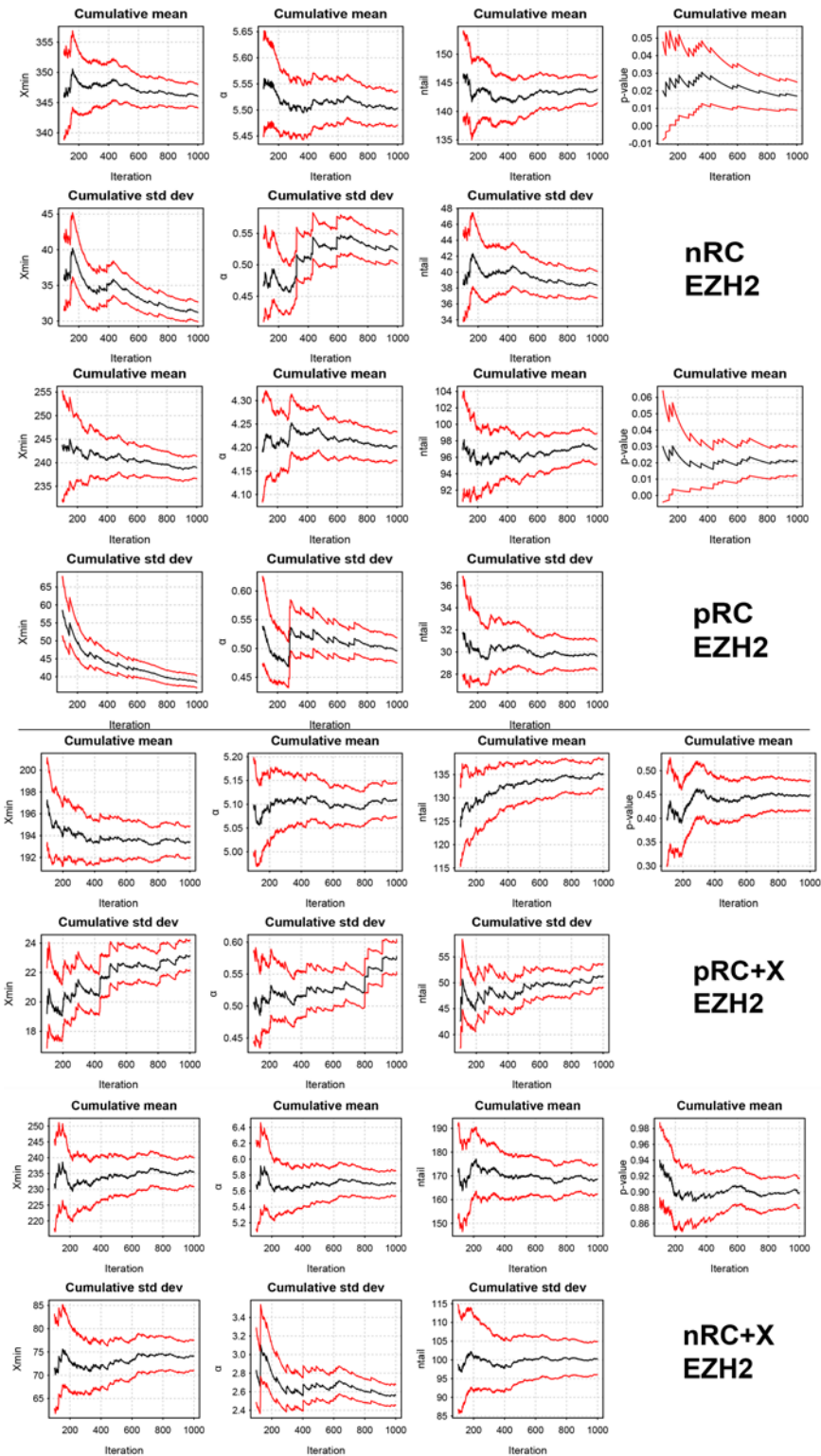


Figure 30. Results from standard bootstrap procedure for the power law model: nuclear area

The black line shows the mean estimate for the model and the red line represent the 95% confidence intervals after 1000 simulations.

Table 5. Goodness-of-fit results for the comparison of truncated power law and alternative methods.

Area									
	Kolmogorov-Smirnov	Anderson-Darling	Cramer Von Mises		BIC	AIC		BIC	AIC
Pareto[489.125, 4.82116]	0.0000257419	0.0000258583	0.0000855345	Pareto	-2185.12	-2197.9			
Frechet[8.57112, 560.682]	0.179595	0.0400546	0.126924	Frechet	2887.95	2900.73			
Weibull[5.30521, 655.759]	4.6585 × 10 ⁻¹⁷	0.	4.79179 × 10 ⁻¹¹	Weibull	Missing[]	Missing[]			
LogNormal[6.40004, 0.158172]	0.000112068	8.28722 × 10 ⁻⁶	0.000079601	LogNormal	-1955.4	-1968.18			
Log-Weibull[565.097, 70.6592]	0.0458799	0.00274829	0.0179056	Log-Weibull	-2417.47	-2430.25			
Exponential[0.00163972]	3.90823 × 10 ⁻¹⁴⁰	0.	2.22045 × 10 ⁻¹⁶	Exponential	921.978	913.455			
Pareto[489.25, 3.62225]	0.262657	0.0583545	0.171656	Pareto	-2154.13	-2166.28			
Frechet[6.09742, 579.721]	0.0337025	0.00140344	0.0155565	Frechet	-1881.83	-1893.98			
Weibull[2.87654, 746.05]	5.31114 × 10 ⁻²⁵	0.	0.	Weibull	214.026	201.877			
LogNormal[6.46895, 0.257502]	6.33478 × 10 ⁻⁸	1.41584 × 10 ⁻⁶	2.10342 × 10 ⁻⁸	LogNormal	-1404.81	-1416.96			
Log-Weibull[590.009, 114.37]	0.000156501	1.86217 × 10 ⁻⁶	0.0000267165	Log-Weibull	-1591.16	-1603.31			
Exponential[0.00149237]	2.67523 × 10 ⁻¹⁰⁰	0.	0.	Exponential	747.717	739.617			
Pareto[489.625, 5.60866]	0.00356315	0.000393315	0.00107065	Pareto	-1877.98	-1890.31			
Frechet[9.88056, 549.736]	0.0757852	0.0387087	0.141402	Frechet	-2358.69	-2371.02			
Weibull[5.56923, 633.496]	3.7402 × 10 ⁻¹⁸	0.	2.8858 × 10 ⁻¹²	Weibull	223.267	210.94			
LogNormal[6.37194, 0.143432]	0.0000615324	3.7696 × 10 ⁻⁶	0.0000633657	LogNormal	-1743.07	-1755.39			
Log-Weibull[553.06, 59.9446]	0.0189593	0.00370318	0.0343157	Log-Weibull	-2126.14	-2138.47			
Exponential[0.00169026]	1.77372 × 10 ⁻¹²⁵	0.	0.	Exponential	792.876	784.658			
Pareto[489.125, 4.73384]	0.0380758	0.0281231	0.0359209	Pareto	-1198.48	-1209.15			
Frechet[8.31339, 560.517]	0.185146	0.0960777	0.179957	Frechet	-1249.95	-1260.63			
Weibull[4.36562, 665.659]	1.8558 × 10 ⁻¹²	2.30982 × 10 ⁻⁶	3.90851 × 10 ⁻⁸	Weibull	118.993	108.311			
LogNormal[6.40386, 0.174089]	0.00100492	0.000281791	0.00127184	LogNormal	-903.719	-914.401			
Log-Weibull[565.453, 74.4646]	0.0422571	0.0132765	0.0408268	Log-Weibull	-1081.46	-1092.14			
Exponential[0.00162809]	2.09694 × 10 ⁻⁶⁹	0.	0.	Exponential	461.586	454.465			
H2A.Z									
Pareto[489.35, 6.36131]	0.519299	0.501103	0.858944	Pareto	-395.542	-402.905			
Frechet[10.2937, 538.24]	0.0649594	0.0921501	0.153233	Frechet	-280.858	-288.221			
Weibull[6.03206, 618.439]	0.000522516	0.00153965	0.00272763	Weibull	47.6732	40.3101			
LogNormal[6.35028, 0.141046]	0.0767154	0.0150602	0.0258348	LogNormal	-224.186	-231.549			
Log-Weibull[541.221, 57.0126]	0.0470853	0.0467882	0.0933678	Log-Weibull	-259.211	-266.574			
Exponential[0.00172809]	2.12883 × 10 ⁻²⁵	0.	1.9984 × 10 ⁻¹⁵	Exponential	156.978	152.069			
Pareto[489.031, 3.86522]	0.280902	0.106471	0.440198	Pareto	-716.631	-726.021			
Frechet[6.26928, 570.745]	0.000345858	0.00192266	0.0057684	Frechet	-481.974	-491.364			
Weibull[3.41625, 723.201]	2.13642 × 10 ⁻⁸	4.46779 × 10 ⁻⁶	2.63206 × 10 ⁻⁶	Weibull	72.837	65.4473			
LogNormal[6.45114, 0.241395]	0.0000202233	0.0000496177	0.000127806	LogNormal	-383.086	-392.476			
Log-Weibull[579.83, 108.309]	0.0000171419	0.000121909	0.000607818	Log-Weibull	-421.588	-430.897			
Exponential[0.00152891]	7.9805 × 10 ⁻⁴²	0.	0.	Exponential	302.669	296.409			
Pareto[490.337, 6.46919]	0.997135	0.336955	0.99759	Pareto	-288.376	-294.505			
Frechet[10.4154, 537.455]	0.488178	0.241915	0.330052	Frechet	-197.723	-203.852			
Weibull[5.35265, 622.049]	0.00178144	0.00320938	0.00501287	Weibull	33.221	27.0919			
LogNormal[6.34967, 0.14917]	0.0383591	0.030502	0.0424334	LogNormal	-150.337	-156.466			
Log-Weibull[540.469, 57.031]	0.216023	0.116091	0.180179	Log-Weibull	-180.262	-186.391			
Exponential[0.00172658]	3.90887 × 10 ⁻¹⁷	0.000010527	1.38562 × 10 ⁻¹⁰	Exponential	105.713	101.627			
Pareto[490.228, 6.75221]	0.974914	0.548183	0.983532	Pareto	-892.48	-901.869			
Frechet[10.6983, 534.486]	0.346937	0.217785	0.305402	Frechet	-625.752	-635.142			
Weibull[5.18553, 618.362]	0.000726883	0.00202453	0.00325185	Weibull	236.407	227.018			
LogNormal[6.34297, 0.149011]	0.0566111	0.0258627	0.040944	LogNormal	-496.613	-506.003			
Log-Weibull[537.389, 55.4166]	0.216097	0.109143	0.180675	Log-Weibull	-574.335	-583.725			
Exponential[0.00172658]	2.855 × 10 ⁻¹⁷	0.0000105269	1.20784 × 10 ⁻¹⁰	Exponential	231.277	225.018			
EZH2									
Pareto[325.19, 4.37817]	0.455857	0.19567	0.298558	Pareto	-835.261	-844.755			
Frechet[7.05582, 374.462]	0.159689	0.042823	0.0942659	Frechet	-681.322	-690.817			
Weibull[4.63684, 452.993]	3.26881 × 10 ⁻⁶	0.0000854062	0.000264914	Weibull	318.314	308.82			
LogNormal[6.01282, 0.192491]	0.00145986	0.00324808	0.00685177	LogNormal	-517.163	-526.658			
Log-Weibull[378.85, 58.9849]	0.0237887	0.0105531	0.0283294	Log-Weibull	318.314	308.82			
Exponential[0.0023999]	8.49913 × 10 ⁻⁴⁶	0.	0.	Exponential	313.149	306.82			
Pareto[327.639, 4.183]	0.550469	0.204339	0.627825	Pareto	-136.116	-141.107			
Frechet[6.95982, 377.061]	0.17073	0.17367	0.213252	Frechet	-118.423	-123.414			
Weibull[3.11093, 478.869]	0.00676952	0.00486506	0.00542634	Weibull	77.3057	72.315			
LogNormal[6.03098, 0.246529]	0.010733	0.025825	0.0255069	LogNormal	-93.4939	-98.4846			
Log-Weibull[382.264, 66.6564]	0.033262	0.0467325	0.0674682	Log-Weibull	77.3057	72.315			
Exponential[0.0023051]	1.84184 × 10 ⁻¹⁰	0.0000193533	1.49652 × 10 ⁻⁶	Exponential	73.6422	70.315			
Pareto[341.145, 6.74096]	0.977773	0.404466	0.575054	Pareto	-47.3482	-49.2654			
Frechet[10.3587, 371.716]	0.794436	0.758898	0.702549	Frechet	-36.1594	-38.0766			
Weibull[5.92792, 428.09]	0.357509	0.305331	0.292076	Weibull	30.7202	28.803			
LogNormal[5.98065, 0.143665]	0.397909	0.492166	0.438215	LogNormal	-26.7985	-28.7156			
Log-Weibull[373.76, 39.3989]	0.654532	0.63414	0.58932	Log-Weibull	30.7202	28.803			
Exponential[0.00249981]	0.0006080918	0.00357305	0.00191285	Exponential	28.0812	26.003			
Pareto[331.526, 7.04934]	0.922721	0.314276	0.96459	Pareto	-185.742	-191.026			
Frechet[11.3175, 361.097]	0.725675	0.601568	0.650686	Frechet	-160.941	-166.224			
Weibull[4.92823, 413.753]	0.00138194	0.00639619	0.0111831	Weibull	84.5572	79.2736			
LogNormal[5.94556, 0.137828]	0.249383	0.155375	0.20262	LogNormal	-127.856	-133.14			
Log-Weibull[362.909, 34.8588]	0.588665	0.450176	0.513468	Log-Weibull	84.5572	79.2736			
Exponential[0.00259023]	2.37615 × 10 ⁻¹³	0.0000140115	1.53615 × 10 ⁻⁸	Exponential	80.796	77.2736			

Testing our experimental datasets against simulated true power-laws models (Figure 25-27) revealed the presence of power laws in all H2A.Z distributions ($p > 0.1$ for naïve, XJB-treated primed and XJB-treated naïve RC, and $p > 0.05$ for primed RC respectively). Likewise, power laws were found in all nuclear area distributions ($P > 0.1$) except in naïve RC. In contrast, EZH2 distributions were not adequately fitted to power law model in naïve and primed RC and thus remained inconclusive. However, power law was significantly manifested ($P > 0.1$) in XJB-treated naïve and primed RC. Importantly, as with previous results, XJB-5-131 successfully restored the scaling exponent of H2A.Z, as well as the absolute count and relative abundance of the tail population in primed RC, and has no significant effects on the naïve RC. In similar fashion, XJB-5-131 completely restored the scaling exponent of the nuclear area distribution in primed RC. However, it did reduce the absolute count of the tail occurrences and their relative abundance to levels that are lower compared to naïve RC. Those effects are in contrast to the slight increase in scaling exponential and reduced loss of the tail population compared to XJB-treated primed RC ($n=86 / 8.73\%$, $n=246 / 27.34\%$, $n=111 / 10.17\%$ and $n=58 / 8.7\%$ for naïve, primed, XJB-treated primed and XJB-treated naïve RC respectively). Notwithstanding, the extent of power laws are present in EZH2 distributions.

XJB-5-131 treatment of primed RC effectively restored the scaling exponential and sensibly enhanced the absolute count of tail population realizations while leaving their relative abundance practically unchanged. To confirm our results, we also used Vuong's test statistic to compare the power law models against other alternative distributions. However, p values were large, and the test sign was not reliable in favoring either model over the other (data not shown). Therefore, to compare the power law models to other competitive models, we used the power law model with a cut-off (truncated power law) with a minimum value parameter k and shape

parameter α . The choice of the truncated power law is justified by the fact that finite-size systems often show an exponential cut-off below the system size. Indeed, it is crucial to emphasize the asymptotic nature of power laws. The assumption of power law scaling is always of approximative nature, and its validity is restricted to a given range between cutoffs at small and large scales that achieve momentous regularity (Jensen, 1998). To further confirm our power law model, we therefore compared truncated power law models to alternative distributions (Figure 25) and evaluated them by using the AD, KS and CVM tests in combination with the BIC and AIC estimates (Table 3). Both EZH2 and H2A.Z truncated tails were significantly fitted by the Pareto distribution more than any other competitive function we tried across all conditions. More importantly, primed RC progenies have lower Pareto index, α , and, thus, fatter tails, whereas XJB-5-131 significantly opposed this effect and rather increased the Pareto index α . In contrast, the nuclear area truncated tails of naïve and primed progenies were differently best fitted with the Frechet and Pareto distributions respectively. XJB-5-131 treatment converted the primed RC Pareto distribution to a Frechet distribution with minor changes in the shape and scale parameters compared to control.

To quantify the tails behavior of the RC, we also estimated the complementary cumulative distribution (also called survival or reliability function), with and without truncation (Figure 25), and numerically computed their exceedance probabilities at different empirical thresholds. These calculations further corroborated our graphical analyses and demonstrated that the primed RC progeny exhibited survival function tails that are "fatter" in the sense that they decrease algebraically for large values of a given quantity, whereas those of the naïve RC and XJB-treated (naïve and primed) progenies decreased fast exponentially for large values (Table 4). Additionally, graphical analysis further supported the power law models when plotted in

double logarithmic scale as demonstrated by their straight line (Fig.4b). Collectively, statistical and graphical analyses converge to support the presence of power law scaling in key epigenetic memory modifiers, suggesting the occurrence of critical state dynamics in RC progenies populations. The latter are optimally modulated by the mitochondrial functionality and are consistent with the scaling and fractal properties of the mitochondrial networks(Aon, Cortassa, & O'Rourke, 2004), as clearly demonstrated by XJB-5-131 effects.

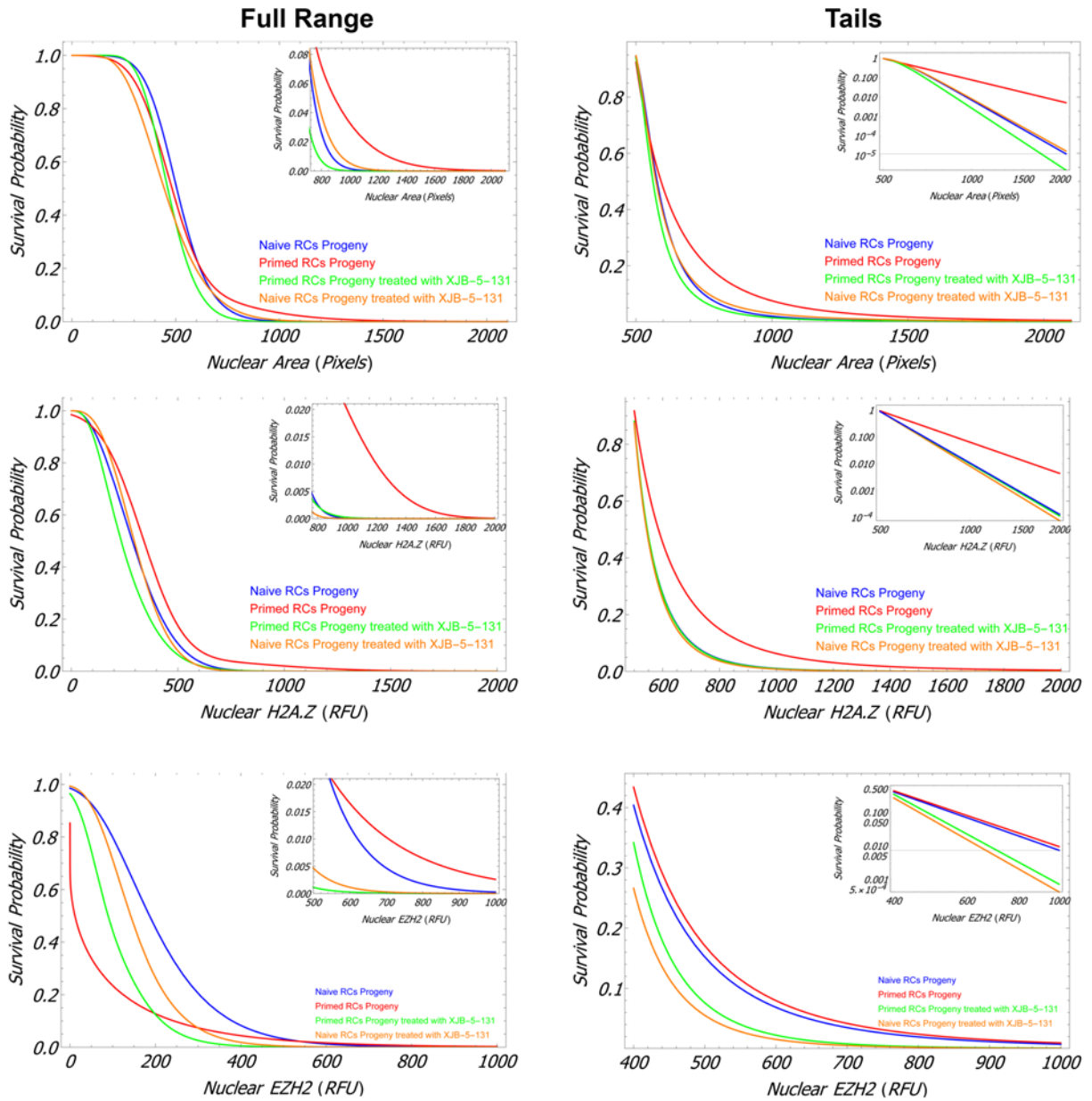


Figure 31. Truncated power law fitting of XJB-5-131 reversion of nuclear area and protein expression

Survival function maximum likelihood fitting of the best PDFs confirmed the “tail fatness” and power law behavior of primed RCs progeny protein expression and nuclear area distributions. The survival function analysis give the probability that an observed value is greater than a specific threshold and are equivalent to 1-CDF (Cumulative Density Function). The insets show the typical power-law affine relation in a log-log plot.

3.3.5 Mitochondria optimize bivalent chromatin domains

It has been suggested that histone H2A.Z and DNA methylation are mutually antagonistic epigenetic marks (Zilberman, Coleman-Derr, Ballinger, & Henikoff, 2008). It is also hypothesized that the acetylated form of H2A.Z (H2A.Zac) may constitute a stable regulator of inducible genes by promoting a more open conformation state of nucleosomes. This open conformation thereby permits the binding of transcription factors and chromatin remodelers, which in turn facilitates the initiation of transcription by Pol II (Colino-Sanguino, Clark, & Valdes-Mora, 2016). To test our hypothesis that mitochondrial functionality and dynamics dictate cellular memory and to demonstrate the functionality of imprinted changes in H2A.Z and EZH2, we focused on epigenetic regulation of expression of the housekeeping, DNA methyltransferase 1 (DNMT1) that propagates clonal inheritance of static methylation patterns (Jones, 2012), and the redox dependent *de novo* DNA methyltransferase DNMT3a, which is involved in dynamic addition and removal of methylation marks (C.-C. Chen, Wang, & Shen, 2012). We found that DNMT3a mRNA levels were elevated in skeletal muscle of mice exposed for five weeks to 100 µg/L of arsenic in their drinking water (control: 1.0 ± 0.1 vs arsenic: 2.0 ± 0.3 fg/ml qRT-PCR product, $p < 0.05$, $n = 8$). Remarkably, arsenic has also been shown to promote a two-fold increase in EZH2 and DNMT3a at the promoters of myogenic genes in C2C12 cells (Hong & Bain, 2012). We found increased transcript levels for both DNMT1 and DNMT3a in primed RC progeny (Figure 26). Using ChiP with antibodies specific for regulating enzymes or modified histones, we found that the strong induction of the DNMT3A in primed RC progeny was associated with gain of Pol II and acetylated H2A.Z, as well as loss of DNMT3a, DNMT1, and EZH2 in the promoter (Figure 26).

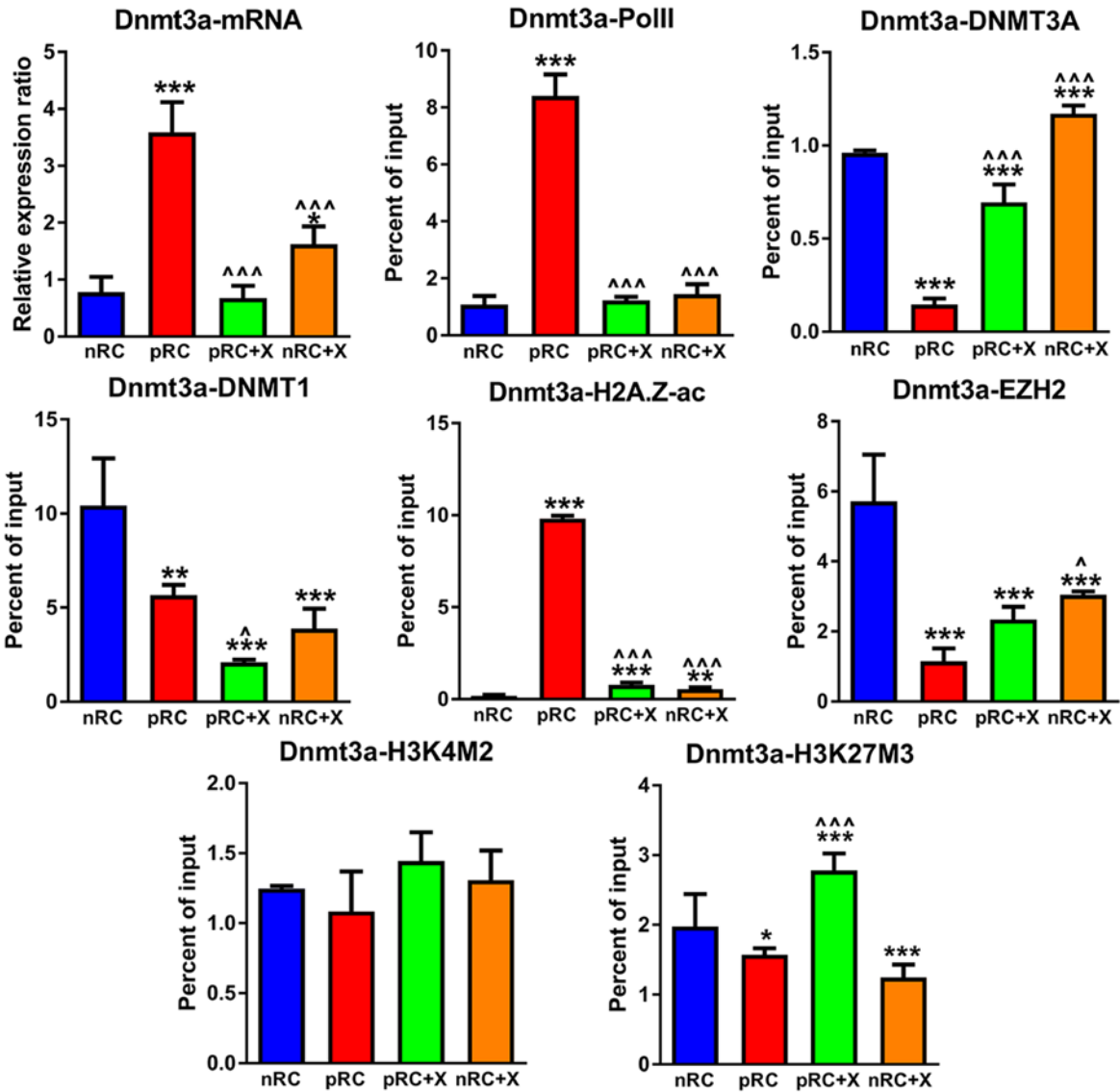


Figure 32. Regulation of memory for expression of DNA methyltransferases: DNMT3A

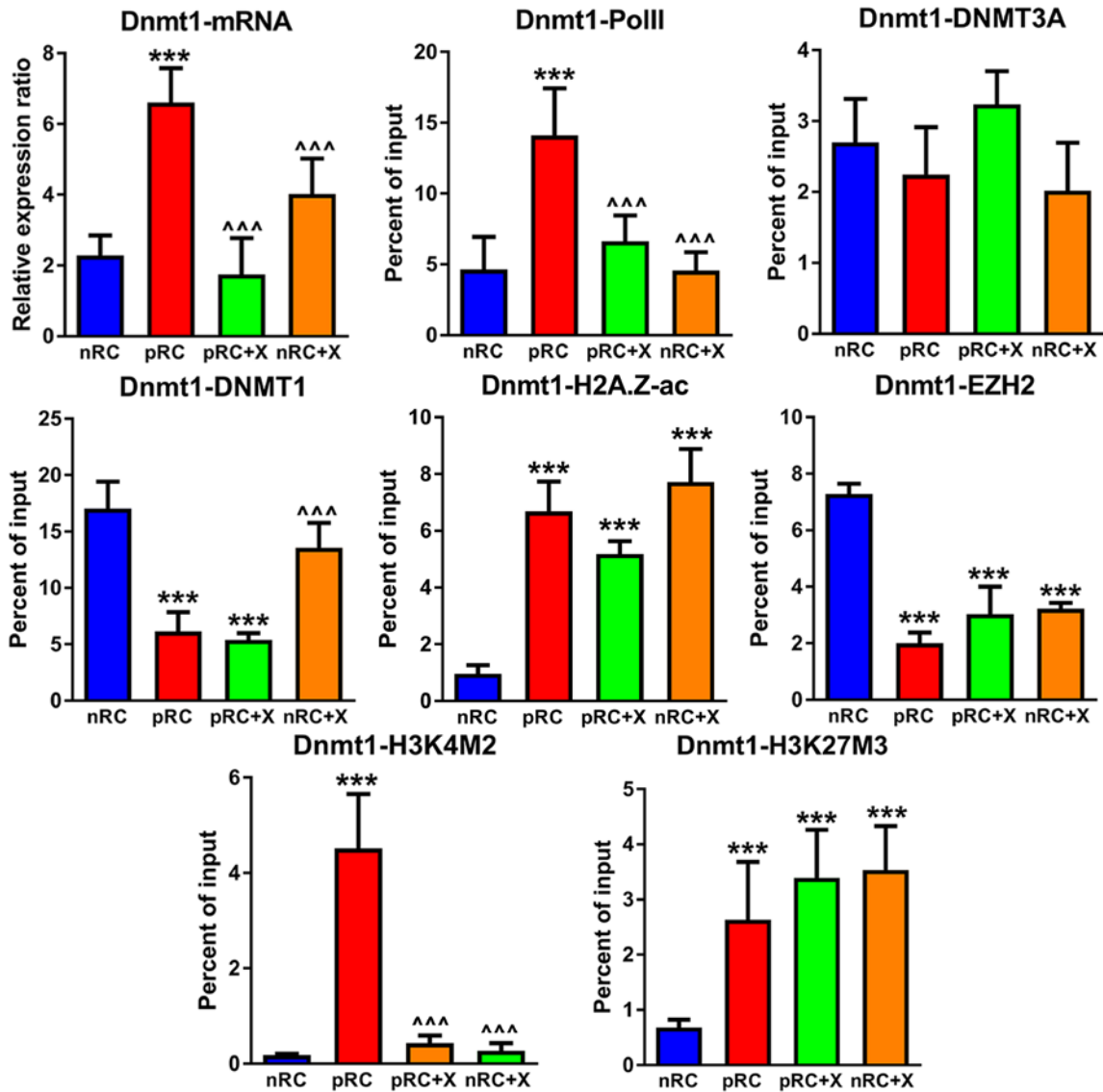


Figure 33. Regulation of memory for expression of DNA methyltransferases: Dnmt1

Transcript levels of DNA methyltransferases, DNMT1 and DNMT3a, were measured by quantitative RTPCR with normalization to expression of Rpl19. ChIP with antibodies specific to the enzymes or modified histones indicated by capitalized labels was followed by PCR for the Dnmt1 or Dnmt3a promoters. Data are mean + sd relative expression ratio for mRNA or percent of input of DNA extracts from four separate experiments. Significant differences from control nRC are designated by * $p < 0.05$ and *** $p < 0.001$, while differences from primed pRC are designated by ^ $p < 0.05$ and ^^ $p < 0.001$, as determined by one-way ANOVA followed by Tukey's ad hoc multiple comparison test.

The DNMT3a promoter exhibited activating and repressive marks, H3K4me3 and H3K27me3, respectively, across all conditions, indicating the presence of bivalent chromatin domains. Indeed, the enrichment of acetylated H2A.Z at bivalent promoters has been recently

reported (Menno P Creyghton et al., 2008). XJB-5-131 intervention modestly induced the re-binding of DNMT3a, DNMT1, and EZH2 in DNMT3a promoter along with a strong exclusion of acetylated H2A.Z. Thus, upon XJB intervention, the primed RC progeny DNMT3a resolved into a predominantly repressed state as manifested by its loss of Pol II, increased H3K27me3, but unchanged H3K4me3 levels. This promotion of the H3K27me3 mark suggests that bivalent domains could be poised for repression post-differentiation (Manching Ku et al., 2008). Indeed, H2A.Z is known to promote a permissive chromatin state by mediating nucleosome turnover (Talbert & Henikoff, 2010). In similar vein, DNMT1 also resolved into a repressed state following XJB-5-131 addition, but as a result of a significant decrease in H3K4me3 and increase in DNMT3a and DNMT1 binding to its promoter. Thus, the combination of activating and repressive DNA and histone modifications reiterates the co-existence of balancing mechanisms and emphasizes the role of poised state in cellular memory. Collectively, the emerging picture from XJB-5-131 intervention is of a myriad of correlated epigenetic regulatory mechanisms including chromatin remodeling, DNA methylation and histone modifications that converge to reset the cellular memory of the primed RC progeny and result in their exit from the poised state. Thus, this data provided the first evidence for mitochondrial role in the optimization of both static and dynamic methylation patterns that contribute to the creation of the cellular memory (Shipony et al., 2014).

3.4 DISCUSSION

How does a stem cell remember its own identity throughout a regenerative event and how is its identity transmitted to its progeny upon activation and proliferation? While the mechanistic

details of the transcriptional and epigenetic circuitries that perpetuate or erase cellular memories are being revealed, the mechanisms that coordinate these circuitries and enable their integrated outputs are less well known. Indeed, much of the emphasis over the past two decades or so has focused on detailed studies of individual molecules and their functions, despite the fact that cellular states often arise from a complex interplay of function and activity between thousands of cell constituents. Inevitably, this fragmented knowledge about these molecular systems has left gaps in understanding of how cell fate decisions are made. There is growing consensus that mitochondria are uniquely poised to provide an integrative interface between intrinsic and extrinsic mechanisms regulating the cell identity owing to their dynamic cell-wide autonomous and long range cell-to-cell non-autonomous signaling capacity. Here, we report that the mitochondria crucially optimize cellular memory and consequential fate-decisions.

Our studies provided evidence that mitochondria possess a record of the cell history and that they actively contribute to the maintenance of cellular memory. Our data revealed that mitochondrially-based fundamental mechanisms operate by driving key aspects of the collective cell population dynamics, including proliferation, cell marker expression, and distribution of crucial epigenetic modifiers. We presented a model whereby a hyperfused state of mitochondrial networks, concomitant hyperpolarization of mitochondrial membrane and enhanced generation of mitochondrial ROS promotes a poised cell state by balancing H2A.Z ac-rich bivalent domains and RNA Polymerase II activity. Thus, we identified mitochondrial functionality and morphological transitions as an integrative mechanism that optimize static and dynamic cellular memory processes by regulating several aspects of epigenetic modifiers including their expression levels, post-translational modifications, promoter activities, protein distribution and correlations. Moreover, our studies also revealed an intimate relationship

between mitochondrial and nuclear morphologies, further emphasizing a vital role of mitonuclear communications. Importantly, we provide, for the first time, statistical evidence that power laws govern these mitonuclear communications.

A stem cell must permanently fulfill the critical requirement to keep genes silent and maintain its quiescent state and yet remain transcriptionally competent to respond swiftly to unpredictable environmental fluctuations and regenerative cues. Understanding the regulatory mechanisms of this vital balance is, therefore, consequential for understanding the regenerative capacity of stem cells, notably muscle satellite cells (Asp et al., 2011). Our results constitute a paradigm shift in our understanding of regulation of the gene poising phenomena and cellular memory, as well as the relationship between mitochondria and the nucleus, and have practical and far-reaching implications both for basic mitochondrial and stem cell research as well as for regenerative medicine and the quest for novel therapeutic strategies.

4.0 MITOCHONDRIAL DYNAMICS REGULATE MYOGENIC RESERVE CELL CELL-STATE TRANSITIONS

4.1 ABSTRACT

Mitochondrial dysfunction can severely compromise stem cell functionality. During stem cell state transitions mitochondria change their morphology from discrete fragmented organelles to large continuously fused networks. However, the functional significance underlying these network dynamics is still incompletely understood. Recent studies linked stemness to mitochondrial potential and suggested that mitochondria control proliferation and early differentiation events of stem cells. We therefore investigated mitochondrial potential in myogenic RC during their transition from quiescence into an activated proliferating state. In addition, we induced aberrant mitochondrial fusion by low dose arsenite to clarify the structural properties of the mitochondrial networks during this transition using the formalism of graph theory. Our data show that excessive mitochondrial fusion promoted hyperproliferation and prolonged the activated state duration. These cellular effects coincided with enhanced mitochondrial membrane potential, augmented mitochondrial mass, the formation of giant mitochondrial network components and culminated in a robust stimulation of non-apoptotic caspase 3/7 activity, suggesting an alteration of the reserve cell self-renewal capacity. Taken together, our data demonstrated that increased mitochondrial activity and mitochondrial fusion

strike a critical balance between stemness and commitment to differentiation by controlling caspase-depend self-renewal and the duration of proliferation.

4.2 INTRODUCTION

C2C12, a subclone of Mouse C2 myoblast (Yaffe & Saxel, 1977), is a primary murine cell line that represent one of the best experimental models (Burattini et al., 2004) to investigate cell-fate decisions in general and myogenesis in particular (Blau, Chiu, & Webster, 1983). Proliferating myoblasts are the equivalent of activated satellite cells in muscle fibers, whereas the undifferentiated cells that refract from differentiation are referred to as reserve cells (N. Yoshida, S. Yoshida, K. Koishi, K. Masuda, & Y.-i. Nabeshima, 1998), and correspond to the quiescent satellite cells. The transition from undifferentiated myogenic state into fused myotubes involves a profound remodeling of mitochondrial architecture and concomitant metabolic reprogramming of the cell switching from a highly glycolytic regime to a heavy reliance on oxidative phosphorylation (Polletta et al., 2015; Sin et al., 2016; X. Wang et al., 2014). Indeed, it is now well established that mitochondrial dysfunction compromises myogenic differentiation (Wagatsuma & Sakuma, 2013). However, little is known about the interplay of mitochondrial functionality and morphology dynamics with cellular processes that govern the much earlier reversible transitions between the quiescent and activated states. Understanding the mitochondrial role in these critical transitions will provide a valuable insight into the underlying mechanisms that define cell fate decision-making and thus the homeostasis of the stem cells pool. Aberrant self-renewal and proliferation in skeletal muscle stem cells constitute convergence points of many muscular disorders (Motohashi & Asakura, 2014; Tierney & Sacco,

2016). Interestingly, mitochondria are emerging as major regulators of self-renewal (Gao et al., 2016; Hsu, Wu, Yu, & Wei, 2016; M. Khacho et al., 2016; Kofman, Huszar, & Payne, 2013) and proliferation (Mitra, 2013; Zhan et al., 2016). Thus, it was shown that mitophagy is required for the progress of C2C12 differentiation (Sin et al., 2016). In line with this requirement, inhibition of mitochondrial fission has been reported to block myogenesis (Kim et al., 2013). In this study we opposed mitochondrial fission and mitophagy by arsenic-induced mitochondrial fusion and investigated the interplay of proliferation and self-renewal with mitochondrial morphology transitions and functionality during the exit of myogenic C2C12 reserve cells from quiescence and their entry into an activated state.

4.3 RESULTS

4.3.1 Transient arsenic exposure hyperpolarizes mitochondria and causes aberrant mitochondrial dynamics

JC-1 is a cyanine dye that exhibits a fluorescence shift to longer wavelengths as it accumulates in mitochondria. JC-1 Monomers excited at 488 nm emit with a green light at 525 nm indicating a low mitochondrial potential. As the dye compartmentalizes and achieves high local mitochondrial concentrations that lead to the formation of the so-called J-aggregate, it emits also at 590 nm, indicating a higher mitochondrial potential. Because JC-1 exists in two distinct and easily detected states, JC-1 is left in excess in wells with cells during the plate-based assay with both the green 488 nm and the red 590 nm fluorescence being read for up to three hours as traces of $\Delta\Psi_m$. We cultured low-passaged C2C12 cells in growth medium until they reached near

confluence, and then switched the cell culture to a low serum medium to induce differentiation in absence or presence of 20 nM arsenite. The cells were left to differentiate for four days without changing the medium. On the fourth day, we discarded the differentiated myotubes and isolated the undifferentiated RC. Using flow cytometry, we compared JC1 staining in control and arsenic-exposed reserve cells and observed a hyperpolarization of mitochondrial membrane potential (Chapter 3, Figure 5). The fluorescent dye 10-N-nonyl acridine orange (NAO) staining, conventionally used to quantify the inner mitochondrial phospholipid cardiolipin in living cells, showed an attenuation of red fluorescence emitted by formation of NAO dimers (Figure 34).

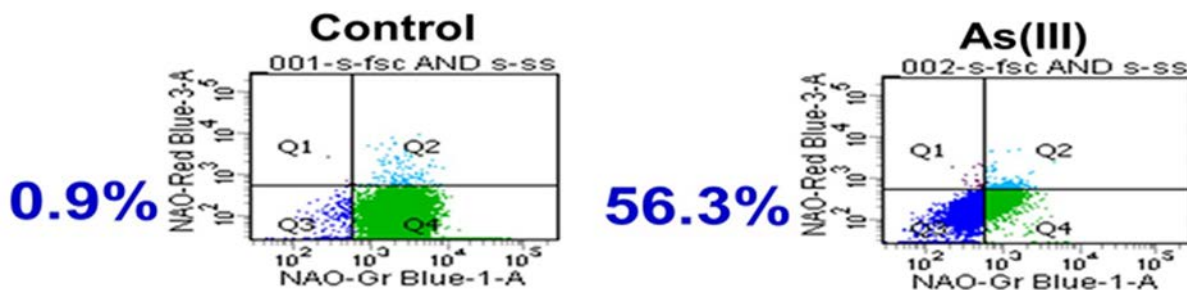


Figure 34. Arsenic decreases cardiolipin in RC mitochondria

Flow cytometric analysis for with control or arsenic exposed RC stained with NAO. The plots present results from fluorescent counts in 100,000 cells and are representative of three separate experiments.

This data indicated a decrease in cardiolipin synthesis (Gallet, Maftah, Petit, Denis-Gay, & Julien, 1995; Kaewsuya, Danielson, & Ekhterae, 2007), that seems to be compensated by the increase of cardiolipin synthase expression levels in Chapter 3, Figure 7. Next, we examined the inner and outer mitochondrial membrane and cristae shaping proteins using immunoblotting to confirm the increasing trend of Cardiolipin synthase, membrane potential and mitochondrial mass. We found a significant increase in the expression levels of the mitochondrial pro-fusion

proteins including Mfn1, Mfn2 (Figure 35) and opa1 (Figure 36). This upregulation of the mitochondrial fusogenic proteins was accompanied by an alteration of their processing and oligomeric state. Specifically, we found an extensive Oma1 and Yme11 –dependent processing of OPA1 and enhanced formation of high order opa1 oligomers (Figure 36). Moreover, the oligomeric state of the metalloprotease Oma1 and its processing were also altered (Figure 36).

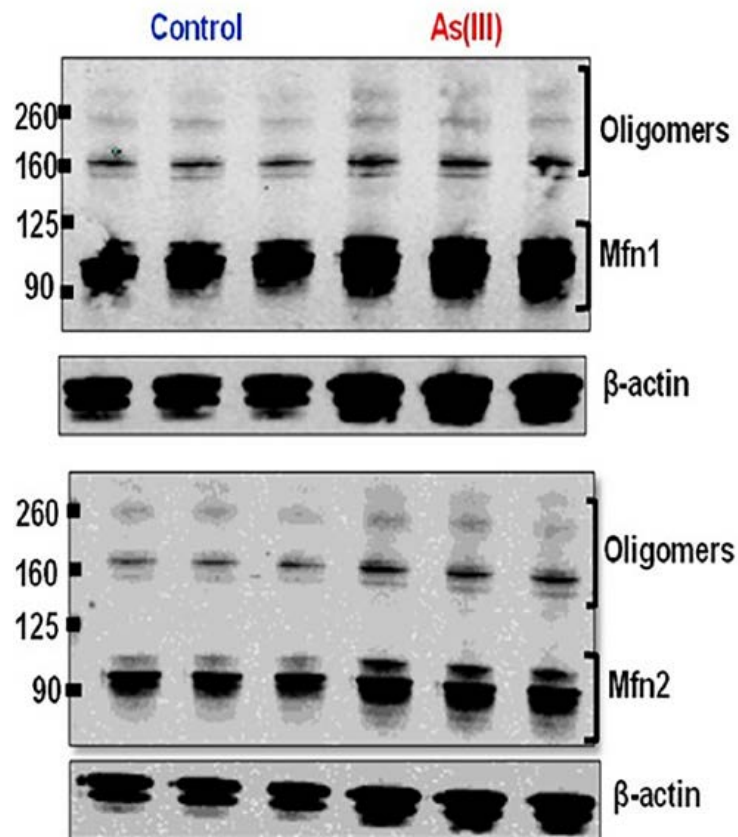


Figure 35. Arsenic increases the abundance of RC mitochondrial outer membrane pro-fusion processing proteins Mfn1 and Mfn2

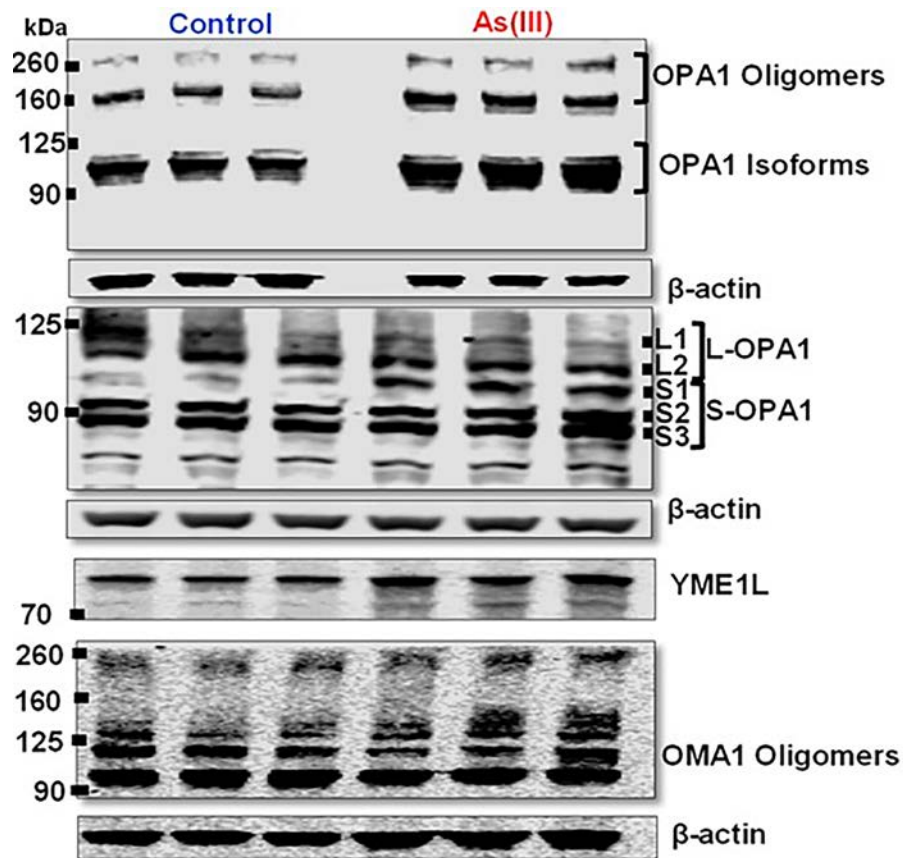


Figure 36. Arsenic-stimulation of inner mitochondrial membrane structural protein and protease processing and remodeling.

It has been shown that mitochondria control proliferation. Therefore we assessed proliferation using Carboxyfluorescein succinimidyl ester (CFSE) (Quah & Parish, 2010). CFSE covalently labels long-lived intracellular molecules with the carboxyfluorescein. Thus, as the cells divide, the progeny CFSE content is diluted. This process can be monitored by flow cytometry; lower fluorescence signals indicated higher dilution rate and thus higher proliferative capacity. We found that arsenic-exposed reserve cells have a higher proliferation rate (Figure 37) that is consistent with their enhanced cycling capacity (Chapter 3, Figure 4). Collectively these data suggest that arsenic exposed reserve cells were less prone to exit their cell cycle and commit

to differentiation. These results also suggest an important role of mitochondrial morphology dynamics in defining the RC identity.

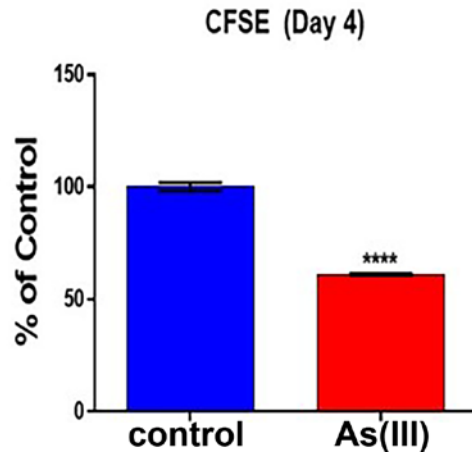


Figure 37. Arsenic stimulates RC proliferation

CFSE dye dilution was used to measure arsenic- stimulated RC proliferation. Data presented as the mean fluorescence as a percentage of naïve RC + SEM (n=3, p<0.001).

4.3.2 Aberrant mitochondrial fusion prevents resolution of cell Identity and fate decisions

Recent studies found that mitochondrial fusion was required for proper cardiomyocyte differentiation (Atsuko Kasahara, Cipolat, Chen, Dorn, & Scorrano, 2013). This mitochondrial fusion-dependent mechanism was contingent on Notch1 cleavage (NCID) (Atsuko Kasahara et al., 2013). In C2C12 cells, the upregulation or over-activation of Notch signaling through the cleaved intracellular domain leads to the downregulation of the pro-differentiation genes and consequent blockage of differentiation (Andrew S Brack, Conboy, Conboy, Shen, & Rando, 2008; Nofziger, Miyamoto, Lyons, & Weinmaster, 1999; Wilson-Rawls, Molkentin, Black, & Olson, 1999). Consistently, downregulation of Notch1 abrogated the proliferation of porcine muscle stem cells; whereas Nocht1 upregulation stimulated their proliferation (Qin et al., 2013).

Notch 1 was also required to produce a subpopulation of CD34 negative C2C12 reserve cells in an undifferentiated state. Taken together, these studies support an important role of Notch1 in muscle progenitor cells fate decisions. However, the interplay of Notch1 (NCID) and mitochondrial fusion in undifferentiated cell-state transitions has not been addressed. Flow cytometry analysis showed a 20 % increase in CD34^{Pos} / Notch1 (NICD)^{Pos} cell population in arsenic-exposed RC indicating an enhancement of the uncommitted activated state (Figure 38) and the upregulation of Notch1 activation was confirmed by immunoblotting quantification of NCID (Figure 39).

CD34 promotes satellite cell motility and entry into proliferation (Alfaro et al., 2011). To more specifically look at the importance of mitochondrial role in proliferation in affecting cell identity and fate decisions. We labeled the reserve cells after their isolation, switched them to proliferate for 3-4 days, and then co-labeled them again with the mitochondrial mass dye mitotracker deep red, the mitochondrial potential dye TMRM and the surface marker of self-renewal marker CD34. Flow cytometry showed that the primed reserve cells progeny have three-fold higher mitochondrial mass and potential population compared to naïve reserve cells progeny (Figure 33). Consistent with its proliferative role, CD34 was upregulated in primed reserve cells progeny. These results directly link the mitochondria to the emerged uncommitted proliferative reserve cells progeny subpopulation. These data also suggest that this behavior is cell-autonomous in the sense that it is inherited by the primed reserve cells progeny independent of the medium in which the cell were cultured.

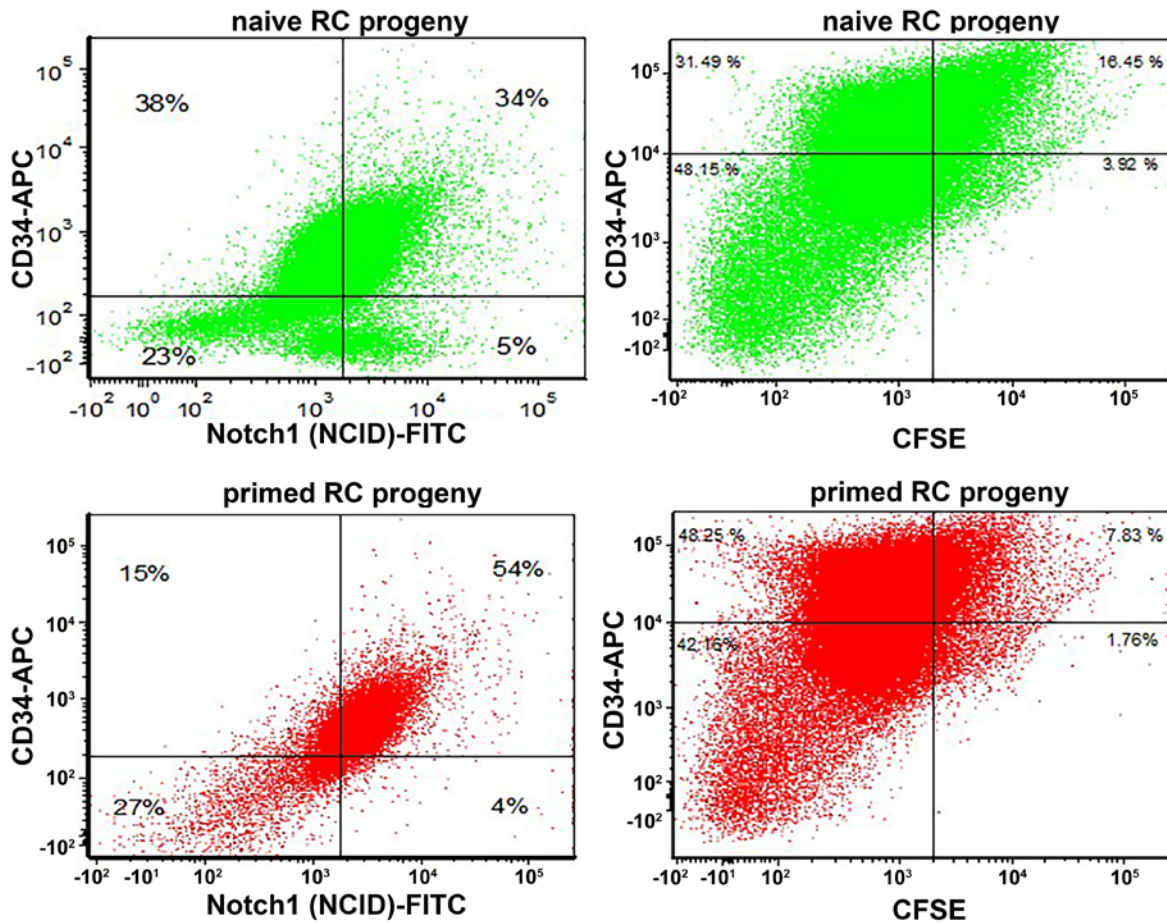


Figure 38. Arsenic-stimulated upregulation of Notch1 signaling and CD34 is associated with increased RC proliferation

Flow cytometric analysis of differentiation day 4 (DD4) reserve cells were immunostained with antibodies to the Notch1 intracellular domain and CD34. Additionally cells were stained with CFSE for four days and then immunostained with antibody to CD34. Plots are from 100,000 cells and representative of three experiments.

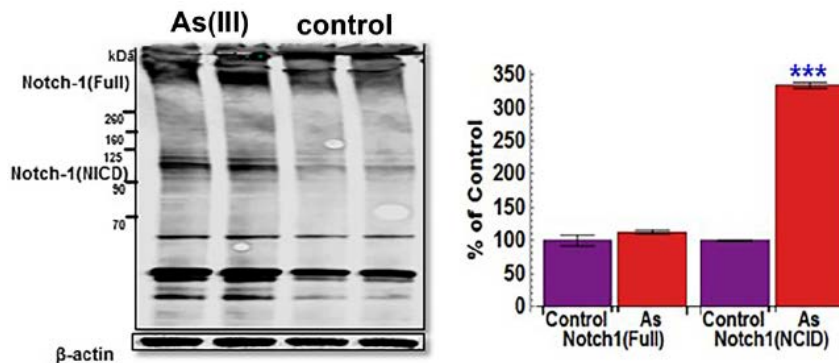


Figure 39. Confirmation of arsenic-stimulated increase in NICD variants

Whole cell protein lysates were isolated, crosslinked to capture oligomeric states and analyzed western blotting.

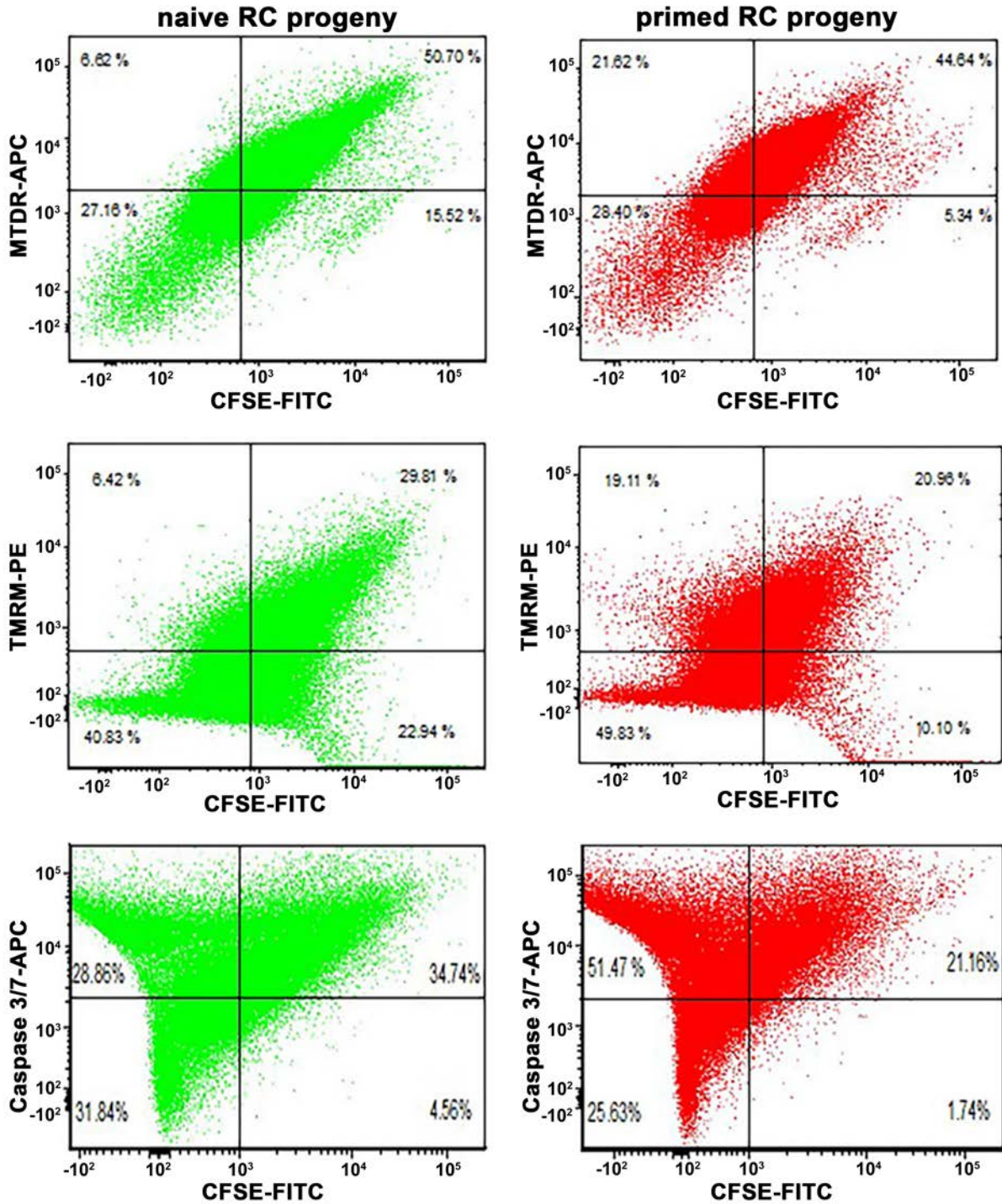


Figure 40. Arsenic increased proliferation correlates with increased mitochondrial mass, membrane potential, and non-apoptotic caspase activity
 Plots are representative of three experiments.

4.3.3 Mitochondrial hyperfusion stimulates non-apoptotic Caspase 3/7 activation

Persistent mitochondrial hyperfusion promotes caspase-dependent cell death (Westrate, Sayfie, Burgenske, & MacKeigan, 2014). However, caspase 3 has also a non-apoptotic role in myogenic cells (Bell & Megeney, 2017). In fact, Pax7 processing by caspase-3 inhibits self-renewal of skeletal muscle stem cells, suggesting the possibility of yet another mechanism that mediates mitochondrial dynamic influence on cell fate decisions. We therefore labeled the isolated reserve cells with CFSE and let them proliferate for 3 to 4 days. The cells were then co-labeled with caspase3/7 fluorescent inhibitor probe FAM-DEVD-FMK to measure caspase3/7 activity by flow cytometry. Primed proliferating cells exhibited a twofold increase in caspase 3/7 activity (Figure 40). However, the RC and RC progeny showed no cell death as evidenced by no change in Annexin V and PI double staining before and after proliferation respectively (Figure 41).

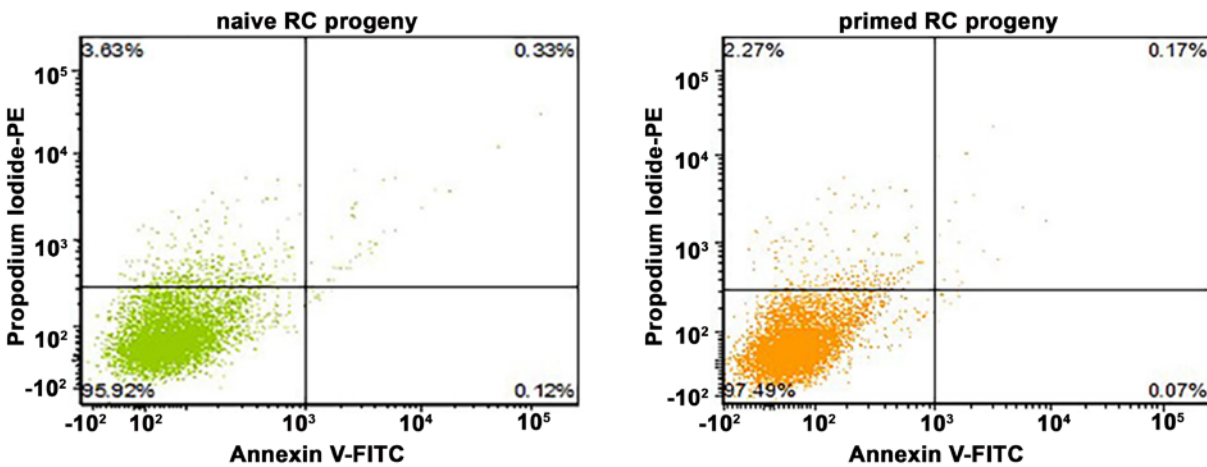
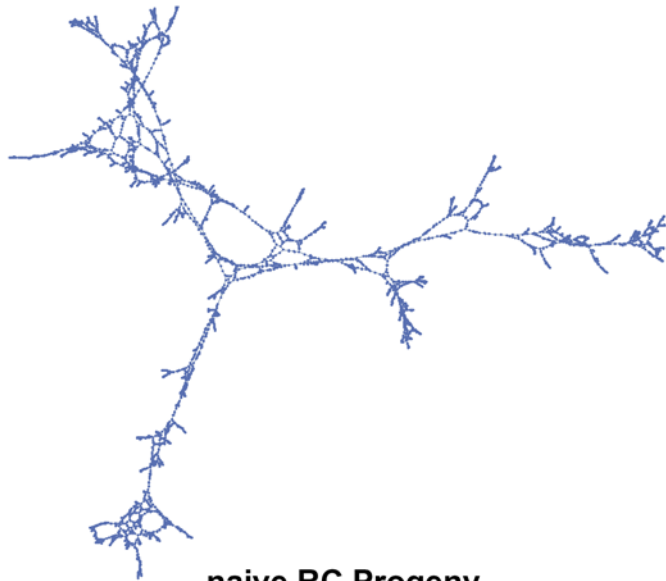
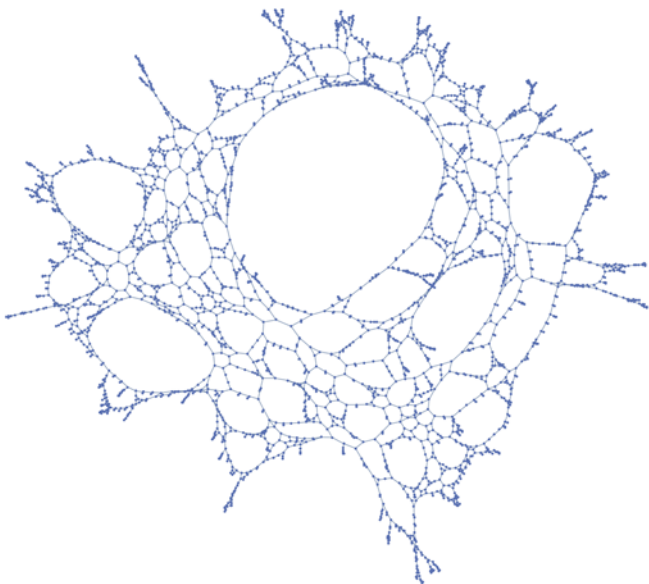
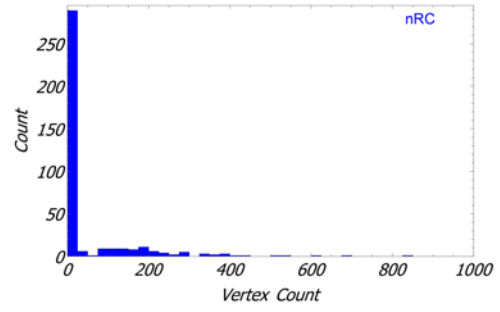


Figure 41. Arsenic does not promote apoptosis in RC



naive RC Progeny



primed RC progeny

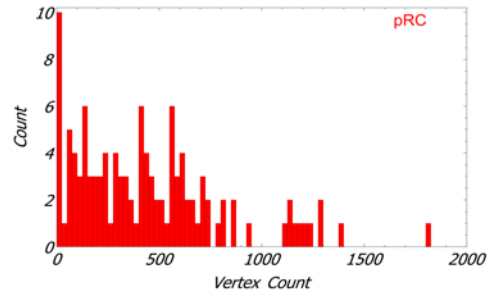


Figure 42. Arsenic increases mitochondrial network connectivity and mass

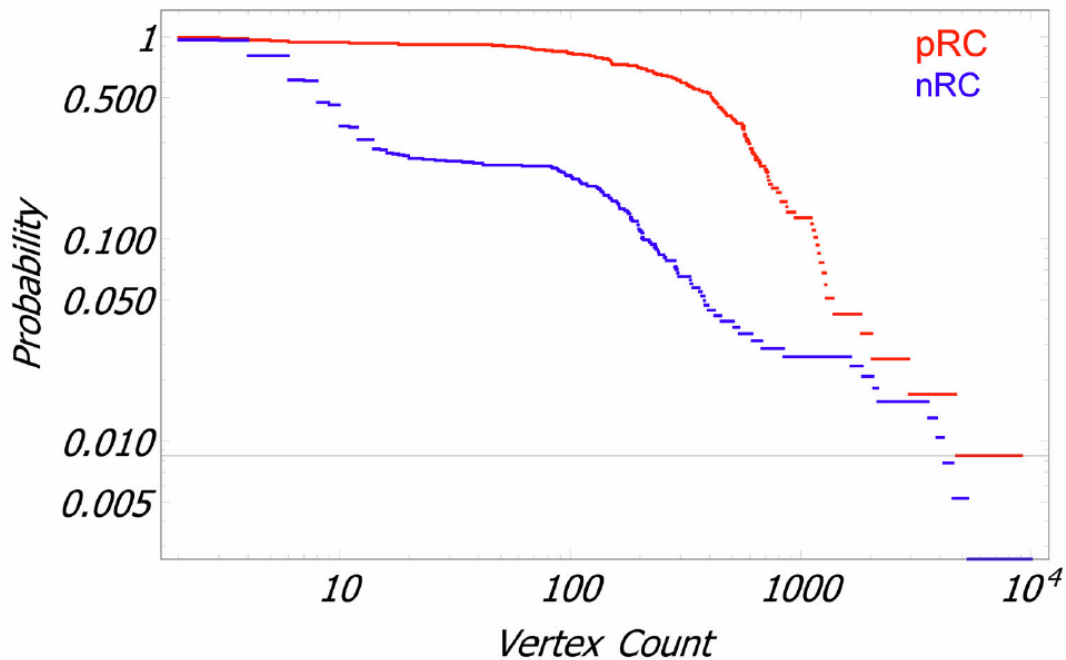


Figure 43. Increased probability of higher connectivity in arsenic-exposed RC

To investigate the mitochondrial dynamics underlying the hyperproliferative behavior of primed RC progeny, we fixed RC progeny and labeled mitochondria with Tom20. Consistent with the immunoblotting profile of the profusion proteins, confocal imaging revealed a more connected network in primed RC progeny. To gain more insight into the structural properties of the mitochondrial networks, we skeletonized binarized mitochondria images and we performed a recursive Otsu's cluster variance maximization to probe the level of the networks connectivity. Primed RC progeny displayed more giant network components (Figure 35) (Strogatz, 2001) corresponding to hyperfused mitochondrial networks and supporting the notion of long range physical cell-to-cell signaling via mitochondria (Scholkmann, 2016). Quantification of nodes (i.e. vertex) count showed that they are more abundant in primed RC progeny compared to naïve

progeny (Figure 42) further confirming the hyperfused state of their mitochondrial networks in Chapter 3, Figure 12 . Collectively, these data suggest that mitochondrial fusion plays a crucial role in determining the self-renewal potential of the myogenic cells.

4.4 DISCUSSION

This study demonstrated that mitochondrial dynamics play a dual role in regulating the fate of myogenic cells. Taken together the experimental data suggest that mitochondrial fusion maintains a subpopulation of myogenic cells in a cycling activated state by promoting proliferation and thus preventing the exit from the cell cycle and commitment to differentiation. On the other hand, mitochondrial fusion limits the self-renewal potential of cycling cells and therefore prevents them from reverting to their ground quiescent state.

Mitochondrial networks exhibit three broad regimes of behavior: hyperfused, fused, and fragmented. In the hyperfused regime, mitochondria adopt a static configuration of constant activity. This is manifested by the formation of cell-wide and long-range connected mitochondrial clusters, or giant mitochondrial components co-existing with fragmented mitochondria whose activities are fluctuating and complex. Under this regime cell-state transitions are de facto put on hold and the cells enter a poised cellular state that when prolonged leads to pathological outcomes

5.0 CONCLUSIONS

5.1 NOVEL MECHANISMS FOR ARSENIC-INDUCED MALADAPTIVE RESPONSE

The modulation of mitochondrial dynamics and functionality is a powerful integrative mechanism of both intra-cellular and long-range cell-to cell- signaling that enable the complex stem cell behavior. Indeed, beyond the classical bioenergetic and biosynthetic roles of mitochondria, their view as signaling organelles is increasingly recognized. The mito-toxicity of arsenic is well established and is generally explained by the direct and physical interaction with key mitochondrial enzymes leading to their inhibition and thus to a depolarized and dysfunctional mitochondria. This type of arsenical toxicology is typically associated with apoptotic and necrotic endpoints. Our study is concerned with near real-life non-apoptotic pathophysiological basis of arsenic exposure. We provided several lines of evidence for an alternative mechanism that is not based on direct physical influence of arsenic but rather on the re-purposing of mitochondrial functionality in response to the arsenic-imposed redox state that possibly emerge as a consequence of its reactivity with cytoplasmic thiols groups. According to our model, the arsenic influence has to be understood within the framework of its Warburg-like effects leading result to the re-configuration of mitochondrial morphology and functionality that sustain specific epigenetic programs. The latter are responsible for establishing, maintaining and

modulating the cellular memory that enable a stem and many cancer cells to exhibit a remarkable resilience to environmental fluctuation and (mal) adaptive potentials.

5.2 IMPACT OF STRESS MEMORY ON MUSCLE STEM CELL FATE AND LOSS OF HOMEOSTATIC INTEGRITY

The prolonged cellular response to transient regenerative or environmental cues is typical of many differentiation programs including myogenesis. The effectiveness of the latter depends on the tight regulation of the muscle stem cells heterogeneity, which ensure both the repair and replacement of damaged tissue, and the replenishment of the reserve stem cell pool at the completion of a regenerative event. Thus, the heterogeneity of the muscle stem cell population can encode distinct and heritable cell fates derive from the integration of a constellation of mechanisms ranging from subcellular to cell population level. Our study showed that such population level heterogeneity is the fundamental basis of cellular memory and stem cell population plasticity. The conversion of a transient stress exposure into a sustained response alters the stem cell identity; memory of stress lead to chromatin states that impose unexpected constraints on the cell fate-decisions and the persistence of such constraints can ultimately lead to the compromise of the muscle stem cell niche homeostasis.

5.3 IMPLICATIONS OF THE POWER-LAW FOR STEM CELL DECISIONS MAKING

Power-law favor the occurrence of extreme events in the sense that there are a lots of very small (expected) events but also few very large ones. The small events dominate such as the average will be reflective of the small events dynamics whereas the large ones get averaged away and unnoticed. In response to injury, the quiescent stem cells population exit their quiescence, become activated and proliferate thus giving rise to a stochastic dynamical system far from equilibrium where cell contents are constantly synthesized and degraded; simultaneously, cells grow, divide, and transmit their properties to their progeny. Because of this inherent stochasticity in the collective dynamics of stem cell populations, they are diverse in their properties, even though they are genetically identical. Power law has implications for performance optimization of these collective dynamics: to find and to optimize the distribution of cell states that maintain the homeostasis of a given tissue and its stem cell reserve pool. It explains why major cellular defects can remain hidden for years and years. Because they are extremely rare and operate under a law that mask their presence and their slowly progressing effects. Most cellular alterations will occur in a few places and most of the cell functionality will remain stable and unchanging. However, as the usage of these cellular processes increase, say with aging, the impact of their alteration will be sensed far more often and the stem cell functionality and integrity become increasingly compromised. From therapeutic perspective, since it is difficult to know in advance which parts of the stem cell functionality need intervention (power law implications) , it's important to understand the integrative mechanism that are built-in the cell so we can modulate them to account for extremes occurrences . Just because some function has not changed in the last year does not mean it will not change again soon. The fact that the cell is

using it shows it is more likely to change. Most of the biomedical decisions on a normal distribution are wrong. There is an urgent need to learn to investigate the stem cell in power law rationale.

5.4 SUMMARY AND FUTURE DIRECTIONS

In the present study, the role of mitochondrial dynamics and functionality in cellular memory, cell population heterogeneity, and cell-fate decisions, during the transition of myogenic reserve cells from quiescence into an activated state was explored. We pioneered an in vitro natural cellular memory model, arsenic-induced stress memory in myogenic reserve cells. We determined the functional profile of mitochondria including ROS production, mitochondrial membrane potential, mitochondrial mass, mitochondrial bioenergetics, mitochondrial ultrastructural remodeling and mitochondrial morphology dynamics, during cell-state transitions, of both naïve and primed reserve cells as well as their progeny after several generations after transient exposure to a single 20 nM of arsenic, a concentration that is highly relevant to real-life human exposure. We reported that mitochondria dynamics and functionality control the overall cell population dynamics including proliferation and self-renewal. Consistently with its known Warburg-like effects, arsenic promoted proliferation. Our study also revealed that arsenic limits the self-renewal potential of the stem cell. The convergence of these two arsenical effects resulted in cellular poised state, indicating an active role of mitochondria in the cell-fate decisions-making. Further investigations led us to discover a previously unknown role of mitochondria in controlling cellular memory. Using a combination of cell culture, mitochondrial assays, imaging, non-Gaussian statistical analysis and epigenetic techniques, we described the

details of mitochondrial role in optimizing cellular memory mechanisms that confer memory including the modulation of major epigenetic modifiers expression levels and distribution in the cell population and post-translational . This in turn led to the conclusion that cellular memory is a statistical property that is encoded in the cell population heterogeneity. Specifically, the progeny of a subpopulation of primed myogenic reserve cells inherited the memory of stress according to distributions of nuclear metrics that obey power law. Moreover, our study also revealed an intimate relationship between mitochondrial and nuclear morphologies that is being reported for the first time. Importantly, mitochondrially-targeted intervention with XJB-5-131 was effectively successful in reversing all the above described arsenic-induced alterations. Thus, given the role of mitochondrial dysfunction in wide array of pathologies including neuromuscular degenerative diseases, our work suggests the possibility of a novel therapeutic window and identify mitochondria as one of the primary target for drug discovery to cure these diseases.

We intend to continue our effort in capitalizing on mathematical, physical and computational technical and conceptual tools to further clarify the mitochondrial mechanisms that coordinate cell autonomous and non-autonomous processes as well as mitochondrial long-range functions at the cell population and beyond.

BIBLIOGRAPHY

- Aballay, LR, Díaz, MP, Francisca, FM, Muñoz, SE. 2012. Cancer incidence and pattern of arsenic concentration in drinking water wells in Córdoba, Argentina. *Int J Environ Health Res.* 22(3):220-31
- Abernathy, CO, Thomas, DJ, Calderon, RL. 2003. Health Effects and Risk Assessment of Arsenic. *The Journal of Nutrition* 133:1536S-1538S.
- Akaike, H. 1973. Information theory and an extension of the maximum likelihood principle. In *Proceedings of 2nd International Symposium on Information Theory, Budapest, Hungary*, pp. 267–281
- Arsenic: Assembly of Life Sciences (U.S.) Committee on Medical and Biologic Effects of Environmental Pollutants. 1977. Washington: National Academy of Sciences.
- Agency for Toxic Substances and Disease Registry (ATSDR). Toxicological profile for arsenic. 2007.
- Baastrup, R, Sørensen, M, Balstrøm, T, Frederiksen, K, Larsen, CL, Tjønneland, A, et al. 2008. Arsenic in drinking-water and risk for cancer in Denmark. *Environ Health Perspect* 116(2):231–237.
- Bates, MN, Smith, AH, Cantor, KP. 1995. Case-control study of bladder cancer and arsenic in drinking water. *Am J Epidemiol* 111:523-530
- Bates, MN, Rey, OA, Biggs, ML, Hopenhayn, C, Moore, LE, Kalman, D, et al. 2004. Case-control study of bladder cancer and exposure to arsenic in Argentina. *Am J Epidemiol* 159(4):381–389.
- Begum, M., Horowitz, J., and Hossain, M.I. 2012. Low-Dose Risk Assessment for Arsenic: A Meta-Analysis Approach. *Asia Pac J Public Health*. DOI: 10.1177/1010539512466568.
- Bhattacharya, P, Welch, AH, Stollenwerk, KG, McLaughlin, MJ, Bundschuh, J, Panaullah, G. 2007. Arsenic in the environment: Biology and Chemistry. *Sci Total Environ* 379: 109-120.

- Biswas, A, Biswas, S, Santra, SC. 2012. Risk from winter vegetables and pulses produced in arsenic endemic areas of Nadia District: field study comparison with market basket survey. *Bull Environ Contam Toxicol* 88:909-914.
- Braun, A, Zhang, S, Miettinen, HE, Ebrahim, S, Holm, TM, Vasile, E, et al. 2003. Probuocol prevents early coronary heart disease and death in the high-density lipoprotein receptor SR-BI/apolipoprotein E double knockout mouse. *Proc. Natl. Acad. Sci. USA* 100, 7283–7288.
- Brown, KG and Ross, GL. 2002. Arsenic, drinking water, and health: a position paper of the American Council on Science and Health. *Regul Toxicol Pharmacol* 36: 162-174,
- Carey, AM, Lombi, E, Donner, E, de Jonge, MD, Punshon, T, Jackson, BP, Guerinot, ML, Price, AH, Meharg, AA. 2012. A review of recent developments in the speciation and location of arsenic and selenium in rice grain. *Anal Bioanal Chem* 402:3275-3286.
- Casarett & Doull's Essentials of Toxicology, 2010. Second Edition ISBN:9780071622400
- Challenger, F. 1947. Biological methylation. *Sci. Prog.* 35, 396–416.
- Challenger, F. 1951. Biological methylation. *Adv. Enzymol. Relat. Subj. Biochem.* 12, 429–491.
- Chen, CJ, Chuang, YC, Lin, TM, Wu, HY. 1985. Malignant neoplasms among residents of a blackfoot disease-endemic area in Taiwan: high-arsenic artesian well water and cancers. *Cancer Res* , 45: 5895–5899.
- Chen, CJ, Chuang, YC, You, SL et al. 1986. A retrospective study on malignant neoplasms of bladder, lung and liver in blackfoot disease endemic area in Taiwan. *Br J Cancer*, 53: 399–405. PMID:3964542
- Chen CJ, Kuo TL, Wu MM. 1988. Arsenic and cancers [Letter]. *Lancet* ii:414-415
- Chen, CJ, Kuo, TL, Wu, MM 1988a. Arsenic and cancers. *Lancet*, 331: 414–415.
- Chen, CJ, Wu, MM, Lee, SS et al. 1988b. Atherogenicity and carcinogenicity of high-arsenic artesian well water. Multiple risk factors and related malignant neoplasms of blackfoot disease. *Arteriosclerosis*, 8: 452–460.
- Chen, CJ and Wang, CJ. 1990. Ecologicalal correlation between arsenic level in well water and age-adjusted mortality from malignant neoplasms. *Cancer Res*, 50: 5470–5474.
- Chen, CJ, Chen, CW, Wu, MM, Kuo, TL. 1992. Cancer potential in liver, lung, bladder and kidney due to ingested inorganic arsenic in drinking water. *Br J Cancer*. 66:888-892

- Chen, CL, Chiou, HY, Hsu, LI, Hsueh, YM, Wu, MM, Chen, CJ. 2010a. Ingested arsenic, characteristics of well water consumption and risk of different histological types of lung cancer in northeastern Taiwan. *Environ Res* 110(5):455–462.
- Chen, CL, Chiou, HY, Hsu, LI, Hsueh, YM, Wu, MM, Wang, YH, et al. 2010b. Arsenic in drinking water and risk of urinary tract cancer: a follow-up study from northeastern Taiwan. *Cancer Epidemiol Biomarkers Prev* 19(1):101–110.
- Chen, CL, Hsu, LI, Chiou, HY et al. Blackfoot Disease Study Group. 2004. Ingested arsenic, cigarette smoking, and lung cancer risk: a follow-up study in arseniasis endemic areas in Taiwan. *JAMA*, 292: 2984–2990.
- Chen, YC, Su, HJ, Guo, YL et al. 2003. Arsenic methylation and bladder cancer risk in Taiwan. *Cancer Causes Control*, 14: 303–310.
- Chen, YC, Su, HJ, Guo, YL et al. 2005. Interaction between environmental tobacco smoke and arsenic methylation ability on the risk of bladder cancer. *Cancer Causes Control*, 16: 75–81.
- Chen, Y, Hall, M, Graziano, JH, Slavkovich, V, van Geen, A, Parvez, F, Ahsan, H. 2007. A prospective study of blood selenium levels and the risk of arsenic-related premalignant skin lesions. *Cancer Epidemiol Biomarkers Prev* 16:207-213.
- Chen, Y, Graziano, JH, Parvez, F, Liu, M, Slavkovich, V, Kalra, T, Argos, M, Islam, T, Ahmed, A, Rakibuz-Zaman, M, et al. 2011. Arsenic exposure from drinking water and mortality from cardiovascular disease in Bangladesh: prospective cohort study. *BMJ* 342:d2431.
- Chiang, HS, Guo, HR, Hong, CL et al., 1993. The incidence of bladder cancer in the black foot disease endemic area in Taiwan. *Br J Urol*, 71: 274–278.
- Chiou, HY, Hsueh, YM, Liaw, KF et al. 1995. Incidence of internal cancers and ingested inorganic arsenic: a seven-year follow-up study in Taiwan. *Cancer Res*, 55: 1296–1300.
- Chiou, HY, Chiou, ST, Hsu, YH et al. 2001. Incidence of transitional cell carcinoma and arsenic in drinking water: a follow-up study of 8,102 residents in an arseniasis-endemic area in northeastern Taiwan. *Am J Epidemiol*, 153: 411–418.
- Christoforidou, EP, Riza, E, Kales, SN, Hadjistavrou, K., Stoltidi, M, Kastania, AN,,Linos, A. 2013. Bladder cancer and arsenic through drinking water: a systematic review of epidemiologic evidence. *J Environ Sci Health A Tox Hazard Subst Environ Eng* 48:1764-1775.
- Collingridge, D. 2014. Three countries - half of the global cancer burden. *The Lancet Oncology* 15:483.

- Crump, KS. 1984. A new method for determining allowable daily intakes. *Fundam Appl Toxicol* 4:854-871.
- Currier, JM, Saunders, RJ, Ding, L, Bodnar, W, Cable, Matousek, T, Creed, JT, Styblo, M. 2013. Comparative oxidation state specific analysis of arsenic species by high-performance liquid chromatography- inductively coupled plasma-mass spectrometry and hydride generation-cryotrapping-atomic absorption spectrometry. *J. Anal. Atom. Spectrom.* 28(6):843-852.
- Cuzick ,J, Sasieni, P, Evans, S 1992. Ingested arsenic, keratoses, and bladder cancer. *Am J Epidemiol*, 136: 417–421.
- Daugherty, A, and Whitman, SC. 2003. Quantification of atherosclerosis in mice. *Methods Mol. Biol.* 209, 293–309.
- Davis, MA, Mackenzie, TA, Cottingham, KL, Gilbert-Diamond, D, Punshon, T, Karagas, MR. 2012. Rice consumption and urinary arsenic concentrations in US children. *Environ Health Perspect* 120:1418-1424.
- De Backer, GG. 2009. The global burden of coronary heart disease. *Medicographia.* 31:4
- Diaz-Barriga F, Santos MA, Mejia JJ, Batres L, Yanez L, Carrizales L, Vera E, del Razo LM, and Cebrian ME. Arsenic and cadmium exposure in children living near a smelter complex in San Luis Potosi, Mexico. *Environ Res* 62: 242-250, 1993.
- Diaz, OP, Leyton, I, Munoz, O, Nunez, N, Devesa, V, Suner, MA, Velez, D, Montoro, R. 2004. Contribution of water, bread, and vegetables (raw and cooked) to dietary intake of inorganic arsenic in a rural village of Northern Chile. *J Agric Food Chem* 52:1773-1779.
- Dittmar, J, Voegelin, A, Maurer, F, Roberts, LC, Hug, SJ, Saha, GC, Ali, MA, Badruzzaman, ABM, Kretzschmar, R. 2010. Arsenic in Soil and Irrigation Water Affects Arsenic Uptake by Rice: Complementary Insights from Field and Pot Studies. *Environmental Science & Technology* 44:8842-8848.
- Dopp, E, von Recklinghausen, U, Diaz-Bone, R, Hirner, AV, Rettenmeier, AW. 2010. Cellular uptake, subcellular distribution and toxicity of arsenic compounds in methylating and non-methylating cells. *Environ. Res.* 110:435-442.
- Duker AA, Carranza EJ, and Hale M.2005. Arsenic geochemistry and health. *Environ Int* 31: 631-641
- Edmonds JS, and Francesconi KA. 2003. Arsenic in seafoods-human health-aspects and regulations. *Marine Pollutants Bulletin* 26, 665-674.

- El-Masri, HA, and Kenyon, EM. 2008. Development of a human physiologically based pharmacokinetic (PBPK) model for inorganic arsenic and its mono- and di-methylated metabolites. *J. Pharmacokinet. Pharmacodyn.* 35(1):31-68.
- European Food safety Authority. 2009. EFSA panel on contaminants in the food chain (contam): Scientific opinion on arsenic in food. *EFSA J.* 7:60-71.
- Ferreccio, C, Gonzalez, C, Milosavjlevic, V et al. 2000. Lung cancer and arsenic concentrations in drinking water in Chile. *Epidemiology*, 11: 673–679.
- Ferreccio, C, Yuan, Y, Calle, J, Benitez, H, Parra, RL, Acevedo, J, Smith, AH, Liaw, J, Steinmaus, C. 2013. Arsenic, tobacco smoke, and occupation: associations of multiple agents with lung and bladder cancer. *Epidemiology* 24:898-905.
- Flanagan, SV, Johnston, RB and Zheng, Y. 2012. Arsenic in tube well water in Bangladesh: health and economic impacts and implications for arsenic mitigation. *Bull World Health Organ* 90:839-846.
- Focazio, MJ, Welch, AH, Watkins, SA, Helsel, DR, and Horn, MA. 1999. A Retrospective Analysis on the Occurrence of Arsenic in Ground- Water Resources of the United States and Limitations in Drinking Water Supply Characterizations. *USGS Water-Resources Investigations Report 99-4279*, pp.27.
- Francesconi, KA, Kuehnelt, D. 2002. Arsenic compounds in the environment. In: *Environmental Chemistry of Arsenic. Books in Soils, Plants, and the Environment.* Marcel Dekker, (Ed), New York, 51-94.
- Freeman, GB, Johnson, JD, Killinger, JM, Liao, SC, Davis, AO, Ruby, MV, Chaney, RL, Lovre, SC, Bergstrom, PD. Bioavailability of arsenic in soil impacted by smelter activities following oral administration in rabbits. *Fundam Appl Toxicol* 21: 83-88, 1993.
- Fricke, MW, Zeller, M, Sun, H, Cullen, WR, Shoemaker, JA, Witkowski, MR, Creed, JT. 2005. Chromatographic separation and identification of products from the reaction of dimethylarsinic acid with hydrogen sulfide. *Chem. Res. Toxicol.* 18(12):1821-1829.
- FSA (Food Standards Agency). 2004. Arsenic in seaweed, July 2004. Available from: <http://www.food.gov.uk/multimedia/pdfs/arsenicseaweed.pdf>, p. 4.
- García-Esquinas, E, Pollán, M, Umans, JG, Francesconi, KA, Goessler, W, Guallar, E, Howard, B, Farley, J, Best, LG, Navas-Acien, A. 2013. Arsenic exposure and cancer mortality in a US-based prospective cohort: the strong heart study. *Cancer Epidemiol Biomarkers Prev.* 22(11):1944-53.
- Gibb, H, Haver, C, Gaylor, D, Ramasamy, S, Lee, JS, Lobdell, D, Wade, T, Chen, C, White, P, Sams, R. 2011. Utility of recent studies to assess the National Research Council 2001 estimates of cancer risk from ingested arsenic. *Environ Health Perspect* 119:284-290.

Globocan 2008 (IARC) , Section of Cancer Information (06/10/2013)
<http://globocan.iarc.fr/Default.aspx>

Goss, PE, Strasser-Weippl, K, Lee-Bychkovsky, BL, Fan, L, Li, J, Chavarri-Guerra, Y, Liedke, PER, Pramesh, CS, et al. 2014. Challenges to effective cancer control in China, India, and Russia. *The Lancet Oncology* 15:489-538

Hall, MN and Gamble, MV. 2012. Nutritional manipulation of one-carbon metabolism: effects on arsenic methylation and toxicity. *J Toxicol* 2012:595307.

Hayakawa, T, Kobayashi, Y, Cui, X, Hirano, S. 2005. A new metabolic pathway of arsenite: arsenic-glutathione complex- es are substrates for human arsenic methyltransferase Cyt19. *Archives of Toxicology*, vol. 79, no. 4, pp. 183–191, 2005.

Hopenhayn-Rich, C, Biggs, ML, Fuchs, A et al. 1996. Bladder cancer mortality associated with arsenic in drinking water in Argentina. *Epidemiology*, 7:117–124.

Hopenhayn-Rich, C, Biggs, ML, Smith, AH.1998. Lung and kidney cancer mortality associated with arsenic in drinking water in Cordoba, Argentina. *Int J Epidemiol* , 27: 561–569.

Hsueh, YM, Cheng, GS, Wu, MM, Yu, HS, Kuo, TL, Chen, CJ. 1995. Multiple risk factors associated with arsenic-induced skin cancer: effects of chronic liver disease and malnutritional status. *Br J Cancer* 71:109-114.

Huang, YK, Huang, YL, Hsueh, YM et al. 2008. Arsenic exposure, urinary arsenic speciation, and the incidence of urothelial carcinoma: a twelve-year follow-up study. *Cancer Causes Control*, 19: 829–839.

Hughes, MF, Beck, BD, Chen, Y, Lewis, AS, Thomas, DJ. 2011. Arsenic Exposure and Toxicology: A Historical Perspective. *Toxicological Sciences*. 123:305-332.

International Agency for Research on Cancer (IARC) 2012. Arsenic, metals, fibres, dusts. In *IARC Monographs Vol 100.c*; available from:
<http://monographs.iarc.fr/ENG/Monographs/vol100C/index.php>.

Jacobson, JL, Janisse, J, Banerjee, M, Jester, J, Jacobson, SW, Ager JW. 2002. A Benchmark Dose Analysis of Prenatal Exposure to Polychlorinated Biphenyls. *Environmental Health Perspectives* 110:4

Joint Food and Agriculture Organization of the United Nations (FAO)/World Health Organization (WHO) Expert Committee on Food Additives (JECFA) 2011. Safety evaluation of certain contaminants in food. In *WHO Food Additives Series: 63*, FAO JECFA Monographs. Geneva, Switzerland available at
http://whqlibdoc.who.int/trs/who_trs_959_eng.pdf

- Jones FT. 2007. A broad view of arsenic. *Poult Sci* 86: 2-14.
- Julshamn K, Lundebye AK, Heggstad K, Berntssen MH, Boe B, 2004. Norwegian monitoring programme on the inorganic and organic contaminants in fish caught in the Barents Sea, Norwegian Sea and North Sea, 1994-2001. *Food Additives & Contaminants*. 21(4), 365-376.
- Karagas, MR, Stokel, TA, Morris, JS, Tosteson, TD, Weiss, JE, Spencer, SK, Greenberg, ER. 2001. Skin cancer risk in relation to toenail arsenic concentrations in a US population based case-control study. *Am. J. Epidemiol.*153, 559–565.
- Karagas, MR, Tosteson, TD, Morris, JS, Demidenko, E, Mott, LA, Heaney, J, Schned, A. 2004. Incidence of transitional cell carcinoma of the bladder and arsenic exposure in New Hampshire. *Cancer Causes Control*. 15, 465–472
- Karagas, MR, Tosteson, TD, Blum, J, Klaue, B, Weiss, JE, Stannard, V, et al. 2000. Measurement of low levels of arsenic exposure: a comparison of water and toenail concentrations. *Am J Epidemiol* 152:84–90.
- Kile, ML, Houseman, EA, Rodrigues, E, Smith, TJ, Quamruzzaman, Q, Rahman, M, et al. 2005. Toenail arsenic concentrations, GSTT1 gene polymorphisms, and arsenic exposure from drinking water. *Cancer Epidemiol Biomarkers Prev* 14:2419–2426.
- Kile, ML, Houseman, EA, Breton, CV, Smith, T, Quamruzzaman, Q, Rahman, M, Mahiuddin, G, and Christiani, DC. 2007. Dietary arsenic exposure in bangladesh. *Environ Health Perspect* 115:889-893.
- Kobayashi, Y, Hayakawa, T , Hirano, S. 2007. Expression and activity of arsenic methyltransferase Cyt19 in rat tissues. *Environ. Toxicol. Pharmacol.* 21(1):115-120.
- Kuchenmüller, T, Hird, S, Stein, C, Kramarz, P, Nanda, A, Havelaar, AH. 2009. Estimating the global burden of foodborne diseases- a collaborative effort. *Eurosurveillance* Vol.14, Issue 18.
- Kurtio, P, Pukkala, E, Kahelin, H, Auvinen, A, Pekkanen, J. 1999. Arsenic concentrations in well water and risk of bladder and kidney cancer in Finland. *Environ Health Perspect* 107:705–710
- Kurzius-Spencer, M, Burgess, JL, Harris, RB, Hartz, V, Roberge, J, Huang, S, Hsu, CH, O'Rourke, MK. 2014. Contribution of diet to aggregate arsenic exposures-An analysis across populations. *J Expo Sci Environ Epidemiol* 24:156-162.
- Lemaire, M, Lemarie, CA, Molina, MF, Schiffrin, EL, Lehoux, S, Mann, KK. 2011. Exposure to Moderate Arsenic Concentrations Increases Atherosclerosis in ApoE^{-/-} Mouse Model. *Toxicological Sciences* 122(1), 211–221

- Leonardi, G, Vahter, M et al 2012. Inorganic Arsenic and Basal Cell Carcinoma in Areas of Hungary, Romania, and Slovakia: A Case–Control Study. *Environmental Health Perspectives*. 120:5.
- Liaw, J, Marshall, G, Yuan, Y et al. 2008. Increased childhood liver cancer mortality and arsenic in drinking water in northern Chile. *Cancer Epidemiol Biomarkers Prev* , 17: 1982–1987.
- Lin, S, Shi, Q, Nix, FB, Styblo, M, Beck, MA, Herbin-Davis, KM, Hall, LL, Simeonsson, JB, Thomas, DJ. 2002. A novel S-adenosyl-L-methionine: Arsenic(III) methyltransferase from rat liver cytosol. *J. Biol. Chem.* 277(13):10795-10803.
- Liu, Y, and Wu, F. 2010. Global burden of aflatoxin-induced hepatocellular carcinoma: a risk assessment. *Environ Health Perspect* 118:818-824.
- Meharg, AA, Williams, PN, Adomako, E, Lawgali, YY, Deacon, C, Villada, A, Cambell, RCJ, Sun, G, Zhu, YG, Feldmann, J, Raab, A, Zhao, FJ, Islam, R, Hossain, S, Yanai, J. 2009. Geographical variation in total and inorganic arsenic content of polished (white) rice. *Environmental Science & Technology*. 43(5), 1612-1617.
- Melkonian, S, Argos, M et al., 2011. A Prospective Study of the Synergistic Effects of Arsenic Exposure and Smoking, Sun Exposure, Fertilizer Use, and Pesticide Use on Risk of Premalignant Skin Lesions in Bangladeshi Men. *American Journal of Epidemiology*. 173: 2
- Moon, K, Guallar, E, and Navas-Acien, A. 2012. Arsenic exposure and cardiovascular disease: an updated systematic review. *Curr Atheroscler Rep* 14:542-555.
- Moon,KA; Guallar, E, Umans, JG, Devereux, RB, Best, LG, Francesconi, KA, Goessler, W, Pollak, J, Silbergeld, EK, Howard, BV, Navas-Acien, A. 2013. Association Between Exposure to Low to Moderate Arsenic Levels and Incident Cardiovascular Disease A Prospective Cohort Study. *Ann Intern Med*.159:649-659
- Morales, KH, Ryan, L, Kuo, TL, Wu, MM, Chen, CJ. 2000. Risk of internal cancers from arsenic in drinking water. *Environ.Health Perspect*.108:655-661.
- Mostafa, MG, McDonald, JC, Cherry, NM 2008. Lung cancer and exposure to arsenic in rural Bangladesh. *Occup Environ Med*, 65: 765–768.
- Muñoz, O, Diaz, OP, Leyton, I, Nuñez, N, Devesa, V, Súnier, MA, Vélez, D, Montoro, R. 2001. Vegetables Collected in the Cultivated Andean Area of Northern Chile: Total and Inorganic Arsenic Contents in Raw Vegetables. *J Agric Food Chem* 50:642-647.
- Murray, CJL, Lopez, AD, editors. 1996. *The global burden of disease: a comprehensive assessment of mortality and disability from diseases, injuries, and risk factors in 1990 and projected to 2020*. Cambridge (MA): Harvard University Press.

- Naranmandura, H, Suzuki, N, Suzuki, KT. 2006. Trivalent arsenicals are bound to proteins during reductive methylation. *Chem Res Toxicol.* 19(8):1010-8.
- National Research Council (NRC): Critical Aspects of EPA's IRIS Assessment of Inorganic Arsenic: Interim Report. Washington DC. National Academies Press. 2013
- Nischwitz, V, Pergantis, SA, 2005. First report on the detection and quantification of arsenobetaine in extracts of marine algae using HPLC-ES-MS/MS. *Analyst* 130 (10), 1348-1350.
- Nordstrom, DK. 2002. Worldwide occurrences of arsenic in ground water. *Science* 296, 2143–2145.
- National Research Council (NRC): Critical aspects of EPA's IRIS assessment of inorganic arsenic: Interim Report. Washington, DC: National Academy Press, 2013
- National Research Council (NRC): Risk Assessment in the Federal Government: Managing the Process. Washington, DC: National Academy Press, 1983
- National Research Council (NRC): Science and Judgement in Risk Assessment. Washington, DC: National Academy Press, 1994.
- Navas-Acien, A, Umans, JG, Howard, BV, Goessler, W, Francesconi, KA, Crainiceanu, CM, Silbergeld, EK, Guallar, E. 2009. Urine arsenic concentrations and species excretion patterns in American Indian communities over a 10-year period: the Strong Heart Study. *Environ Health Perspect.* 117(9):1428-33
- Omenn, GS. 2000. The genomic era: a crucial role for the public health sciences. *Environ Health Perspect* 108(5):A204–205
- Parvez, F, Chen, Y, Brandt-Rauf, PW, Slavkovich, V, Islam, T, Ahmed, A, Argos, M, Hassan, R, Yunus, M, Haque, SE, et al. 2010. A prospective study of respiratory symptoms associated with chronic arsenic exposure in Bangladesh: findings from the Health Effects of Arsenic Longitudinal Study (HEALS). *Thorax* 65:528-533.
- Postma, D, Larsen, F, Hue, NTM, Duc, MT, Viet, PH, Nhan, PQ, Jessen, S, 2007. Arsenic in groundwater of the Red River floodplain, Vietnam: Controlling geochemical processes and reactive transport modeling. *Geochimica et Cosmochimica Acta* 71, 5054-5071.
- Pu, YS, Yang, SM, Huang, YK et al. (2007a). Urinary arsenic profile affects the risk of urothelial carcinoma even at low arsenic exposure. *Toxicol Appl Pharmacol* , 218:99–106.
- Raml, R, Rumpler, A, Goessler, W, Vahter, M, Li, L., Ochi, T, Francesconi. 2007. Thio-dimethylarsinate is a common metabolite in urine samples from arsenic-exposed women in Bangladesh. *Toxicol. Appl. Pharmacol.* 222(3):374-380.

- Reagan-Shaw, S, Nihal, M, Ahmad, N. 2007. Dose translation from animal to human studies revisited. *The FASEB Journal Life Sciences Forum*. 22:659 - 61
- Rehman, K, Naranmandura H. 2012. 2012. Arsenic metabolism and thioarsenicals. *Metallomics*. 4(9):881-92.
- Rivara, MI, Cebrin, M, Corey, G et al. 1997. Cancer risk in an arsenic-contaminated area of Chile. *Toxicol Ind Health*, 13: 321–338.
- Rumpler, A, Edmonds, JS, Katsu, M, Jensen, KB, Goessler, W, Raber, G, Gunnlaugsdottir, H, Francesconi, KA, 2008. Arsenic-containing long-chain fatty acids in cod liver oil: a result of biosynthetic infidelity? *Angewandte Chemie International Edition* 47, 2665-2667.
- Samal, AC, Kar, S, Bhattacharya, P, Santra, SC. 2011. Human exposure to arsenic through foodstuffs cultivated using arsenic contaminated groundwater in areas of West Bengal, India. *Journal of Environmental Science and Health, Part A* 46:1259-1265.
- Sayarath, V, Kamiri, R, Karagas, M et al. 2009. Contribution of foodborne exposure to Arsenic and to Biomarker levels. *Epidemiology*. 20:6.
- Scarborough, P, Bhatnagar, P, Wickramasinghe, K, Smolina, K, Mitchell, C, Rayner, M. 2010. Coronary heart disease statistics. British Heart Foundation Health Promotion Research Group Department of Public Health, University of Oxford.
- Schaeffer, R, Francesconi, KA, Kienzl, N, Soeroes, C, Fodor, P, Váradi, L, Raml, R, Goessler, W, Kuehnelt D. 2006. Arsenic speciation in freshwater organisms from the river Danube in Hungary. *Talanta* 69, 856-865
- Schmeisser, E, Goessler, W, Kienzl, N, Francesconi, KA. 2005. The direct measurement of lipid-soluble arsenic species in biological samples with HPLC-ICPMS. *Analyst* 130, 948-955.
- Schoof, RA, Yost, LJ, Eickhoff, J, Crecelius, EA, Cragin, DW, Meacher, DM, Menzel, DB. 1999. A Market Basket Survey of Inorganic Arsenic in Food. *Food and Chemical Toxicology* 37:839-846.
- Scientific Cooperation (SCOOP), 2004. SCOOP Report of experts participating in Task 3.2.11.. Assessment of the dietary exposure to arsenic, cadmium, lead and mercury of the population of the EU Member States. Available from: http://ec.europa.eu/food/food/chemicalsafety/contaminants/scoop_3-2-11_heavy_metals_report_en.pdf. pp. 125
- Signes, A, Mitra, K, Burló, F, Carbonell-Barrachina, AA. 2008. Effect of cooking method and rice type on arsenic concentration in cooked rice and the estimation of arsenic dietary intake in a rural village in West Bengal, India. *Food Additives & Contaminants: Part A* 25:1345-1352.

- Siroto, V, Guérin, T, Volatier, JL, Leblanc, JC. 2009. Dietary exposure and biomarkers of arsenic in consumers of fish and shellfish from France. *Science of the Total Environment* 407 (6), 1875-1885
- Slejkovec, Z, Bajc, Z, Doganoc, DZ. 2004. Arsenic speciation patterns in freshwater fish. *Talanta* 62 (5), 931-936.
- Sloth, JJ, Larsen, EH, Julshamn, K. 2005. Survey of inorganic arsenic in marine animals and marine certified reference materials by anion exchange high-performance liquid chromatography- inductively coupled plasma mass spectrometry. *Journal of Agricultural and Food Chemistry* 53 (15), 6011-6018.
- Sloth, JJ, Julshamn, K. 2008. Survey of total and inorganic arsenic content in blue mussels (*Mytilus edulis* L.) from Norwegian fiords: revelation of unusual high levels of inorganic arsenic. *Journal of Agricultural and Food Chemistry* 56 (4), 1269-1273.
- Smedley, PL, Kinniburgh, DG. 2002. A review of the source, behaviour and distribution of arsenic in natural waters. *Applied Geochemistry* 17 (5), 517-568.
- Smith, AH, Marshall, G, Liaw, J, Yuan, Y, Ferreccio, C, Steinmaus, C. 2012. Mortality in Young Adults following in Utero and Childhood Exposure to Arsenic in Drinking Water. *Environ Health Perspect.* 120(11), 1527-1531.
- Smith, AH, Goycolea, M, Haque, R, Biggs, ML. 1998. Marked increase in bladder and lung cancer mortality in a region of Northern Chile due to arsenic in drinking water. *American Journal of Epidemiology* 147:660-669.
- Smith, AH, Ercumen, A, Yuan, Y, and Steinmaus, CM. 2009. Increased lung cancer risks are similar whether arsenic is ingested or inhaled. *J Expo Sci Environ Epidemiol* 19:343-348.
- Smith, AH, Marshall, G, Yuan, Y, Ferreccio, C, Liaw, J, von Ehrenstein, O, Steinmaus, C, Bates, MN, Selvin, S. 2006. Increased mortality from lung cancer and bronchiectasis in young adults after exposure to arsenic in utero and in early childhood. *Environ. Health Perspect.* 114(8), 1293-1296
- Soeroes, C, Goessler, W, Francesconi, KA, Schmeisser, E, Raml, R, Kienzl, N, Kahn, M, Fodor, P, Kuehnelt, D, 2005. Thio arsenosugars in freshwater mussels from the Danube in Hungary. *Journal of Environmental Monitoring.* 7, 688-692.
- Srivastava, S, D'Souza, SE, Sen, U, States, JC. 2007. In utero arsenic exposure induces early onset of atherosclerosis in ApoE^{-/-} mice. *Reprod Toxicol* 23:449-456.
- Srivastava, S, Vladykovskaya, EN, Haberzettl, P, Sithu, SD, D'Souza, SE, States, JC. 2009. Arsenic exacerbates atherosclerotic lesion formation and inflammation in ApoE^{-/-} mice. *Toxicol Appl Pharmacol* 241:90-100.

- States, JC, Barchowsky, A, Cartwright, I, Reichard, JF, Futscher, BW, Lantz, RC. 2009. Arsenic Toxicology: Translating between Experimental Models and Human Pathology. *Environmental Health Perspectives*.119: 10
- Steinmaus, C, Bates, MN, Yuan, Y et al. 2006. Arsenic methylation and bladder cancer risk in case– control studies in Argentina and the United States. *J Occup Environ Med*, 48: 478–488.
- Steinmaus, C, Yuan, Y, Bates, MN, Smith, AH. 2003. Case–control study of bladder cancer and drinking water arsenic in the western United States. *Am J Epidemiol* 158(12):1193–1201
- Straif, K et al. 2009. A review of human carcinogens – Part C: Metals, arsenic, dusts, and fibers. *Lancet Oncology* 10:453-4.
- Strong Heart Study (SHS): Cardiovascular Disease in American Indians (Phase V) Operations Manual. 2006. Center for American Indian Health Research. College of Public Health. <http://strongheart.ouhsc.edu/manual/PhaseV/Vol01.pdf>
- Su, CC, Lu, J, Tsai KY, Lian, L. 2011 Reduction in arsenic intake from water has different impacts on lung cancer and bladder cancer in an arseniasis endemic area in Taiwan. *Cancer Causes Control* 22:101–108
- Sun, GX, Williams, PN, Carey, AM, Zhu, YG, Deacon, C, Raab, A, Feldmann, J, Islam, RM, Meharg, AA, 2008. Inorganic arsenic in rice bran and its products are an order of magnitude higher than in bulk grain. *Environmental Science and Technology* 42 (19), 7542-7546.
- Taleshi, MS, Jensen, KB, Raber, G, Edmonds, JS, Gunnlaugsdottir, H, Francesconi, KA, 2008. Arsenic- containing hydrocarbons: Natural compounds in oil from the fish capelin, *Mallotus villosus*. *Chemical Communications* 39, 4706-4707.
- Thomas, DJ, Styblo, M, Lin, S. The cellular metabolism and systemic toxicity of arsenic. *Toxicol Appl Pharmacol* 176: 127-144, 2001.
- Tsai, SM, Wang, TN, Ko, YC. 1999. Mortality for certain diseases in areas with high levels of arsenic in drinking water. *Arch Environ Health* , 54: 186–193.
- Tseng, WP, Chu, HM, How, SW et al. 1968. Prevalence of skin cancer in an endemic area of chronic arsenicism in Taiwan. *J Natl Cancer Inst*, 40: 453–463.
- Tsuda, T, Babazono, A, Yamamoto, E et al. 1995. Ingested arsenic and internal cancer: a historical cohort study followed for 33 years. *Am J Epidemiol*, 141: 198–209.
- Uneyama, C, Toda, M, Yamamoto, M, Morikawa, K. 2007. Arsenic in various foods: cumulative data. *Food Addit Contam* 24:447-534.

- United States Environmental Protection Agency (USEPA) Toxicological Review of n-Butanol. In Support of Summary Information on the IRIS. 2011. US Environmental Protection Agency Washington, DC
http://ofmpub.epa.gov/eims/eimscomm.getfile?p_download_id=504786
- United States Environmental Protection Agency (USEPA): Guidelines for Carcinogen Risk Assessment. 2005. Risk Assessment Forum. US Environmental Protection Agency, Washington, DC
http://www.epa.gov/raf/publications/pdfs/CANCER_GUIDELINES_FINAL_3-25-05.PDF
- United States Environmental Protection Agency (USEPA) Integrated Risk Information System (IRIS) 1998. Arsenic, inorganic. Washington DC
<http://www.epa.gov/iris/subst/0278.htm>.
- United States Environmental Protection Agency (USEPA) Risk Assessment: Basic Information. Available from: <http://epa.gov/riskassessment/basicinformation.htm#risk>
- Benchmark Dose Technical Guidance. 2012. Risk Assessment Forum U.S. Environmental Protection Agency Washington, DC 20460 EPA/100/R-12/001
- Vahter, M. 2002. Mechanisms of arsenic biotransformation. *Toxicology* (181-182):211-217.
- von Ehrenstein, OS, Mazumder, DN, Yuan, Y, Samanta, S, Balmes, J, Sil, A, Ghosh, N, Hira-Smith, M, Haque, R, Purushothamam, R, et al. 2005. Decrements in lung function related to arsenic in drinking water in west bengal, India. *Am.J.Epidemiol.* 162:533-541.
- Waalkes, MP, Liu, J, Diwan, BA. 2007. Transplacental arsenic carcinogenesis in mice. *Toxicol Appl Pharmacol.* 222: 271–280.
- Watanabe C. 2001. Environmental arsenic exposure in Bangladesh: water versus extra-water intake of arsenic. *Environ Sci* 8:458–466.
- World Health Organization (WHO) consultation to develop a strategy to estimate the global burden of foodborne diseases. Geneva: World Health Organization; 2006. p. vii.
 Available from:
http://www.who.int/foodsafety/publications/foodborne_disease/fbd_2006.pdf
- World Health Organization (WHO). Arsenic. 2000.
http://www.euro.who.int/__data/assets/pdf_file/0014/123071/AQG2ndEd_6_1_Arsenic.PDF
- Wignall JA, Shapiro AJ, Wright FA, Woodruff T, Chiu WA, Guyton KZ, Rusyn I. 2014 Standardizing Benchmark Dose Calculations to Improve Science-Based Decisions in Human Health Assessments. *Environmental Health Perspectives*. Advance publication February 25.

- World Health Organization (WHO) - Global Environment Monitoring System-Food Contamination Monitoring and Assessment Programme (GEMS/Food). 2006. Geneva, Switzerland. <http://www.who.int/foodsafety/chem/gems/en/index1.html>.
- World Health Organization (WHO). 2011. Arsenic in drinking water, background document for development of WHO Guidelines for Drinking Water Quality. Geneva, Switzerland available from: http://www.who.int/water_sanitation_health/dwq/chemicals/arsenic.pdf
- Wu, MM, Kuo, TL, Hwang, YH, Chen, CJ. 1989. Dose-response relation between arsenic concentration in well water and mortality from cancers and vascular diseases. *American Journal of Epidemiology* 130:1123-1132.
- Yang, CY, Chang, CC, Chiu, HF. 2008. Does arsenic exposure increase the risk for prostate cancer? *J. Toxicol. Environ. Health A* 71(23):1559-1563.
- Yost, LJ, Schoof, RA, Aucoin, R. 1998. Intake of inorganic arsenic in the North American diet. *Human and Ecological Risk Assessment* 4:137-152.